Arsenic distribution and speciation in antigorite-rich rocks from Vermont, USA

By

Lijie Niu

A thesis submitted to the School of Graduate Studies and Research
in partial fulfillment of the requirements
for the degree of M.Sc. in Biology

University of Ottawa

August, 2011

Summary

Serpentinites from the northern Vermont were examined for the distribution and abundance of As. XRD and electron microprobe showed the samples are composed of antigorite, chromite, magnetite, and carbonate minerals (magnesite, dolomite, calcite). The concentration in As when the samples were dissolved in H_3PO_4 was 10% of the concentration in As when the samples were dissolved in concentrated HF/HNO_3, suggesting that As is mainly incorporated in the structure of antigorite. X-ray absorption near-edge structure spectra showed that the As is As(III) in the samples. Extended X-ray absorption fine structure spectra suggested that the As has a tetrahedral coordination and is located in the Si-site in serpentine.

Résumé

Des échantillons de serpentinite du nord du Vermont ont été analysés par diffraction de rayons X et microsonde de Castaing afin de déterminer leur composition et l'abondance en Arsenic. Ces échantillons se sont révélés principalement composés d'antigorite, de chromite, de magnétite et de minéraux carbonatés (magnésite, dolomite, calcite). La concentration en Arsenic pour les échantillons dissous à l'aide de H_3PO_4 est égale à 10% de la concentration en Arsenic pour les échantillons dissous à l'aide de HF/HNO_3, suggérant que l'Arsenic est principalement contenu dans la structure de l'antigorite. L'étude de ces échantillons par XANES (spectroscopie de structure près du front d'absorption de rayons X) indique que l'Arsenic a une coordination tétraédrique et qu'il est contenu dans le site Si de la serpentine.

Acknowledgements

First of all, I would like to thank my thesis supervisor, Dr. Kéiko Hattori, without whose constant support, encouragement, and help in all aspects, this project would not have been possible. I would like to thank Dr. Yoshio Takahashi, co-supervisor of this project, for providing an excellent opportunity to work, and experience the warm welcome in Japan. I deeply appreciate the opportunity given by Dr. Hattori and Dr. Takahashi for this extremely valuable experience of learning many advance analytical techniques and living in a spectacular country, and the great amount of time that was dedicated to complete this project. All two chapters benefited from edits, comments and suggestion from Dr. Takahashi and especially Dr. Hattori, for her ceaseless help and incredible patience with my many mistakes made during thesis completion.

There are numbers of people that had made the route of my research smooth and joyful. Besides Dr. Hattori, Dr. Takahashi, I thank Dr. Danielle Fortin for the support not only in the graduate school years but also her enormous help during the undergraduate school years. I wish to thank Dr. André E. Lalonde, Dr. Jeremy Kerr, Dr. Richard Blute that have helped and supported me spiritually and financially. Mr. Yasuyuki Shibata from Hiroshima University (Japan) provided many hours of help on the EPMA analysis. All the members in Dr. Tahakashi's laboratory have provided me many helps in the

laboratory as well as living in Japan, especially Mika Sakamitsu for providing me her large amount of unpublished data, the calculated results, as well as the diagrams that she had generated. They are used in the second part of my thesis. Special thanks also need to be delivered to Yuka Yokoyama, Sakiko Kikuchi for the ICP-MS/AES as well as XRD analysis.

I wish to thank many great friends whom have proved me a very joyful time in the years of graduate study. I would like to deliver my special thanks to Emmanuel, Sarah and Angelina for the constant supports, the laugh and good times. One special thanks to Jesse for many years of enlightening, supports in my study and life. Friends I have made in Japan had added so much color and support during my living there. I have to thank Ricardo for his assistance while living in Japan. I would like to thank Nicolas for his contribution on preparing my thesis defense as well as his great encouragement and support for me to complete my thesis writing.

Last but not least, I sincerely thank my parents and grandparents for providing me with everything unconditionally, and the love and care they had put on me in all time. I have to thank my uncle and his family providing financial supports during my study in Ottawa.

Table of Contents

List of Figures

List of Tables

List of Appendices

Introduction

Arsenic has been studied over many years; however, its behavior is still not fully understood. With increased attention on As poisoning and increased As found in various areas in the world, locating the source of As and understanding its behavior has become more crucial to prevent As entering water for consumption.

Arsenic is known for its potent toxicity; it is a semi-metal element naturally present, but determining its occurrence is difficult in the earth crust. It can enter human or live stocks' diets through drinking water, as well as plants that are grown on arsenic contaminated soil due to natural deposit, or human activities.

The difficulty in determining the source of As has been the most intriguing field of As study. Although high As can be found in the groundwater in one area, the adjacent groundwater can contain insignificant amount of As (Smedley and Kinniburgh, 2002). Some studies of As has looked at its relation to antigorite (Hinkle and Polette, 1999) and suggested that in New England, U.S.A., As is mainly located in serpentine and shales, whereas most other minerals contain relatively low concentrations of As. Thus, it is in our interest to gain the knowledge of the source of the As, its speciation, its structural property, as well as its concentration in various minerals obtained from Vermont U.S.; in addition, we determined the diffusion coefficient of various As species.

This thesis addresses objectives related to As characteristics, such as to describe the As occurrence, its location and distribution, in natural rock samples.

Thesis objective

The purpose of this thesis is to document the distribution of As in serpentinites collected from the northern Vermont, United States;

Statement of original contribution

To my knowledge, this thesis is the first report on the distribution of As in the rock samples that were obtained from the northern Vermont, U.S.A. The chapter attached in appendix of the thesis is a continuation of research carried out by Mika Sakamitsu as her Master's thesis project under the supervision of Dr. Takkahashi. I have followed the same method and produced several more data to increase the quality of the results.

The Contribution of the Author and the Collaborating Researchers

This study involved 10 months of research in Hiroshima University, Japan. Prior to my research, Rock samples were collected by Peter Ryan of Middlebury College and Keiko Hattori of the University of Ottawa in outcrops in northern Vermont. George Mrazek made polished-thin sections of samples for microscope examination, and EPMA analysis. I prepared the remaining

samples for other analysis.

The data presented in this thesis include my original data, as well as the data obtained by Dr. Keiko Hattori, Dr. Yoshio Takahashi, and Mika Sakamitsu. The preliminary analysis of minerals in polished sections was carried out by Dr. Keiko Hattori with the assistance of Peter Jones at Carleton University. A detailed analysis was carried out by Mr. Yasuyuki Shibata (Hiroshima University, Japan); X-ray Absorption Spectroscopy (XAS) analytical procedures were partially accomplished by Dr. Takahashi as well as myself at Spring-8 synchrotron facility (Hyogo, Japan), and the Micro XRF elemental mapping was performed at the BL4A, Photon Factory (Tsukuba, Japan) by Dr. Takahashi. The majority of data along with the calculations generated on these data presented in the attached chapter in appendix are produced by Mika Sakamitsu at Hiroshima University. I have produced 4 data points with calculation generated on these data points that made the interpretation convincing and possible to made interpretations.

Chapter 1

Distribution and Speciation of Arsenic in Serpentinites obtained in Northern Vermont, USA

Niu, L., Hattori, K., Takahashi, Y. and Ryan, P.C.

1.1 Abstract

The high As contents in groundwaters and bedrocks are reported in many parts of New England (Ayotte et al. 2003). The contents of As in hydrated ultramafic rocks in northern Vermont are up to 449 ppm in serpentinites and up to 1,100 ppm in talc-magnesite rocks (Ryan et al. 2009). Serpentinites are commonly present in the Appalachians in New England. The As occurrence in the representative serpentinites collected in northern Vermont would reveal its importance on controlling the local As concentrations, which was the focus of this study. Multiple techniques were employed to examine in this study, such as polished thin sections used for electron microprobe (EPMA) analysis and μ-X-ray fluorescent spectrometer (μ-XRF), powdered samples used in acid leaching and digestion, as well as X-ray absorption (XAS) study of As in mechanically separated mineral fractions. EPMA, μ-XRF and XAS studies showed that most of As is distributed in antigorite, the only identified serpentine phase. In the acid leaching/digestion experiment, As is mainly dissolved in concentrated HF/HNO_3, whereas phosphate acid does not leach high amount of As, suggesting that As is mainly incorporated in the structure of antigorite. Less than 10% As was able to dissolve by long period phosphate leaching. XANES spectra at As K-edge showed that the As(III) was the only detected form in the samples. EXAFS spectra illustrated that the As keeps its tetrahedral coordination, indicating that As is likely at the Si-site in serpentine.

Study by Hattori et al. (2005) of serpentinites in north western Himalayas show that As (V) is fixed in serpentine by replacing Si(IV) in antigorite. The results of this study suggests antigorite is the major fixing agent of As(III) in the samples we collected from North Vermont.

1.2 Introduction

1.2.1 Arsenic information

Arsenic is a semi-metal element that has high toxicity and complex geochemical behavior. The World Health Organization (WHO) and U.S.Environmental Protection Agency (EPA) drinking water guidelines for arsenic are 10μg/L, and it should not excess 50μg/L (WHO 2003; EPA 2009). Several areas have reported As poisoning due to high concentrations of As in waters. Groundwaters that contained high concentration of As have been found in Argentina, Chile, Mexico, China, Hungary, and some countries in southern and southeast Asia (Smedley and Kinniburgh, 2002; Polizzotto et al. 2008). One of well-known cases occurs in Bangladesh; where people suffer from As poisoning from consuming groundwater containing high As (Stollenwerk, et al. 2007). Ahamd, et al.(1997) reported that 29% of 294 wells in the village of Rajarampur of the Nawabganj district contain As exceeding 50μg/L, It is suggested that As in this area is naturally occurring and it is believed that it is originated from the Himalayan catchments sediments

(McArthur et al. 2001; Harvey et al. 2002). In northern Vermont, U.S., the concentrations of As are high in groundwater reaching up to 300ppb (Ryan, 2009).

The distribution of As in natural minerals and environments is of great interest due to its toxicity and its high solubility, especially As (III), in waters (Smedley and Kinniburgh, 2002). A good understanding of the As distribution and the migration of As species is crucial for the development of techniques for effective removal of As from groundwaters. The technique commonly uses adsorbents, such as iron oxide (Su and Puls, 2001; Lakshmipathiraj et al. 2006).

1.2.2 Geochemistry of arsenic

In the natural environment, As is present in many oxidation states, such as +5, +3, +1, -3 (Welch et al. 1988). Arsenic is rarely found in its elemental state, and it can substitute anions or cations (O'Day, 2006). The bio-availability of As depends on the oxidation states of As, due to the difference between their solubility in water. The behavior of phosphate is considered to be similar to arsenate (Cotton and Wilkinsone, 1988, Butler, 1998).

In aqueous environments, the oxidative states of As can be interchanging depending on the Eh, pH. The Eh-pH diagram (Fig. 1.1) for As-O_2-H_2O species in aqueous condition under 25^0C and 1 bar atmospheric pressure

shows that under oxidizing environment at pH< 2.2, the dominate specie is $H_3AsO_4^0$; at pH between 2.2 - 6.9, $H_2AsO_4^-$ is the major presenting specie; and between pH 6.9 – 11.7, $HAsO_4^{2-}$ become the dominating specie; at pH higher that 11.7, AsO_4^{3-} is the major specie. At low Eh value (reducing environment), at pH < 9.2, the major specie is $H_3AsO_3^0$, and from pH 9.2 – 12.2, $H_2AsO_3^-$ becomes the major specie; and at pH at 12.2 – 13.6, $HAsO_3^{2-}$ is the dominating specie; and AsO_3^{3-} is dominant at pH > 13.6; in factor, the sensitivity of As species towards Eh change can be used as an indicator for redox potential measurements (Fig. 1.1; Smedley and Kinniburgh, 2002).

The solubility of As also depends on some other factors, such as its affinity with metal oxides, such as Fe oxides, and Al oxides (Smedley and Kinniburgh, 2002). The study done by Jonsson and Sherman (2008) suggested that Fe(II) or the mixed Fe(II)/Fe(III) minerals such as fougerite, magnetite, and siderite are able to sorb As(V) to form inner-sphere surface complexes at pH >8, and As(III) and the sorption increases with increasing pH.

Besides some metal oxides, organic material is also suggested to affect As mobility in aqueous solutions (Welch et al. 1988). Xu et al. (1991) demonstrated the effect of acidity and organic materials on the As mobility; it suggested that As adsorption on alumina is generally reduced in fulvic acid that is over 10 mg/L at pH 5 - 7.

Relatively high HCO^{3-} concentrations resulting from the ultramafic rock

dissolution also affected As mobility in groundwater for the enhanced alkalinity (Ryan et al. 2011).

Arsenic is usually high in groundwater from inland or closed basins in arid or semi-arid areas, or in geologically young rocks, and high As concentrations in groundwater are likely to be found in highly reducing environments with slow moving aquifers (Smedley and Kinniburgh, 2002). However, the source and distribution of As in groundwater and fresh water remains unclear; its concentrations in fresh water can vary by four orders of magnitude (Smedley and Kinniburgh, 2002). Smedley and Kinniburgh (2002) also suggested that the groundwater concentration of As is strongly influenced by the chemical, physical conditions of the local environment, as well as the water-rock, water-soil interactions, thus it is crucial to study the source and distribution of As in rocks and minerals, and soils.

There are more than 200 minerals that contains As as their major component (Smedley and Kinniburgh, 2002). Arsenic-bearing minerals and solids include realgar ($As^{I}S$), orpiment ($As^{III}_2S_3$), arsenopyrite ($FeAs^{0}S$), claudetite ($As^{III}_2O_3$), arsenolite ($As^{III}_4O_6$), arsenic pentoxide ($As^{V}_2O_5$) and scorodite ($FeAs^{V}O_4.2H_2O$) (Welch et al. 1988). Sedley and Kinniburgh (2002) reviewed that the As can reach up to 1000 mg/kg in apatite; As can also replace Si(IV), Al(III), Fe(III) and Ti(IV) in mineral structures, and its concentration in silicate minerals, such as quartz, feldspar, micas, amphiboles are about 1mg/kg; while it is less than 10 mg/kg in most common carbonate

minerals.

There are many researches on the speciation and distribution of As in rocks and minerals. In the study by Charnock et al. (2007), XAS measurement of the garnet obtained from the Central Oslo Rift showed direct evidence that As was present as As(V) is replacing the Si^{4+} tetrahedral site.

Hattori et al. (2005) examined As concentration, its distribution and speciation of serpentinites in the Indus suture zone, northwest Himalayas which are, associated with the Tso Morari eclogitic rocks. The serpentinites contain total As concentrations from 6 to 275 ppm. Arsenic in antigorite is mostly As(V) and bonds with O.

In the fractured bedrock aquifer of northern Vermont, USA, the data obtained in a recent study by Ryan et al. (2011) showed As concentrations in groundwater ranged from <1 to 327μg/L and it seems to correlate to the spatial distribution of ultramafic rock bodies which are serpentinites and talc–magnesite rocks. In comparison, the other lithologies in the study area contain low As relative to the ultramafics: the As concentration in metabasaltic, phyllites and schists was much lower in comparison. The majority of the As is located in antigorite and magnesite compare to magnetite (Fe_3O_4).

The fate of As in soil highly depends on the water contents of soil due to its influence on the soil oxidative state, its pH value, and ion contents and speciation. The paper by Takahashi et al. (2004) described the observation of As behavior in rice paddy fields (Japan). In soil, As was hosted in

Fe-(hydr)oxide. In irrigation waters, As was incorporated in Fe-(hydr)oxide in soil during the non-flooded period, but it was quickly released from soil to water during the flooded period because of the reduction of As from As(V) to As(III) thus the mobility of As was also increased.

1.3 Study locations

Rock samples were taken from northern Vermont; arsenic concentrations reach as high as 300 ppb in groundwater from public and private domestic bedrock wells (Ryan et al. 2009). The geology of Vermont is rather complex. It is located in the Appalachian Mountain that stretches at least from to Newfoundland (Doolan, 1996).

We examined the As concentrations, speciation, and locations on two representative serpentinite samples BH-4, BH-5. Rock samples were collected in outcrops of small serpentinite ultramafic bodies in northern Vermont; the sample sites are BH-4, BH-5 at UTM coordinates of 4919016 (northing) and 683824 (easting) in NAD 27 (Figs. 1.2a.,2b.).

The sampling location is underlain by metasedimentary and metaigneous rocks; These metamorphic rocks were originated from sediment, lava flows and slivers of ancient oceanic crust and mantle, and they host talc and asbestos deposits; these rocks were proximally 590-550 Ma, (Doolan, 1996, Kim et al. 2003).

1.4 Methods and materials

1.4.1 Sample preparation

BH-4 and BH-5 samples prepared for X-ray deffractometer (XRD), X-ray adsorption spectroscopy (XAS), acid leaching and digestion examination were purified by hand separation and washed by Milli-Q water in ultrasonic water-bath, as illustrated in Fig. 1.3, which is explained as follow:

To separate serpentine from magnetic Fe-oxide grains, BH-4, BH-5 samples were crushed by a hand-held iron hammer into small (< 1 mm) particles in a double zip-locked bags. First dark magnetic fraction (Fraction M) was removed from white portion (serpentine-rich Fraction S). Second, Fractions of S and M were rinsed with Milli-Q water in an ultrasonic bath for 1 day (>24 hrs).Fraction S was further separated in water by applying a hand magnet outside the containers to attract the magnetic fraction (magnetite removed), whereas the non-magnetic portion, which is serpentine-rich, was transferred into a new container. Milli-Q water was added again into the serpentine rich portion and then put it to the ultrasonic water bath for over 8 hrs and repeated the procedure to obtain serpentine-rich fraction (Fraction PS). Pure alcohol was added into Fraction PS to accelerate the evaporation of any moist for over 24 hrs.

1.4.2 X-ray diffractometer

X-ray diffractometer (XRD; M18XHF MAC Sciences Ltd, Yokohama, Japan) was used to determine the mineralogy and purity of serpentine in Fractions of S and PS. The analytical conditions were adopted and modified from Takahashi et al. (2003), Zheng et al. (2007), and Mitsunobu et al. (2009). The XRD was operating with a Cu-Kα source at 40kV, 40 mA. Fine powdered samples hand-milled by acid cleaned agate mortar and pestle and were placed on clean boro-silicate glass holders. Each run scanned from 2 to 80° in 2θ; for each sample, the entire scan takes about 15 minutes, under ambient temperatures. The detection limit of a mineral is considered to be 5 to 10 %, but it is difficult to precisely determine.

1.4.3 Electron Probe Micro Analysis

The micrometer-scale distributions of As, Si, Fe, Mg, Ca, and P contents in the mineral phases were determined using an electron probe micro analyzer (EPMA; JEOL JXA-8200). The aperture was composed of a Cameca SX 50 electron probe equipped with four wave-length energy dispersive spectrometers. The analysis was carried out by Mr. Yasuyuki Shibata at Hiroshima University with appropriate crystal analyzers for different elements, along with according standards for calibration, and appropriate electron beam sizes for the analysis; essential conditions are described as below:

Quantitative analysis of arsenic:

The X-ray peak pattern of As Kα was collected to ensure the presence of As in the areas of analysis (Fig. 1.8). The As Kα peak was measured at 25 kV acceleration voltage with beam current at 10 nA using LiF crystal with 1μm beam size. Counting time for As was 120 sec at the peak position and 60 sec each for the background wavelength positions lower and higher than the peak. The standard used for As was 100 % As metal. The high electron current, voltage and long counting time adopted here lowered the detection limit of As to 100 ppm in all phases.

For other elements, counting time was typically 1 sec with 25 kV acceleration voltage and 100 nA current. The beam size was typically 5-10 μm in diameter. The crystals used for the other elements were TAP, for Si, Mg, Al, and Na, LiF for Fe, Ni, Cr, Ti, and Mn, lastly, PET for Ca and K with K lines.

Elemental mapping

For elemental mapping on the sample thin sections, the beam size was 2 μm while the current and acceleration voltage were 50 nA and 15 kV, respectively. The mapping was carried out by Mr. Yasuyuki Shibata at Hiroshima University with appropriate scanning procedure.

1.4.4 X-ray Absorption Spectroscopy

X-ray Absorption Spectroscopy (XAS) is used to investigate the oxidation

state, the local atomic structure of As, and the distribution of As in samples; the analysis was carried out by Dr. Yoshio Takahashi (Hiroshima University).

1.4.4.1 X-ray Absorption Near Edge Structure (XANES) spectroscopy

Arsenic K-edge XANES spectroscopy was employed to determine the As (III)/As(V) ratios in Fraction PS of two samples. XANES spectra were collected at beamline BL01B1 at SPring-8 (Hyogo, Japan). The X-ray beam was monochromatized with an Si(III) double-crystal monochromator and then focused to 1 X 0.5 mm^2 with a bent cylindrical mirror. All the measurements were carried out under ambient conditions. For all experiments, powder $As^{III}_2O_3$ and $As^{V}_2O_5$ were used as reference materials and the peak maximum of $As^{III}_2O_3$ was set at 11.866 keV. Arsenic K-edge XANES spectra were recorded in the energy range between 11.830 and 11.920 keV. The energy step was 0.25 eV. The energy of the peak top did not shift by more than 0.25 eV throughout all the measurements.

Window of a single-channel analyzers (SCAs) were tuned to count the As K-line fluorescence selectively. The total count entering the detector was kept lower than 200 kcps by adjusting the distance between the 19-element Ge semiconductor detector and the sample. It was necessary to correct the SCAs windowed signal due to the increase in the dead time when the incoming count rate was increased by large intensities of the fluorescence and scattering X-rays. The correction was made by a computer program, CORDT3U. The

analytical procedure is essentially the same as described in Hattori et al. (2005).

1.4.4.2 EXAFS Measurement and Data Analysis

The As K-edge EXAFS spectra were obtained for Fraction S of samples at beamline BL-12C of Photon Factory, KEK (Tsukuba, Japan) under the condition of 2.5 GeV, 450-300 mA. The spectra were collected in the fluorescence mode using a Lytle detector or a 19-element Ge semiconductor detector, whereas transmission mode was employed to measure the spectra for standard materials. The spectra collected in fluorescence mode used shaping time of 0.25 μ sec. Reference AsO_3^{3-} ($Na_3As^{III}O_3$) and As(III) adsorbed on $Fe(OH)_3$ were employed for extended X-ray absorption fine structure (EXAFS) study. EXAFS data were analyzed by REX2000 Version 2.5.9 (Rigaku Co. Ltd., Japan), by Dr. Yoshio Takahashi (Hiroshima University). The oscillation was extracted from the original spectrum by a spline smoothing method. E0 was set at the edge inflection point for the measured samples. The Fourier transformation of the $k3\chi(k)$ EXAFS oscillation from k (1/Å) space to R (Å) space was performed in a range 3.0-12.0 Å-1 to obtain a radial structural function (RSF) for As. The inversely Fourier filtered data were analyzed with a curve fitting method. Theoretical phase shift and amplitude functions employed in this fitting procedure were extracted from FEFF 7.0 (REX 2000, Version 2.5.9 Rigaku Co. Ltd., Japan) by

Dr. Yoshio Takahashi, and the principle of the procedure is as described by Ankudinov and Reher (1997). For this procedure, As-O phase shifts and amplitude functions were extracted from the structure of scorodite ($Fe^{3+}AsO_4 \bullet 2(H_2O)$).

For XAS analysis, two As compounds were used as references: $As^{III}_2O_3$ and $As^{V}_2O_5$, both were purchased from Sigma-Aldrich, Inc.

1.4.5 micro X-ray fluorescence spectrometry (μ-XRF)

μ-XRF elemental mapping was performed at the BL4A, Photon Factory (Tsukuba, Japan) by Dr. Yoshio Takahashi (Hiroshima University). Prior to the analyses, distributions of minerals within the thin section were examined by an optical microscope by Dr. Keiko Hattori. For the μ-XRF analyses, the polished-thin section was positioned at an angle of 45º against the incident beam, and fluorescence X-ray was recorded by a Si semiconductor. The size of incident X-ray scanning beam was fixed at 5 μm x 5 μm, which becomes 7 μm (horizontal) and 5 μm (vertical) on the sample due to the angle of the sample to the incident X-ray beam. Counting time (scanning speed) was 1 sec for 1 pixel. Intensity of incident X-ray was fixed at 12.0 keV. Simultaneous to the scanning, the intensities of fluorescent As Kα were monitored using SCAs tuned for the energy of fluorescence X-ray. The detection limits are difficult to determine due to its dependence on various parameters.

1.4.6 Acid leaching and digestion experiments

Fraction PS from BH-4 and BH-5 samples were selected for leaching and digestion analysis using an Inductively Coupled Plasma Mass Spectrometer (ICP-MS) and Inductively Coupled Plasma Atomic Emission Spectrometry (ICP-AES). In the leaching experiment, about 0.2 g of each Fraction PS samples was submerged in 20 mL of 1M phosphoric acid, which was prepared by dissolving 23.4 g of $NaH_2PO_4.2H_2O$ (Wako Pure Chem., Osaka, Japan) salt in 150 mL Milli-Q water. The pH of the solution was about 4.1 ± 0.5 at the beginning of the leaching experiment.

The weight ratio of sample to solution is about 1:100 to make sure that the acid is sufficient for thorough leaching. The leaching solution was made followed the method described by Keon et al. (2001). The solutions were placed in ambient temperatures for 3 days, with hand shaking in every 10 to 12 hrs.

A different portion of Fraction PS was digested in a 1:3 mixture (~ 3 mL) of conc. HNO_3/HF at 65^0C for over 24 hrs. The reagents were purchased from Wako Chem. Ind., Japan. After the leaching and nitric-HF acid digestion, the solutions were filtered with a Millipore GD/X 0.2um filter, followed by 100 times or 1000 times dilution by 2% HNO_3. The final solutions were analyzed for the concentrations of As by ICP-MS (Agilent HP-7500). Indium solution (~ 1 ppb) was added to the solution to monitor the analysis. The detection limit of As is

10 ppt. Standard solutions were prepared from XSTC-331(SPEX: 100μg/L) by diluting with 2% HNO_3 to be 0, 100 and 500 ng/L, and 1, 5, 10 μg/L as final concentrations of As. Pure He gas was used as a collision gas instead of Ar gas to avoid the interference of ArCl for As analysis.

Elemental concentrations of Mn, Fe, Si, Al, Mg, Ca in the solution were determined by ICP-AES (SII SPS-3100). Standard solutions for ICP-AES analysis were prepared as follows: XSTC-622(SPEX: 10 mg/L) was diluted by 2% HNO_3 to be 0, 0.1, 0.5, 1, 5 mg/L as final concentrations. The precision and accuracy of the analytical values were better than 10%, based on the analysis of the JR-2 reference from the Geological Survey of Japan during the course of this study.

1.5 Results

1.5.1 X-ray diffraction analysis

The peaks on the spectra of XRD for Faction S and Fraction PS of BH4 and BH5 are compared to those of antigorite, lizardite, chrysotile, talc, chromite, magnetite, and carbonate minerals (magnesite, dolomite, calcite) because some carbonate minerals are identified in polished-thin sections and during electron microprobe analysis. Diffraction patterns of Fraction S of BH4 and BH5 samples produced peaks and those greater than 10 % of the highest peak are listed in table 1.1. The peaks are identified as those of antigorite, and likely minor magnetite in Fraction S of BH5, and likely magnesite in Fraction S

of BH4 and BH5. No peaks for lizardite, chrysotile talc and chromite were identified for the Fraction S and PS samples. Three most intense peaks in the samples matched those of antigorite. However, due to low abundance and possible minor sifts of the peaks, only two or even one peak matched with those of magnetite. Therefore the presence of these two minerals can not be certain by looking at XRD patterns (Figs. 1.4 a, b).

The samples show an unidentified peak (Figs. 1.4 c, d). The unidentified peak in Fraction PS of BH4 occurs at d-value of 2.73 A which has 16% of the highest peak at a d-value 7.2017.

1.5.2 Electron microprobe analysis (EPMA)

The electron microprobe was used to identify minerals and mineral compositions in thin sections of BH-4 (Fig. 1.5 b) and BH-5 (Fig. 1.5 m). The analysis was carried out by Mr. Yasuyuki Shibata at Hiroshima University. The major mineral in the samples is serpentine and the minor minerals are chromite, magnetite, dolomite, calcite and magnetite (tables 1.3, 1.4). Minor magnesite was also found in several areas in BH-4 and BH-5 samples. Carbonate minerals are magnesite dolomite, Ca-carbonate in decreasing order of abundance.

Oxide- rich areas contain magnetite including the end-member composition of magnetite. There is no hematite found in the samples.

The distributions of Fe, Si, Ma, Ca, and P of selected areas on thin

sections of BH-4 and BH-5 were mapped and shown on Fig. 1.6. The bright areas on the back scattered electron image (point a.) is magnetite whereas the dark area is chromite (point b.) (Fig. 1.6 a and table 1.3). Circle E in BH 4 (Fig. 1.6 b) shows that the bright area is magnetite (table 1.3.1). On BH-4 Circle F (Fig. 1.6 c), the bring area is magnetite, whereas on the image of Fe Kα, the blue areas is chromite.

Similar back-scattered electron images were observed for sample BH-5, as shown in Fig. 1.6 d and e. In BH-5 Circle A (Fig. 1.6 d), the bright areas are Fe oxide (table 1.3). On BH-5 Circle E (Fig. 1.6 e), the bright areas in back–scattered electron image are magnetite, the blue areas in Fe level image are chromite (table 1.3).

1.5.2.1 Chemical compositions of minerals

Quantitative analysis show the presence of chromite (x13, x20, x17, x36 of Figs. 1.7 a, b. table 1.3.1, Cr bearing magnetite (x14, x21), magnetite (x15, x16 x18, x22 –x26), and serpentine (x19, x27 in table 1.3.2) on BH-4 thin section. Similarly, Cr bearing magnetite (x37), magnetite (x28 – x31, x38 –x40), and serpentine (x35, 41) are identified on BH-5 thin section (Fig. 1.7 f, table 1.3.1)

1.5.2.2 Arsenic contents in minerals

Quantitative analysis on As was done on areas 14, 16, 17, 19, 23, 27 of BH-4 thin section, and areas 29, 31, 33, 34, 37, 39, 41 of BH-5 (Fig. 1.8 a-c). These areas contain Cr^{-} bearing magnetite, magnesite, and serpentine (table 1.3). The results suggest that the concentrations of As were above the detection limits of ~ 100 ppm in only serpentine. Fe oxides contain As below 100 ppm. Fig. 1.8 showed that the areas that were selected for the analysis and the As peak patterns produced from them. The obtained As peak patterns were compared to the As metal peak pattern, thus to determine the presence of As. The areas show positively identified As are the site 27 on HB-4 Circle F (Fig. 1.8 b (2)), and site 41 on BH-5 Circle E (Fig. 1.8 d (3)).

Carbonate minerals

Elemental mappings of Mg, Ca, Si and P show the distribution of carbonate minerals (Figs. 1.9, 1.10, table 1.4). The maximum amount of magnesite was calculated from Mg content, 45800 ppm (= 4.5 wt%), in phosphoric acid leach (table 1.5) assuming all the Mg is from magnesite:

(4.58 % X molecular weight of magnetite ($MgCO_3$))/23

= (4.58 % X 68)/23

=31.14%

Since the phosphoric acid dissolved Mg from serpentine, the amount calculated above is the upper limit of the abundance of magnesite in the sample, BH 4.

Elemental mapping and back scattered electron image also identified apatite ($CaPO_4$) (circle apatite) of Fig. 1.10 a).

Fig. 1.10 b No. 4 and X3 are likely to be calcite, No. 5 and X3 are dolomite, and No.6 and X5 are magnesite. Similarly on Fig. 1.10 c - e, sites No. 7 and X6 are calcite; X7, X10 and X12 are magnesite; X8, X9 and X11 are dolomite. Table 1.4 showed that x1 on Fig. 1.10 a) is likely to be magnesite, whereas x2 to be dolomite.

1.5.3 Micro X-Ray Fluorescence (μ-XRF)

To determine the concentration of As in Fe-rich areas, μ-XRF which has lower detection limit than EPMA, although the exact value is hard to determine, for As was used to map the As and Fe distributions on the Circles B and F of section of BH-4 (Fig. 1.9). The selected areas on the thin sections were already examined by EPMA to identify the Fe^{-} rich area, and then these areas were examined for As abundance for comparing their distribution. μ-XRF scanned image Fig. 1.11 b, c, f, and g illustrated that As is high in areas that are relatively low in Fe; and As shows lower intensity in Fe-rich areas.

1.5.4 X-ray Absorption Spectroscopy (XAS)

XAS was done on Fraction S and PS of both BH-4 and BH-5:

1.5.4.1 X-ray Absorption Near Edge Structure (XANES)

The XANES spectra of fraction S (BH-4, BH-5) sample showed identical absorption patterns as that of reference for As(III) in $As^{III}_2O_3$. Therefore, As in the sample is likely mainly as As(III) (Fig. 1.12).

1.5.4.2 Extended X-ray Absorption Fine Structure (EXAFS)

The EXAFS spectra of As in Fraction S of BH-4 and BH-5 were very similar (Fig. 1.13 a). After background subtraction, the EXAFS spectra were Fourier transformed to separate the neighboring atoms according to their distances from the central atom thus giving the coordination number and the distances. The coordination number and the distances between As and the neighboring atoms are calculated by Dr. Yoshio Takahashi and listed in table 1.6. The calculation shows that As has a tetrahedral coordination in Fraction S of both samples (table 1.6). For BH-4, the As-O distance is 1.78 ± 0.009 Å, As-Si is 3.204 ± 0.070 Å, and As-Mg is 3.491 ± 0.31 Å; for BH-5, the As-O distance is 1.775 ± 0.009 Å, As-Si is 3.188 ± 0.062 Å, and As-Mg is 3.484 ± 0.032 Å.

1.5.5 Acid leaching

Arsenic concentrations in the Fraction PS (BH-4, BH-5) were determined after leaching with 1 N $NaH_2PO_4 \cdot 2H_2O$ solution and digestion in $HF\text{-}HNO_3$ mixture solution. Phosphoric acid is known to leach As that is adsorbed on the mineral surface, as described in Keon et al. (2001), but the leachate contained

high Ca, Mg, Al, Fe, Mn and Si (table 1.5). These data suggest phosphoric acid dissolved minerals in Fraction PS. HF-HNO3 digestion is the near total digestion as it dissolves most minerals except for Cr-rich spinel. Arsenic concentrations in phosphoric acid solution were ~120 (±15) ppm in both samples.

Total As concentration in the Fraction PS (BH4, BH5) determined after HF/HNO_3 digestion was 357 ppm for BH-4 and 756 ppm for BH-5. These results showed that As leached by phosphate acid was about 20% to 30% of the total As in the bulk rock samples.

1.6 Discussion

1.6.1 Arsenic concentration in serpentinites

Arsenic concentrations of Fraction PS of BH-4 and BH-5 samples were examined by phosphate leaching, and concentrated HNO3/HF acid digestion. The phosphate leachates of Fraction PS of BH-4 and BH-5 showed As concentration of 108ppm, 135ppm, respectively. The leachates also contained Ca, Mg, Al, Si, Mn, Fe. Therefore, As could have been contributed from carbonates and silicate minerals. Since calcite ($CaCO_3$) is the only phase containing Ca, the amount of calcite dissolved in phosphoric acid is calculated from Ca, One over 4 lechates contained 2980 ppm Ca and the rest had below the detection limit of 1 ppm in solution, (table 1.5). Therefore, the amount of As that was possibly located in calcite is small.

The Mg concentration is significant in the phosphoric acid leachates (table 1.5, Mg = 4.6%, average). To estimate the contribution of As dissolved from magnesite, the maximum concentration of As that is possibly contributed by magnesite is calculated. Assuming that all Mg is originated from magnesite; taking the maximum Mg concentration (4.83%) in the solution, and the maximum concentration of As in magnesite, determined by EPMA (As < 100 ppm, because As is below detection limit, Fig. 1.8, and because magnesite contains 28.83% Mg, Arsenic from magnesite is less or equal to:

(48300 X 1/1000000) X (100 x 1/1000000) / 28.83%

= 4.83 ppm / 28.83%

= 16.75 ppm

< 17 ppm

Another possible source of As is dissolution of antigorite. Due to long hours of leaching, antigorite was dissolved in phosphoric acid to release Si (~1.81%). Antigorite contains 18.05 wt.% Si (table 1.5).

Antigorite dissolved ppm = (1/ Si %) X Si dissolved ppm

= (1/ 18.05%) X 18100 ppm

= 100,277 ppm

= ~ 10 wt.%

As suggested in XRD analysis discussed in the next section, the only identified minerals above the detection limit in the Fraction PS samples are

antigorite and minor magnesite; therefore, both the leaching experiment as well as the XRD analysis show that the dissolved antigorite is about 10 wt% of the total antigorite. According to HF/HNO_3 acid digestion analysis, the maximum concentration of As is 756 ppm (in Fraction PS of BH-5), and the average concentration is 556 ppm (table 1.5), therefore antigorite contains on average less than 800 ppm As, thus in the phosphoric acid leaching, the dissolved 10 % of antigorite releases less than 80 ppm of As. Compared to the total As in the leachate (108 ~135 ppm), almost all As in the leaching solution could be explained by the dissolution of antigorite.

Therefore, major fractions of As could have been within the crystal structure of antigorite; however, the average of As, detected by ICP-MS, from antigorite dissolved in the phosphoric acid (80 ppm) is less than the total As in phosphoric acid leaching (122 ± 15 ppm).

From the above calculation, the As located in magnetite is < 17 ppm. The major amount of As in phosphoric acid leachate is the addition of antigorite adsorped As, the amount of As from antigorite dissolved in phosphoric acid, and As from magnetite; thus the range of adsorbed As onto antigorite can be calculated:

122 ±15 ppm – 80 ppm -17 ppm = 25 ± 15 ppm

This amount of adsorbed As estimated from leaching experiments by phosphate solution is 1.80 % to 7.19 % of the total As that was from the samples dissolved by HF/HNO_3.

Concluding from the above calculation, the major amount of the As is incorporated in the structure of antigorite. The contents of As in antigorite are measured with an EPMA and EXAFS as shown in Fig. 1.13 and table 1.6. The As within the structure of antigorite is not water leachable or cannot dissolve in water, but As adsorbed onto the surface of antigorite can be more easily released into water, thus serpentine leaching is not the major source of As in groundwater, because water leachable As might regulate As concentration in groundwater through the adsorption-desorption reaction.

1.6.2 Arsenic host phase in serpentines

The XRD spectra of the Fraction S of BH-4 and BH-5 show that these fractions are composed of antigorite, minor magnesite, magnetite, and an unidentified mineral (less than 5 %).

The magnetite present in the samples might have affected the As speciation in the samples, because Fe oxides are considered to host As during its crystallization (Wang et al., 2008; Tokoro et al. 2010). Ferric Fe oxide adsorbs As(V) more than As(III), suggested by Takahashi et al. (2004), whereas Su and Puls (2008) indicated that As(III) has higher sorption affinity with Fe oxides than As(V) in alkaline solution. Thus, the pH of water and the availability of As and Fe oxides can affect the As(III) / As(V) ratios in Fe oxides in BH-4 and BH-5.

The μ-XRF analysis results, obtained by Dr. Yoshio Takahashi (Hiroshima

University), on Fig. 1.11 illustrated the As relative distribution around the boundary between antigorite and magnetite of sample BH-4 Circle B and F (as shown on Fig. 1.5 e, k). The results suggested that As and Fe distributions are opposite from each other. The areas rich in Fe contain relatively low amounts of As, whereas areas low in Fe show high As concentration. This result is opposite from the expectation that As would have high concentration in Fe-rich areas, because previous studies by Moore and Pierce (1980), O'Day (2006), Wang et al. (2008), Su and Puls (2008) suggested that As has affinity for Fe oxides, such as magnetite; our results revealed that As could have higher affinity to serpentine than magnetite.

This μ-XRF result also suggests that As may have been fixed into serpentine (antigorite) during its formation. The comparison of As concentrations of the rock sample in phosphate leaching, and HF/HNO_3 acid digestion also confirmed that As is located in the structure of antigorite. This finding is very important, because it once again illustrates that in our samples, As has higher affinity towards antigorite than Fe oxide, which, once again, was considered to be the best co-precipitant for As in water.

BH-4 and BH-5 samples are composed of antigorite with minor magnetite, and chromites. There are minor carbonate minerals in the samples, such as magnetite, calcite, and dolomite (table 1.4, Fig. 1.10). Chromite is the primary mineral of the ultramafic rock. Antigorite and magnetite form during the hydration at temperatures above 350 ^{0}C (Evans, 2004). Magnesite may form

during this process because minor magnesite is commonly present in serpentinites. Finally, antigorite-rich serpentinites may change to carbonate minerals, such as dolomite, magnesite, and calcite, at low temperatures (Kim et al. 2003).

EXAFS shows that the As-O (BH4: 1.78 ± 0.009 Å; BH5: 1.775 ± 0.009 Å), As-Si (BH4: 3.204 ± 0.070 Å; BH5: 3.188 ± 0.062 Å), and As-Mg (BH4: 3.491 ± 0.031 Å; BH5: 3.484 ± 0.032 Å) distances (table 1.6). The length of As-O is longer than the bond length of Si-O (1.637 - 1.638 Å) in antigorite (Mellini et al. 2002, Capitani and Mellini 2004). In tetrahedral sheet, As (V) has an ionic radius of 0.48. Å, which is smaller than 0.53 Å of As(III),and in octahedral sheet, arsenic (V) has an ionic radius of 0.68. Å, which is smaller than 0.72 of As(III) (Ryan et al. 2011), therefore, As(III) would be difficult to enter the tetrahedral site of antigorite which is mostly made up of Si (IV) with radius of 0.40 Å (Shanoon 1976).

1.6.3 Arsenic structural information

XANES analysis suggested that As in samples of Fraction S and Fraction M of BH-4 and BH-5 is presented as As(III) (Fig. 1.12); In addition, As is concentrated in antigorite, thus As presented in the samples is As (III) in antigorite. This finding suggested that As(III) was incorporated into antigorite structure; in combination with ICP-MS, μ-XRF and EPMA analysis, these results suggested that As(III) can be incorporated into the Si(IV) site of

antigorite.

1.7 Reference

Ayotte, J.D., Montgomery, D.L., Flanagan, S.M., and Robinson, K.W. (2003) Arsenic in groundwater in eastern New England: occurrence, controls, and human health implications. Environ. Sci. Technol. 37(10): 2075-2083

Ahmad, S., Bandaranayake, D., Khan, A.W., Hadi, S., Uddin, G., and Halim, M. A. (1997) Arsenic contamination in ground water and arsenicosis in Bangladesh. International Journal of Environmental Health Research. 7: 271–276.

Ankudinov, A.L., and Rehr, J.J. (1997) Relativistic spin-dependent X-ray absorpion theory. Phys. Rev. B 56: 1712-1715

Butler, J.N. (1998) Ionic Equilibrium: Solubility and pH Calculations. John Wiley & Sons, New York, pp. 559

Capitani G. and Mellini M. (2004) The modulated crystal structure of antigorite: The m=17 polysome. *American Mineralogist.* 89 (1): 147-158

Charnock, J. M., Polya, D. A., Gault, A. G., and Wogelius, R. A. (2007) Direct EXAFS evidence for incorporation of As(V) in the tetrahedral site of natural andraditic garnet American Mineralogist. 92: 1856-1861

Cotton, F.A., and Wilkinson, G. (1988) Advanced Inorganic Chemistry. 5th edition. John Wiley & Sons, New York, pp. 382

Doolan, B. (1996) The Geology of Vermont. Rock and Minerals. 71, 218-2 5.

Evans B.W. (2004) The serpentinite multisystem revisited: chrysotile is metastable. International Geology Review. (46) 479–506

Harvey, C.F., Swartz, C.H., Badruzzaman, A.B.M., Keonblute, N., Yu, W., Ali, M.A., Jay, J., Beckie, R., Niedam, V., Brabander, D., Oates, P.M., Ashfaque, K.N., Islam, S., Hemond, H.F. and Ahmed, M.F.(2002) Arsenic mobility and groundwater extraction in Bangladesh. Science. 298:1602-1606

Hattori, K., Takahashi, Y., Guillot, S., and Johanson B. (2005) Occurrence of arsenic (V) in forearc mantle serpentinites based on X-ray absorption spectroscopy study. Geochimica et Cosmochimica Acta. 69(23): 5585-5596

Jonsson, J.; Sherman, D. M., (2008). Sorption of As (III) and As(V) to siderite, greenrust (fougerite) and magnetite :Implications for arsenic release in anoxic groundwaters. Chem.Geol. 255 (1 -2): 173-181

Keon,N. E., Swartz, C. H., Brabander, D. J. , Harvey, C., and Hemond, H. F. (2001) Validation of an arsenic sequential extraction method for evaluating mobility in sediments. Environ. Sci. Technol. 35 (13): 2778–2784

Kim, J., Coish, R., Evans, M., and Dick, G. (2003) Supra–subduction Zone

Extensional magmatism in Vermont and adjacent Quebec: Implications for Early Paleozoic adjacent Quebec: Implications for Early Paleozoic Appalachian Tectonics. Geological Society of America Bulletin. 115(12):1552–1569

Lakshmipathiraj, P., Narasimhan, B. R. V., Prabhakar, S. and Bhaskar, Raju, G. (2006) Adsorption studies of arsenic on Mn-substituted iron oxyhydroxide. Journal of Colloid and Interface Science, 304: 317–322

McArthur, J. Ravenscroft, P., Safiullah, S. and Thirlwall, M. (2001) Arsenic in groundwater: testing pollution mechanisms for sedimentary aquifers in Bangladesh, Water Resources Research. 37:109-117

Mellini, M., Fuchs, Y., Viti, C., Lemaire, C., and Linares, J. (2002) Insights on the antigorite structure from Mössbauer and FTIR spectroscopies. European Journal of Mineralogy. 1: 97–104

Mitsunobu, S., Takahashi, Y., Saka, Y.,and Inumaru K. (2009) Interaction of synthetic sulfate green rust with antimony(V). Environ. Sci. Technol. 43 (2): 318–323

Pierce, M.L., and Moore, C.B.(1980) Adsorption of arsenite on amorphous iron hydroxide from dilute aqueous solution. Environ. Sci. Technol.14 (2): 214–216

O'Day, P.A. (2006) Chemistry and mineralogy of arsenic. Elements. 2: 77- 83

Polizzotto, M.L., Kocar, B.D., Benner, S.G., Sampson, M. and Fendorf, S. (2008) Near-surface wetland sediments as a source of arsenic release to

ground water in Asia. Nature, 454, 505-508

Ryan, P.C., Kim, J., Clark, A.L., Smith, T.T., Chow, D., Sullivan, C., and Bright, K. (2009) Ultramafic source of arsenic in a fractured bedrock aquifer. Gelogical Society of America Abstracts with Programs. 41(7): 218

Ryan, P.C., Kim, J., Wall, A.J., Moen, J.C., Corenthal, L.G., Chow, D.R., Sullivan, C.M., and Bright, K.S. (2011) Ultramafic-derived arsenic in a fractured bedrock aquifer. Applied Geochemistry. 26: 444–457

Shanoon, R.D. and Prewitt, C.T.（1970）Revised valued of effective ionic radii.Acta Cryst. B.26, 1046-1048

Smedley, P.L., and Kinniburgh, D.G. (2002) A Review of the source, behavior and distribution of arsenic in natural water. Applied Geochemistry. 17(5). 517-568.

Stollenwerka, K.G., Breitb, G.N., Welchc, A.H., Yountd, J.C., Whitneyd, J.W., Fostere, A.L., Uddinf, M.N., Majumderg, R.K., and Ahmedg, N. (2007) Arsenic attenuation by oxidized aquifer sediments in Bangladesh.Science of The Total Environment.379(2-3): 133-150

Su, C., and Puls, R.W. (2008) Arsenate and arsenite sorption on magnetite: relations to groundwater arsenic treatment using zerovalent iron and natural attenuation. Water, Air & Soil Pollution. 193(1-4): 65-78

Su, C., Pulse, R.W. (2001) Arsenate and arsenite removal by zerovalent iron: effects of phosphate, silicate, carbonate, borate, sulphate, chromate, molybdate and nitrate, relative to chloride. Environ. Sci.Technol. 35,

4562–4568

Takahashi, Y., Minamikawa, R., Hattori, K., Kurishima, K., Kihou, N., and Yuita, K. (2004) Arsenic behavior in paddy fields during the cycle of flooded and non-flooded periods. Environ. Sci. Technol. 38 (4): 1038–1044

Takahashi, Y., Ohtaku, N., Mitsunobu, S., and Yuita, K. (2003) Determination of the As(III)/As(V) ratio in soil by X-ray absorption near-edge structure (XANES) and its application to the arsenic distribution between soil and water. Analytical Sciences. 19 (6): 89- 896

Tokoro, C., Yatsugi, Y., Koga, H., and Owada, S. (2010) Sorption mechanisms of arsenate during coprecipitation with ferrihydrite in aqueous solution. Environ. Sci. Technol. 44 (2): 638–643

U.S. Environmental Protection Agency (U.S.EPA)(2009) National primary drinking water regulations; arsenic and clarifications to compliance and new source contaminants monitoring. <http://www.epa.gov/fedrgstr/EPA-WATER/2001/January/Day-22/w1668.htm> Last updated on October, 2009

Wang, Y., Morina, G., Ona-Nguemaa, G., Menguya, N., Juillota, F., Aubryb, E., Guyota, F., Calasa, G.,and Brown, G.E. (2008) Arsenite sorption at the magnetite–water interface during aqueous precipitation of magnetite: EXAFS evidence for a new arsenite surface complex. Geochimica et Cosmochimica Acta. 72(11): 2573-2586

Welch, A.H., Lico, A.S., and Hughes, J.L. (1988) Arsenic in ground water of the

western United States. Ground Water. 26(3): 333- 347

World Health Organization(WHO)(2003)Arsenic in drinking-water background document for development of WHO guidelines for drinking-water Quality. <http://www.who.int/water_sanitation_health/dwq/chemicals/en/arsenic.pdf> 2003

Xu H, Allard B., and Grimvall A. (1991) Effects of acidification and natural organic materials on the mobility of arsenic in the environment. Water, Air, and Soil Pollution. 57-58: 269–278.

Zheng, G. D., Kuno, A., Mahdi, Talib Abdulameer, Evans, D. J., Miyahara, M., Takahashi, Y., Matsuo, M., and Shimizu, H. (2007) Iron speciation and mineral characterization of contaminated sediments by coal mining drainage in Neath Canal, South Wales, United Kingdom. Geochemical Journal. 41(6): 463-474

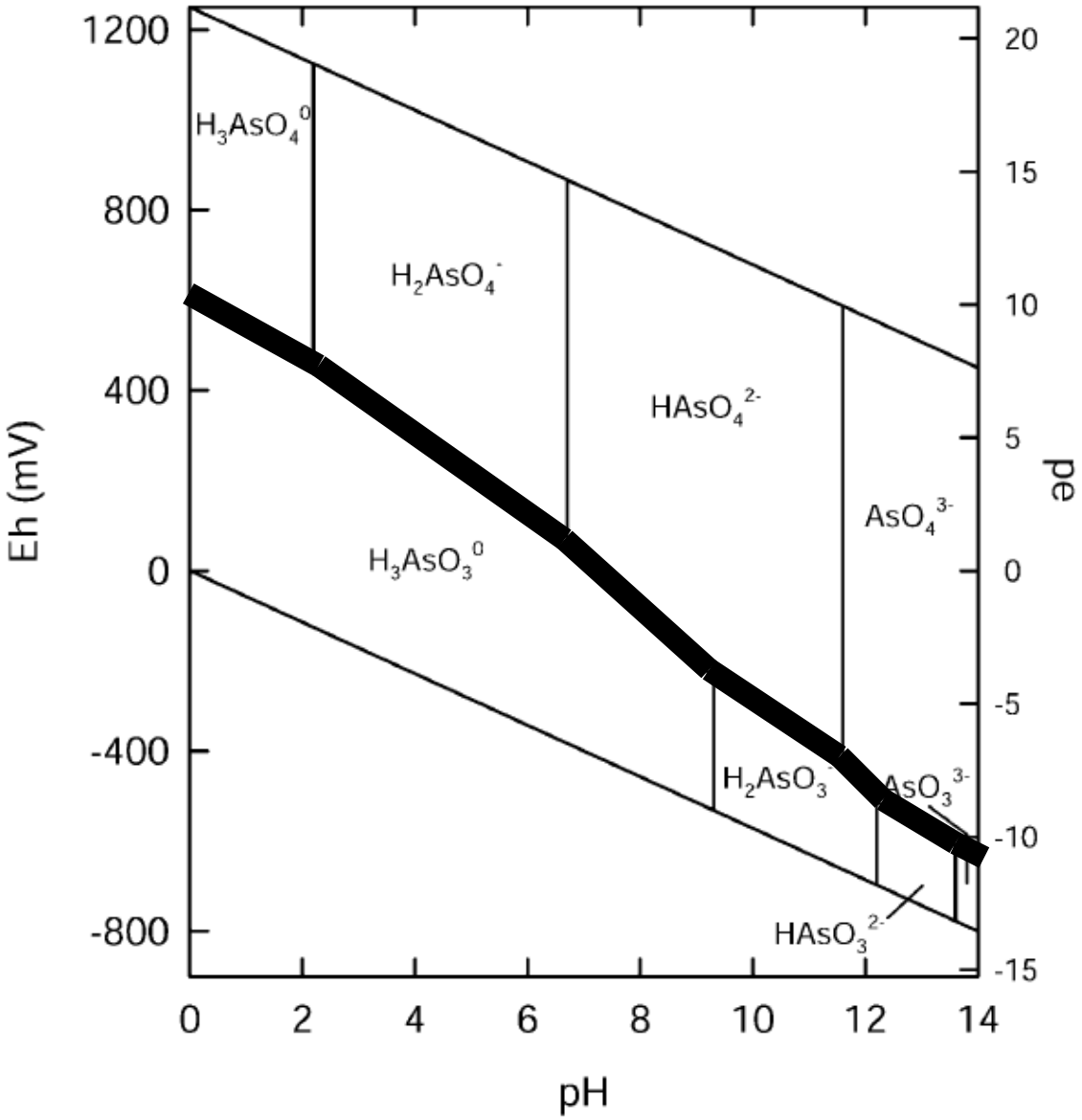

Figure 1.1 Eh-pH diagram for aqueous As species in the system AsO2H2O at 25 C^0 and 1bar total pressure (Smedley and Kinniburgh, 2002). For At high Eh values at pH< 2.2, the dominate specie is H3AsO40; at pH between 2.2 - 6.9, H2AsO4- is the major presenting specie; and between pH 6.9 – 11.7, HAsO42- become the dominating specie; at pH higher that 11.7, AsO43- is the major specie. At low Eh value (reducing environment), at pH < 9.2, the major specie is H3AsO30, and from pH 9.2 – 12.2, H2AsO3- becomes the major specie; and at pH at 12.2 – 13.6, HAsO32- is the dominating specie; and AsO33- is dominant at pH > 13.6; the Thick red line indicates the boundary between As(V) and As(III).

Figure 1.2 The sampling location of the study area on the simplefied map of Vermont. Natural rock samples were collected in northern Vermont, United States (modified from http://upload.wikimedia.org/wikipedia/commons/d/de/Vermont_Locator_Map_with_US.PNG)

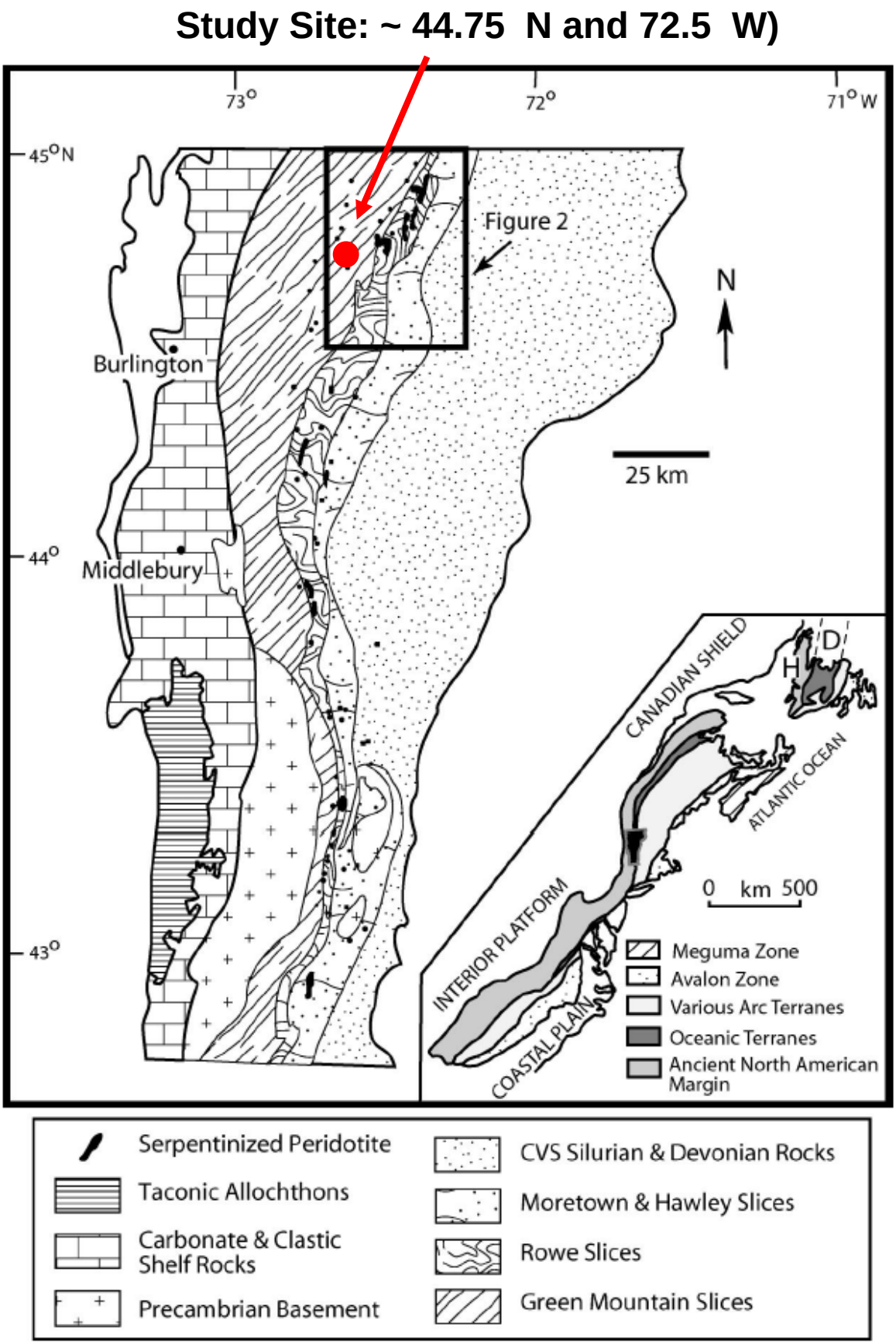

Figure 1.2 b The generalized geological map of the study area in the northern Vermont, United States: ~ 44.75 N and 72.5 W) (modified from Kim, et al. (2003). CVS—Connecticut Valley Sequence. The sampling location belongs to Green Mountains areas, which contains schist, phyllite, quartzite, graywacke, conglomerate, greenstone, dolomite, limestone, gneiss, amphibolite, intruded by ultrabasic rocks, basalte.

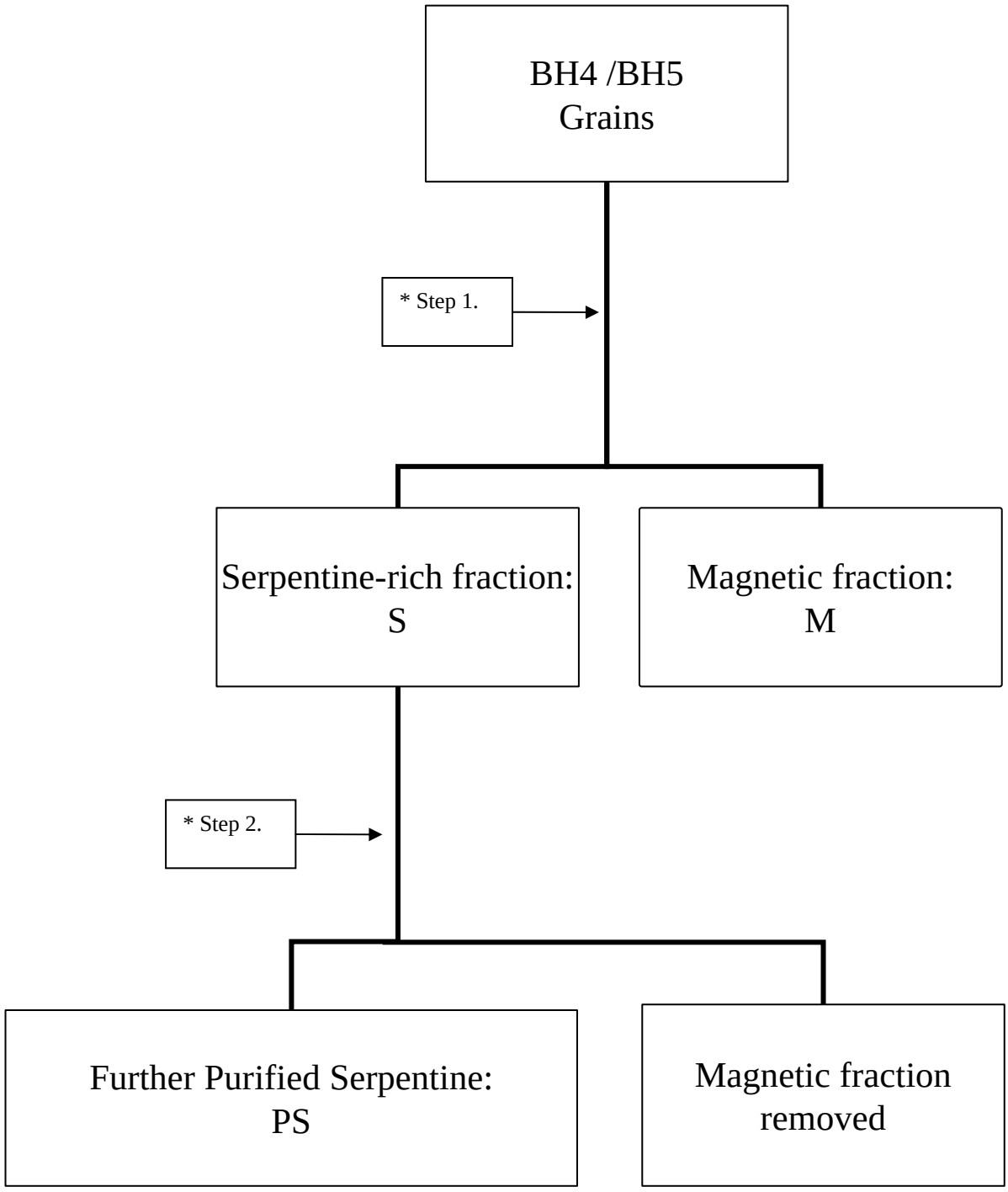

Figure 1.3 Flow chart showing the separation steps of studied samples. *Step 1.: hand-picked serpentine-rich fraction (S) and magnetite-rich fraction (M) using a hand magnet after samples were crushed by an iron hammer into particles(< 1 mm) in double zip-locked bags. *Step 2.: Fraction S was rinsed with ultra-pure water in an ultrasonic bath for 1 day (>24 hrs), then further removed magnetic fragments in water with a hand magnet placed on the side of the vials. The process was repeated.

a)

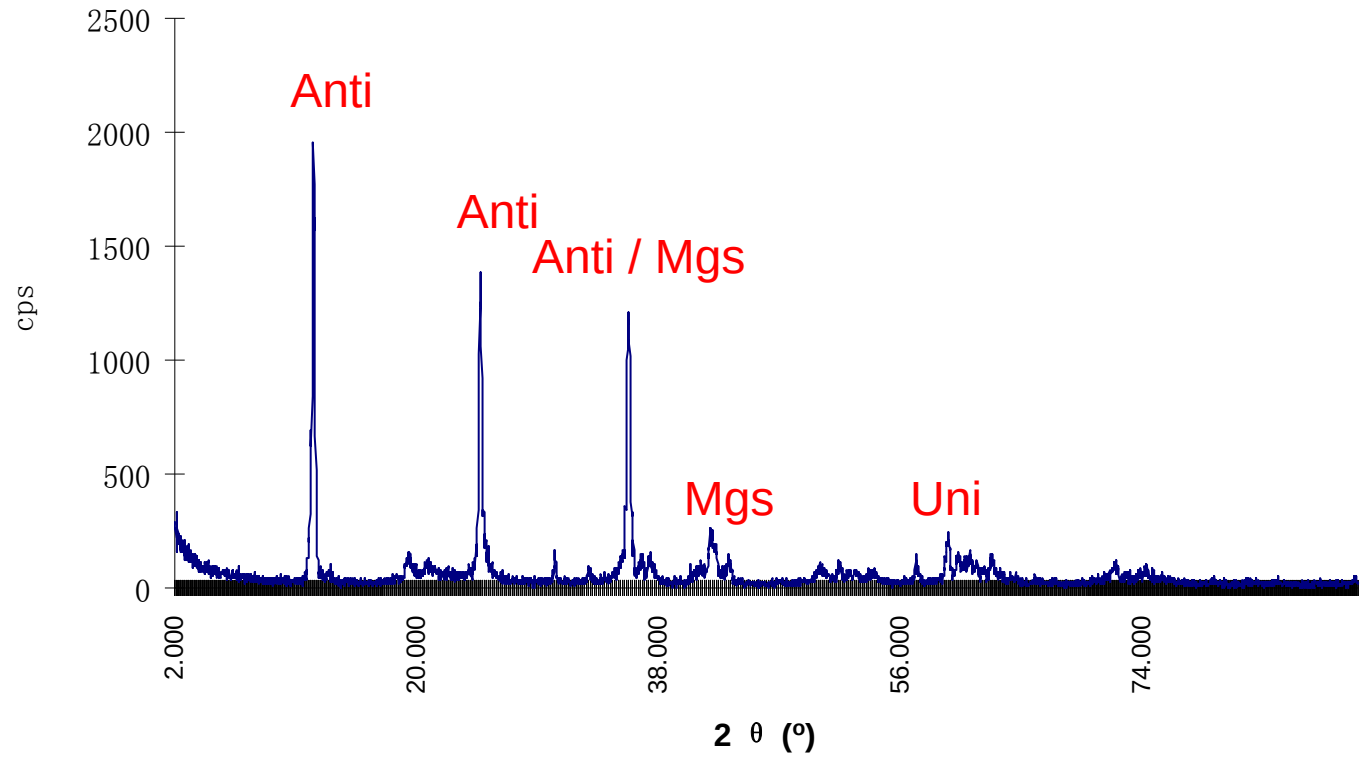
2500
2000
1500
1000
500
0
cps
Anti
Anti
Anti / Mgs
Mgs
Uni
2.000
20.000
38.000
56.000
74.000
2 θ (º)

b)

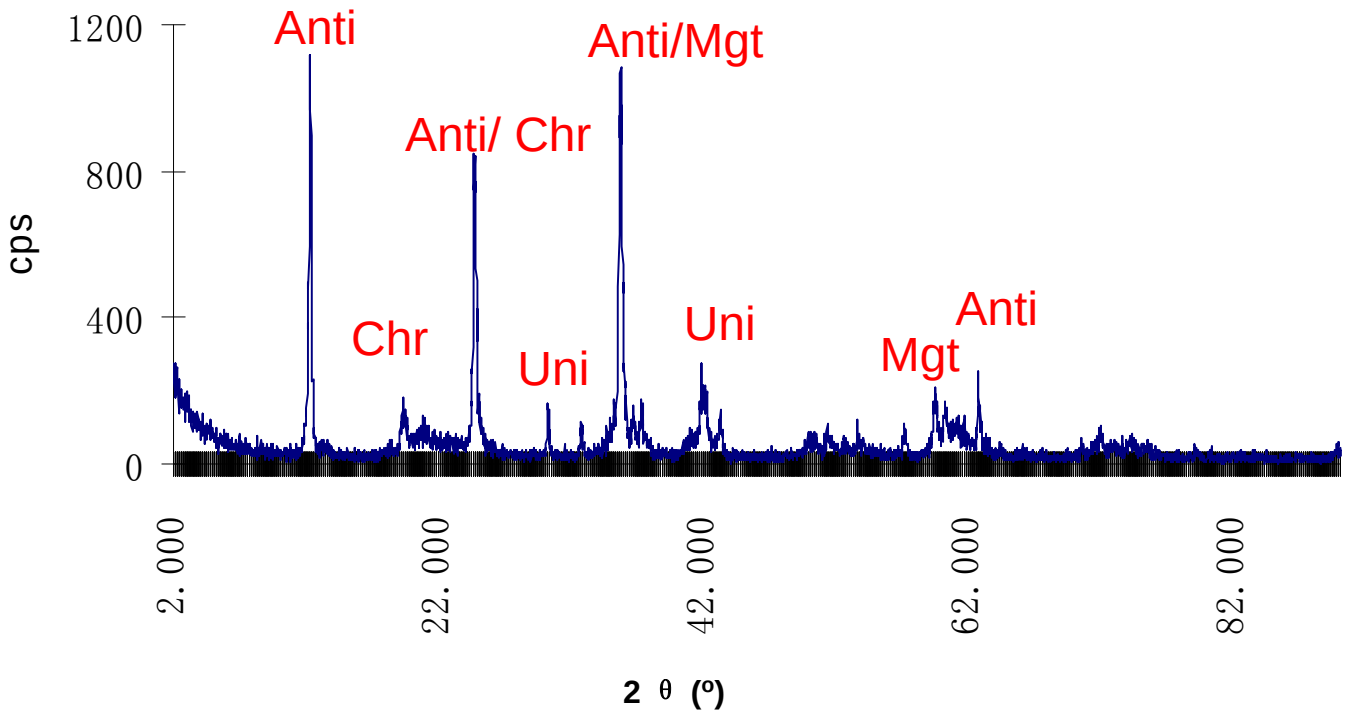
1200
800
400
0
cps
Anti
Anti/Mgt
Anti/ Chr
Chr
Uni
Uni
Mgt
Anti
2. 000
22. 000
42. 000
62. 000
82. 000
2 θ (º)

c)

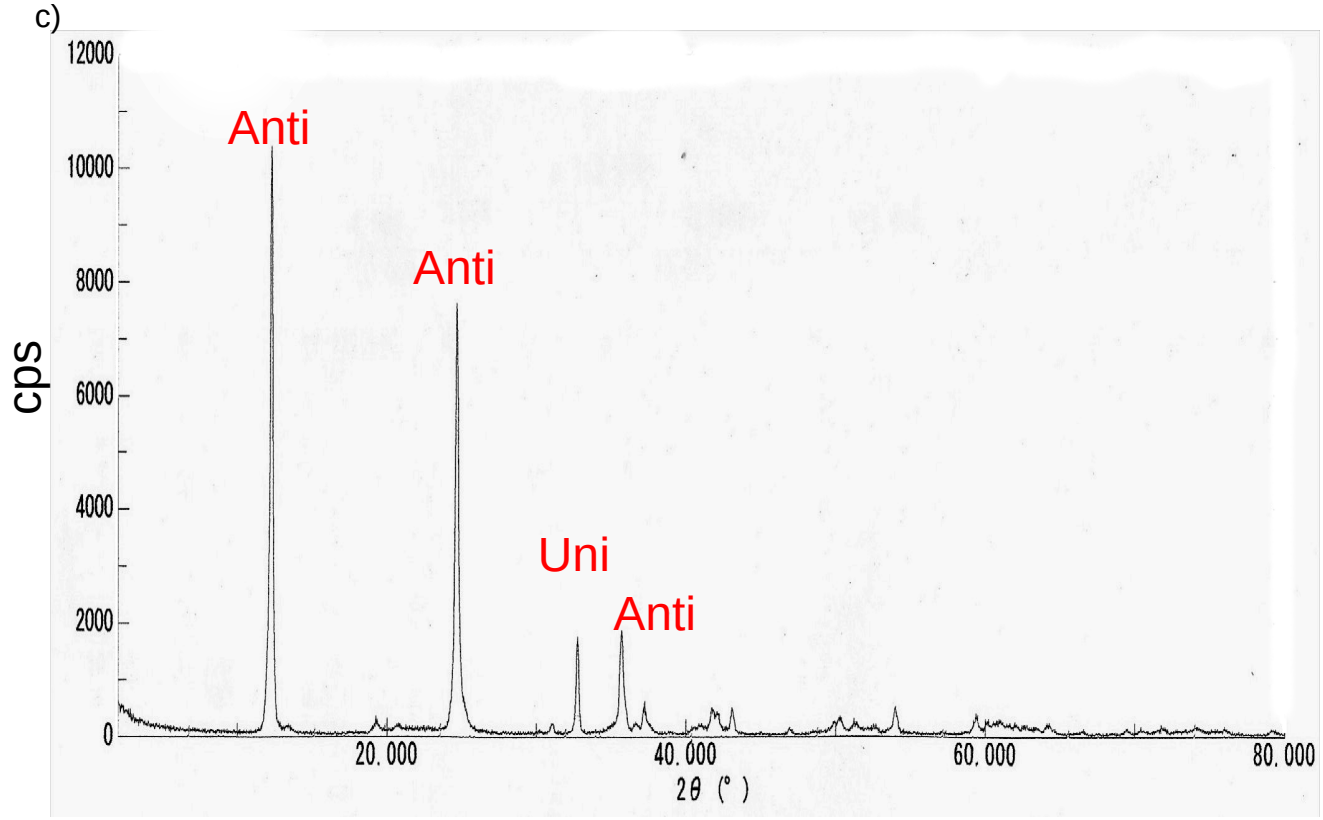
cps
12000
10000
8000
6000
4000
2000
0
Anti
Anti
Uni
Anti
20.000
40.000
60.000
80.000
2θ (°)

d)

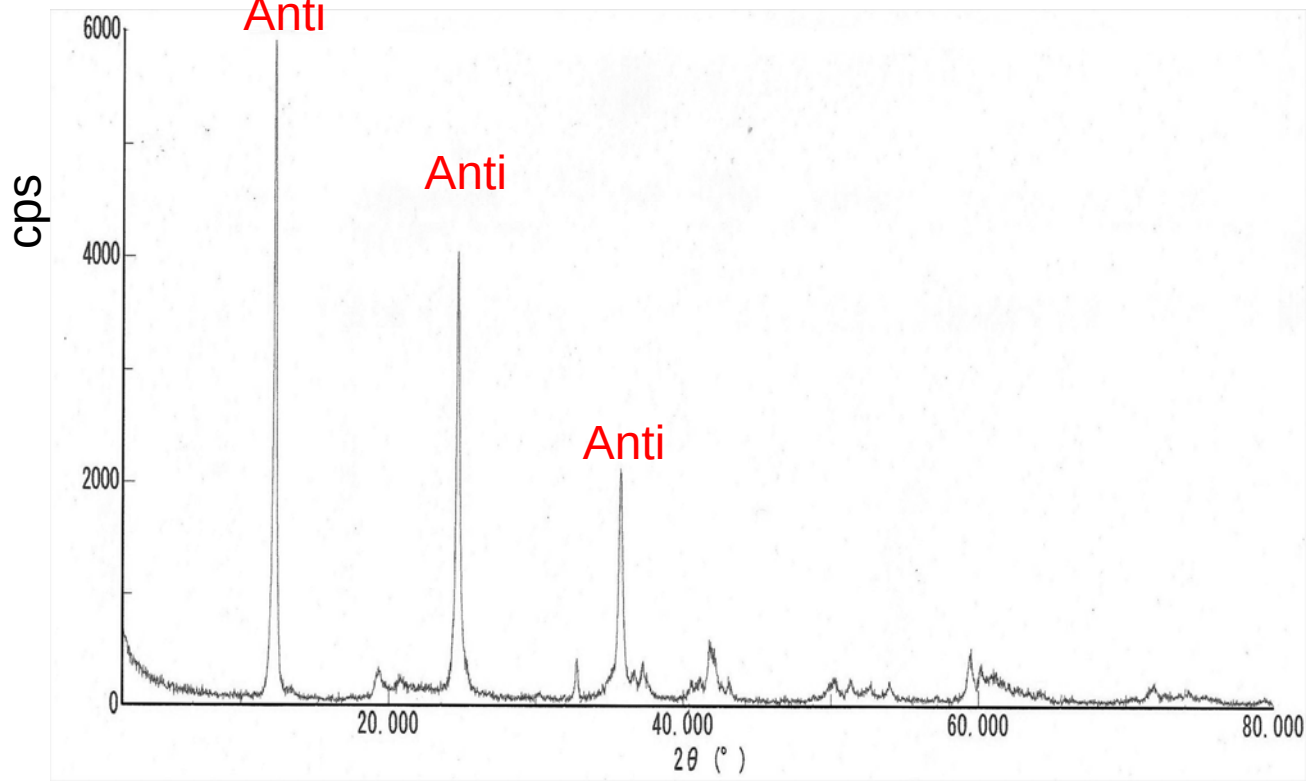
cps
6000
4000
2000
0
Anti
Anti
Anti
20.000
40.000
60.000
80.000
2θ (°)

e)

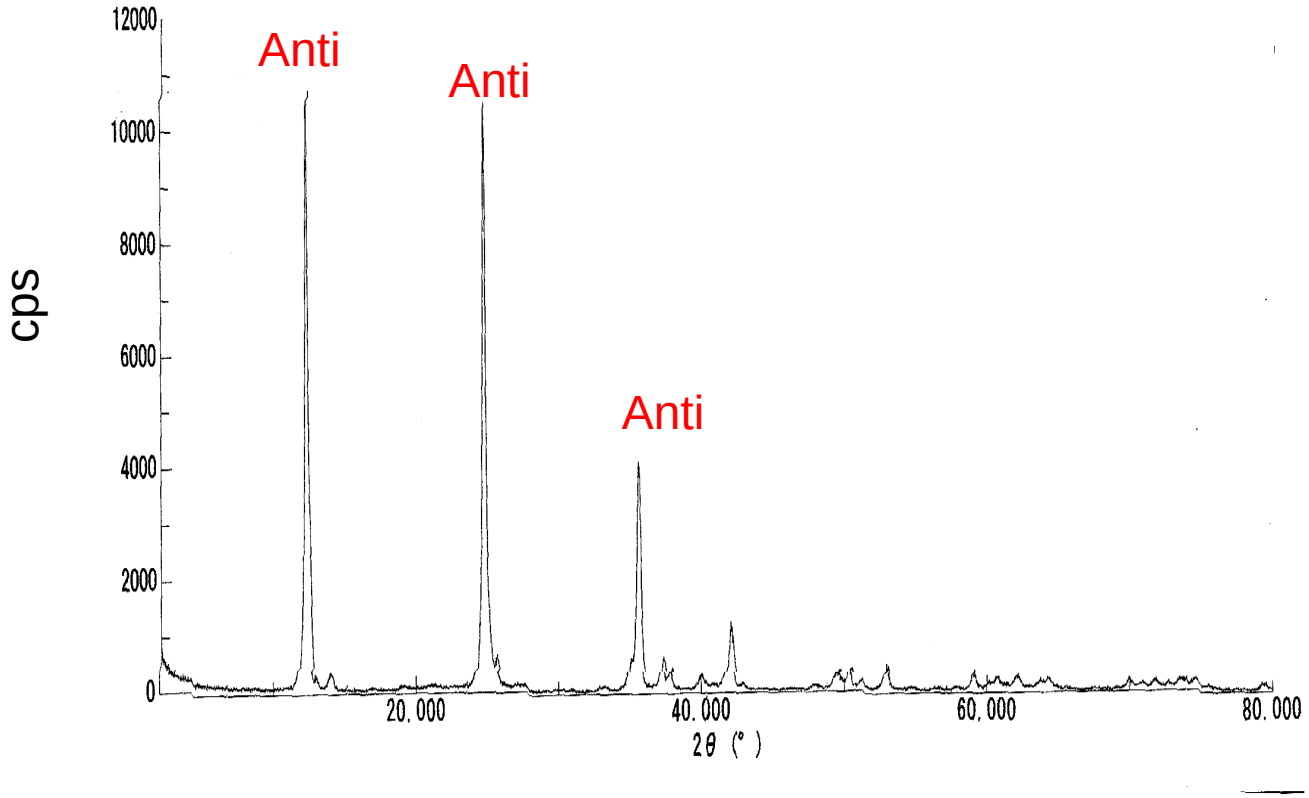

Figure 1.4 Powder X-ray diffraction spectra of Fraction S of BH-4 and BH-5. **a)** Powder X-ray diffraction spectra of Fraction S of BH-4., Antigorite(Anti) is the only indentified serpentine phase, and one peak of magnesite (Mgs) is identified. An unidentified (Uni) peak occurs at the d-value of 1.79 which has 12% of the highest peak. **b)** X-ray diffraction spectrum of fraction S of BH-5. Antigorite is the only indentified serpentine phase, two matching d-value to magnetite, two matching d-value to chrysotile (Chr), and an unidentified (Uni) peak with d-value 1.55(0.18), 2.16(0.24). **c)** Powder X-ray diffraction spectra of Fraction SP of BH-4. In sample, antigorite is the only indentified serpentine phase, and a unidentified (Uni) peak at the d-value of 2.73(0.16). **d)** X-ray diffraction spectra of SP fraction rock powder of BH-5. In sample, the only indentified serpentine phase is antigorite.


a
BH-4
1 cm

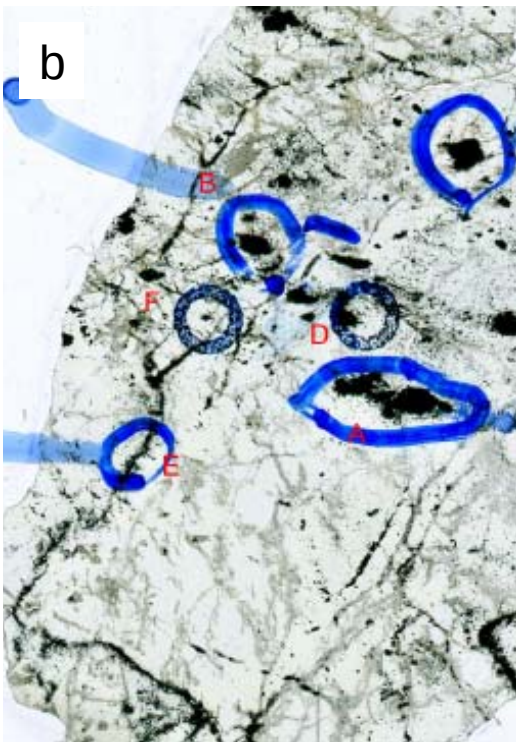
b
B
F
D
A
E
0.5 cm

Circle A

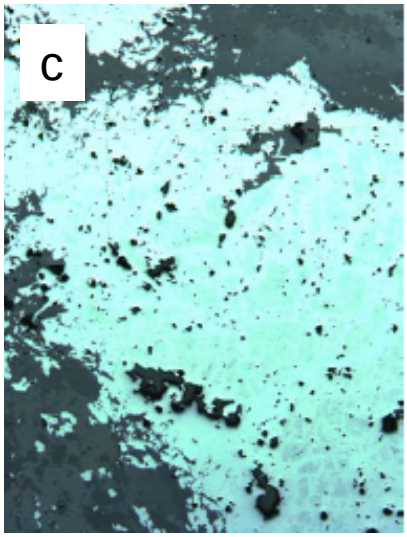

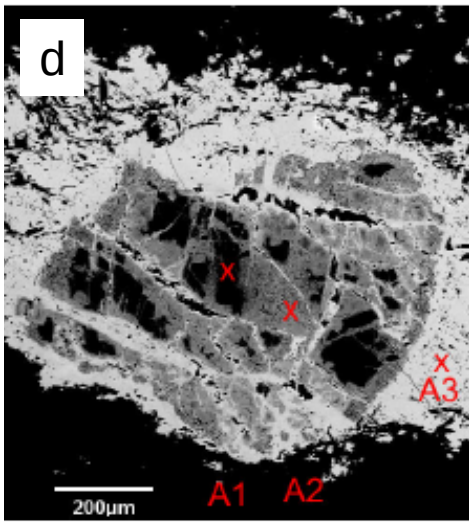

Circle B

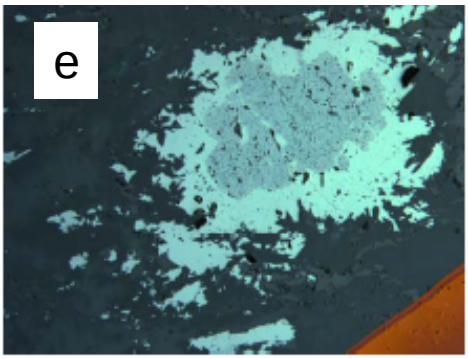

Circle C

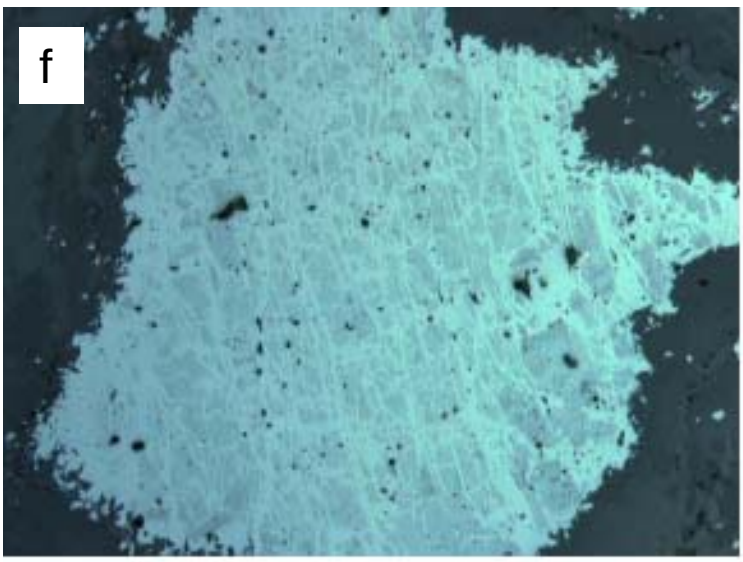

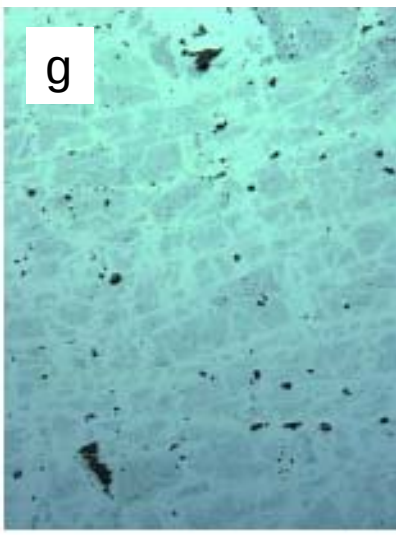

Circle D

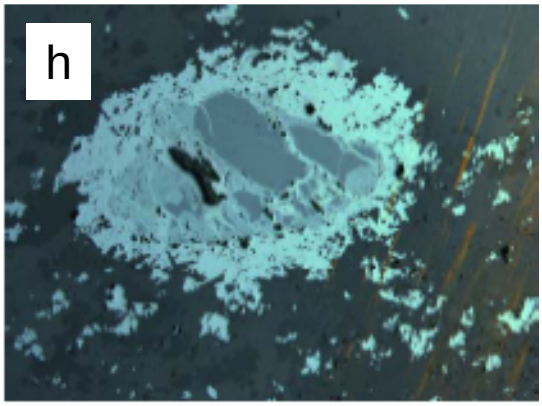

Circle E

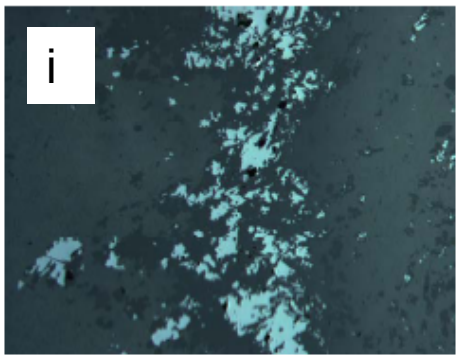

Circle F

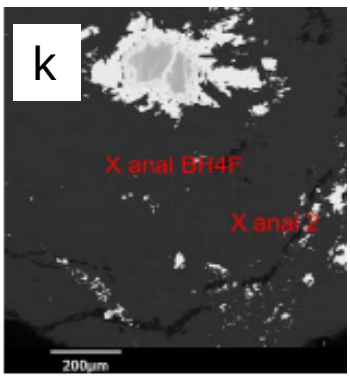

l

1 cm

m

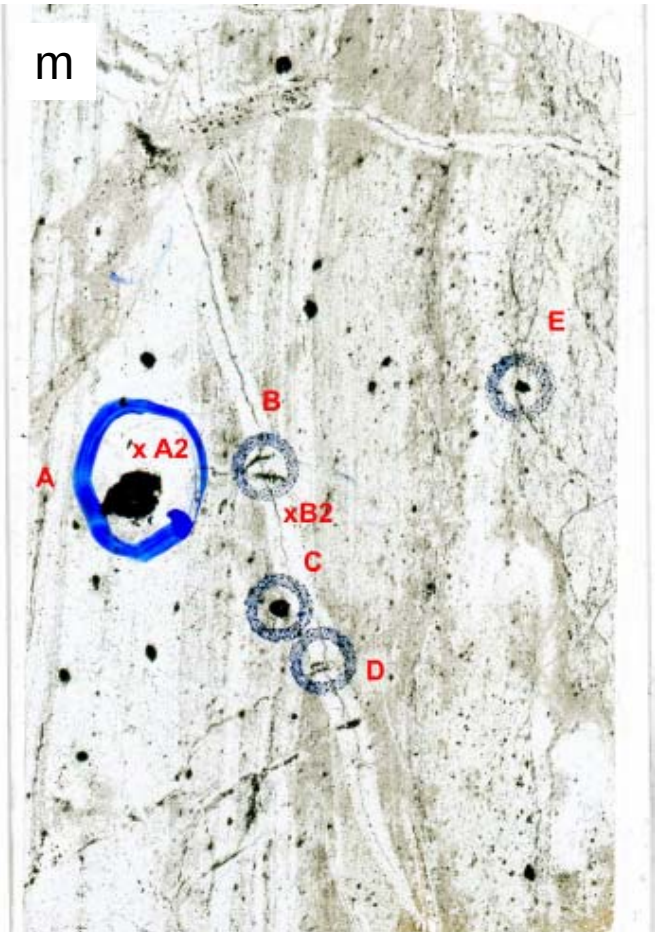

0.5 cm

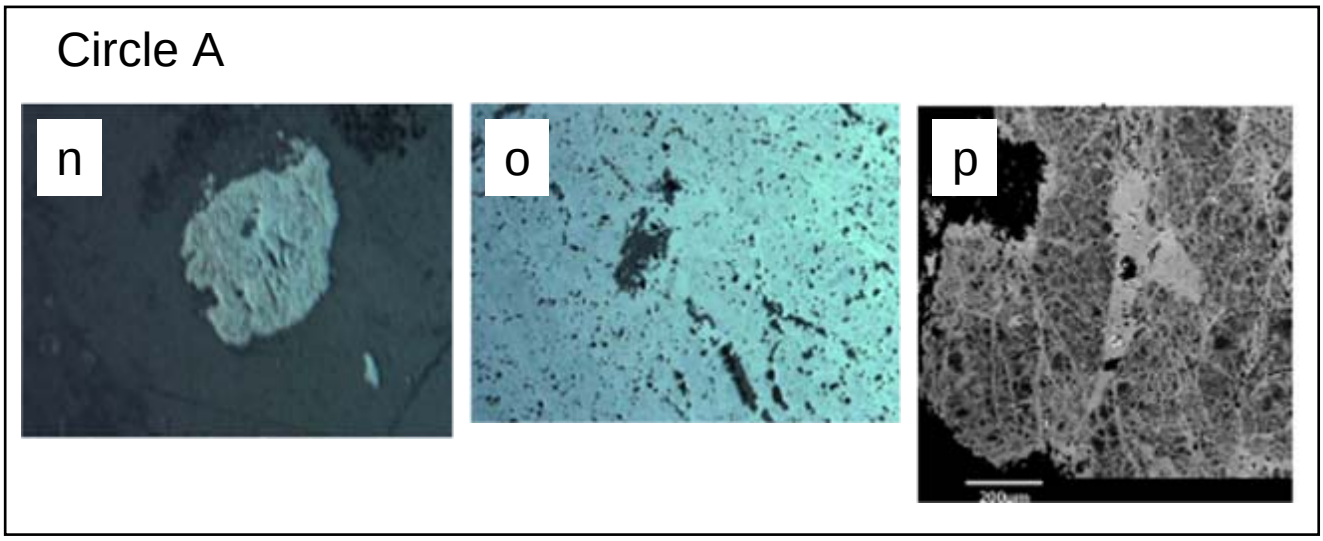

Figure 1.5 Various photos, photomicrographs and Back Scatter Electron (BSE) imagines of sample BH-4 and BH-5 hand samples and thin sections. **a)** Photograph of hand specimen BH-4; **b)** Thin section of BH-4. The major mineral in transparent areas is antigorite, whereas the opaque areas are chromite with magnetite rims; **c)** Photomicrograph of BH-4 circle A. Grey areas majorly contains chromite, and the bright part contains magnetite; **d)** BSE imagine of BH-4 circle A. The dark areas are majorly chromite, where as the bright part is mostly Al-Mg chromite (A1), ferrichromite (high in Cr, low in Mg and Al) (A2), and magnetite (A3); **e)** Photomicrograph of BH-4 circle B. The bright areas are mainly chromite and magnetite, which contains many holes and inclusions, which is serpentine; **f), g)** and **h)** photomicrograph of BH-4 circle C and D. The bright areas are mainly chromite and magnetite; **i), j)** BSE of circle E. Brighter areas majorly contains magnetite, and the bright part contains magnetite. **k)** BSE of circle F. The bright areas are mainly chromite and magnetite; **l)** Photo of hand sample BH-5; **m)** Thin section of BH-5. The major mineral in transparent areas is antigorite, while the opaque areas are chromite with magnetite rims; **n)** Photomicrograph of BH-5 circle A. Grey areas majorly contains Cr-Fe-oxides **o)**, and p) BSE of BH-5 circle A. The dark areas are majorly serpentine; **p)** the dark areas is the remnant of chromite.

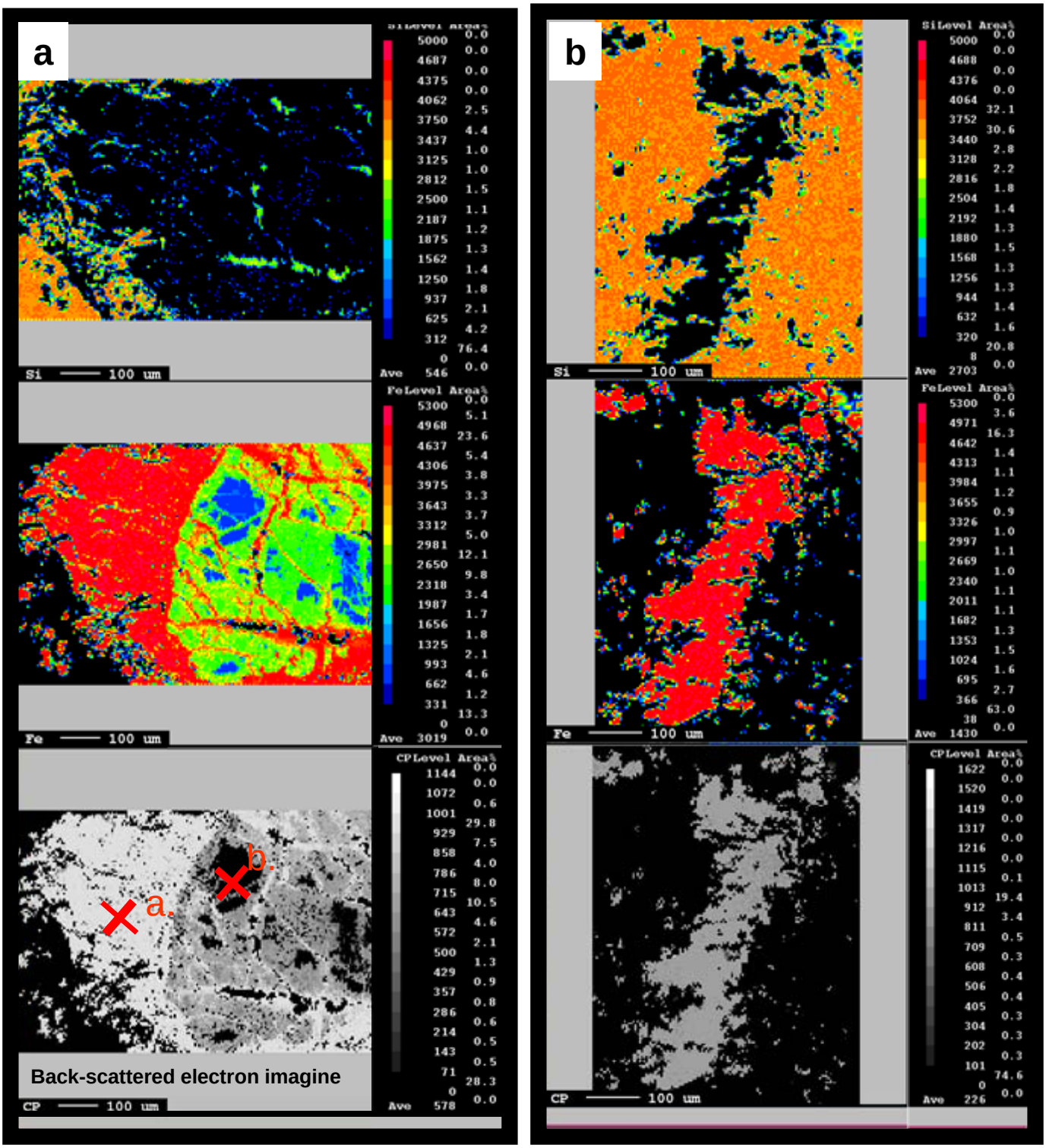
a
b
Si 100 um
Fe 100 um
CP 100 um
a.
b.
Back-scattered electron imagine

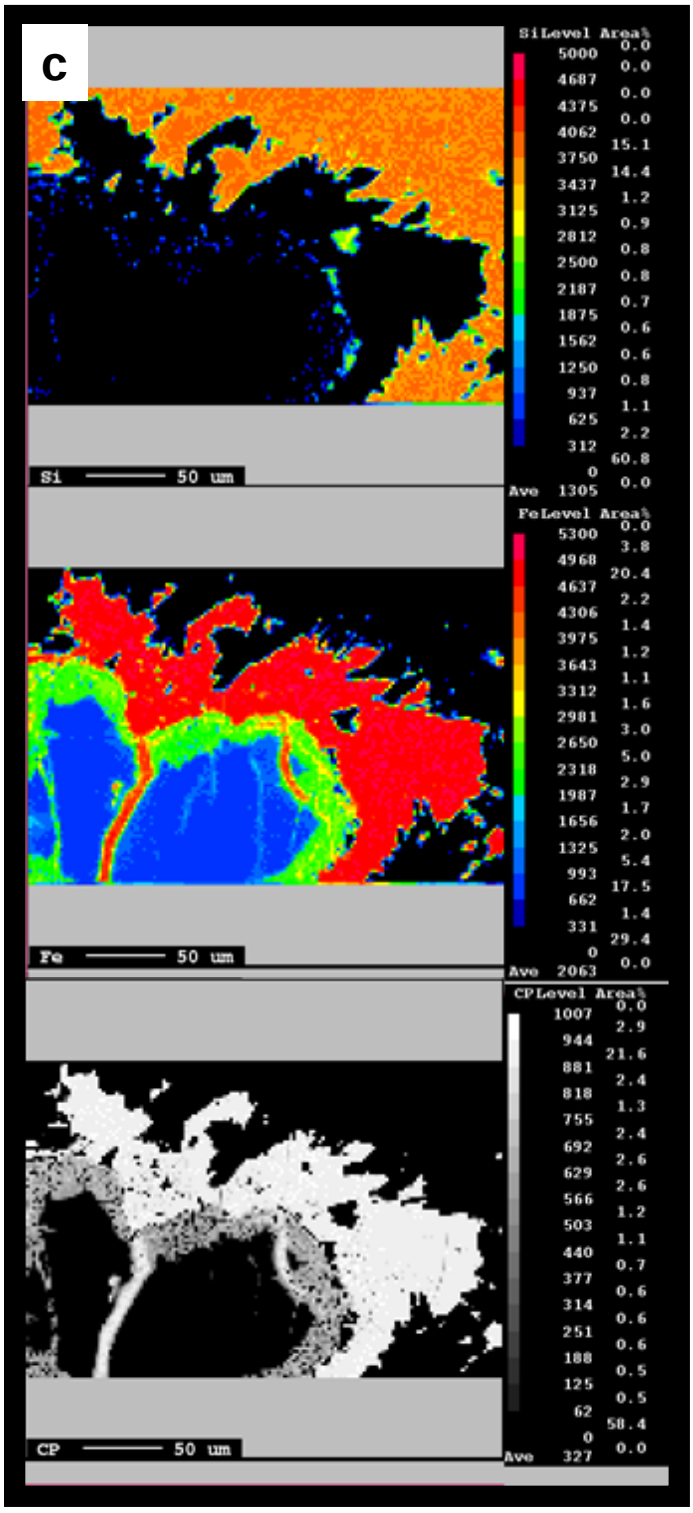
c
SiLevel Area%
5000 0.0
4687 0.0
4375 0.0
4062 0.0
3750 15.1
3437 14.4
3125 1.2
2812 0.9
2500 0.8
2187 0.8
1875 0.7
1562 0.6
1250 0.6
937 0.8
625 1.1
312 2.2
0 60.8
Ave 1305 0.0
Si 50 um
FeLevel Area%
5300 0.0
4968 3.8
4637 20.4
4306 2.2
3975 1.4
3643 1.2
3312 1.1
2981 1.6
2650 3.0
2318 5.0
1987 2.9
1656 1.7
1325 2.0
993 5.4
662 17.5
331 1.4
0 29.4
Ave 2063 0.0
Fe 50 um
CPLevel Area%
1007 0.0
944 2.9
881 21.6
818 2.4
755 1.3
692 2.4
629 2.6
566 2.6
503 1.2
440 1.1
377 0.7
314 0.6
251 0.6
188 0.6
125 0.5
62 0.5
0 58.4
Ave 327 0.0
CP 50 um

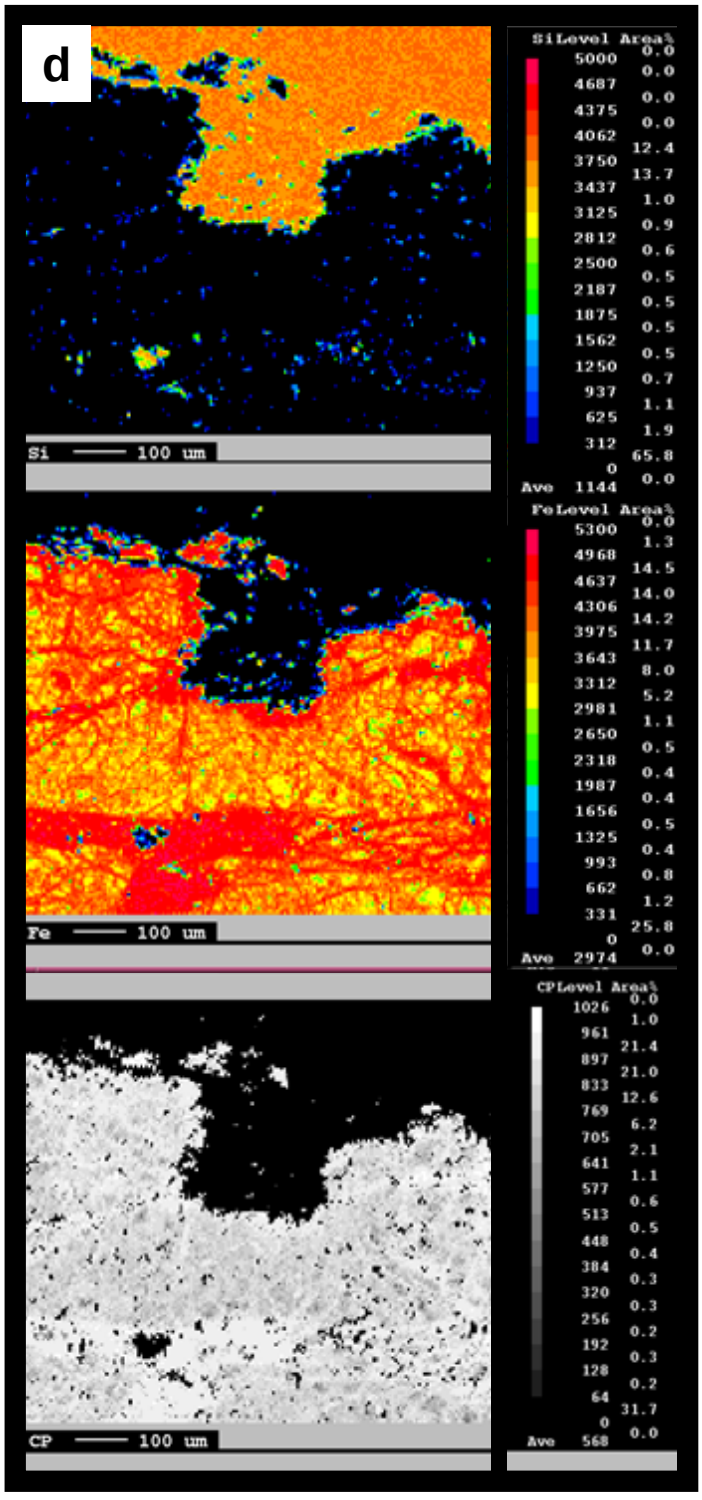
d
SiLevel Area%
5000 0.0
4687 0.0
4375 0.0
4062 0.0
3750 12.4
3437 13.7
3125 1.0
2812 0.9
2500 0.6
2187 0.5
1875 0.5
1562 0.5
1250 0.5
937 0.7
625 1.1
312 1.9
0 65.8
Ave 1144 0.0
Si 100 um
FeLevel Area%
5300 0.0
4968 1.3
4637 14.5
4306 14.0
3975 14.2
3643 11.7
3312 8.0
2981 5.2
2650 1.1
2318 0.5
1987 0.4
1656 0.4
1325 0.5
993 0.4
662 0.8
331 1.2
0 25.8
Ave 2974 0.0
Fe 100 um
CPLevel Area%
1026 0.0
961 1.0
897 21.4
833 21.0
769 12.6
705 6.2
641 2.1
577 1.1
513 0.6
448 0.5
384 0.4
320 0.3
256 0.3
192 0.2
128 0.3
64 0.2
0 31.7
Ave 568 0.0
CP 100 um

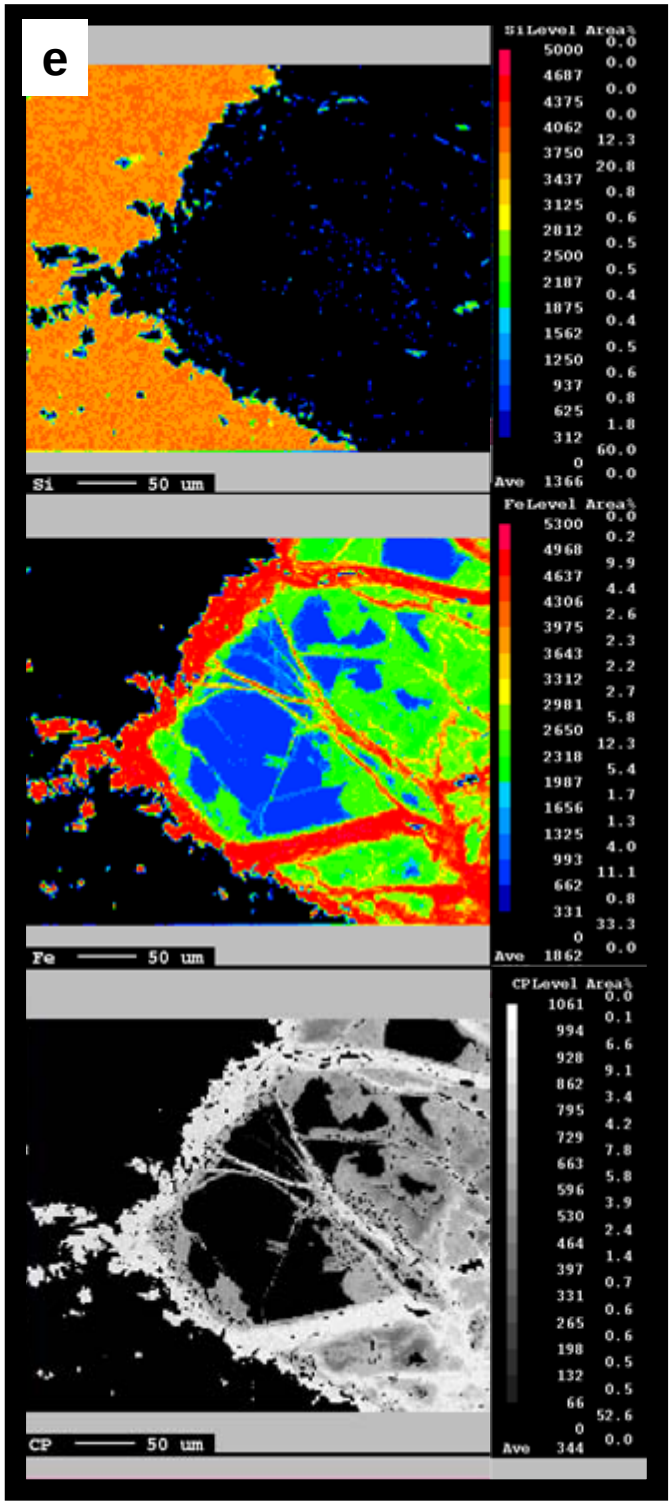

Figure 1.6 X-ray maps of Mg, Ca, Si, P and back scatter electron images collected by Mr. Shibata (Hiroshima University). CP stands for Back-scattered electron image. **a)** image of thin section of sample BH4 at “circle B” in thin section shown in Fig.5 e): the white part (X a.) in CP image is magnetite, determined on the quantitative analysis shown in Table 4. The dark part is chromite (X b.), listed in Table 4; **b)** on BH4 circle E of section shown in Fig. 5 i, j), the entire white area is possibly magnetite, based on the quantitative analysis; **c)** BH-4 circle F in the section of Fig. 5 k) shows in the CP image, the bright part is magnetite, whereas the blue part is chromite. The analyses of these grains are shown in Table 4; **d)** on BH-5 circle A in Fig. 5 n, o, p), the white area is possibly magnetite; **e)** on BH-5 circle E, the white part in CP imagine is likely to be magnetite, based on the quantitative analysis shown in Table 3.

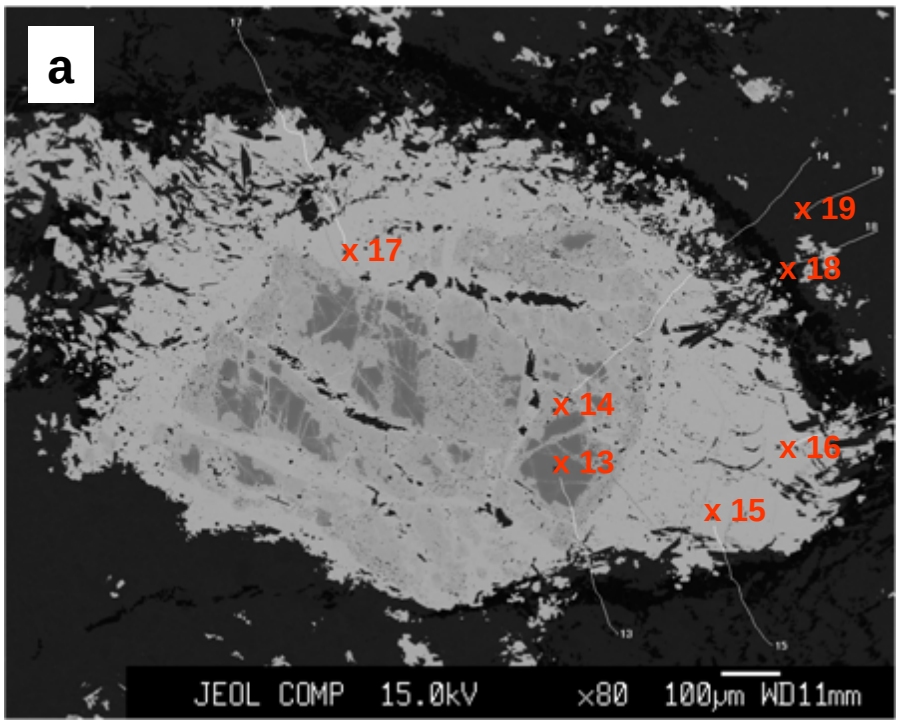
a
x 17
x 19
x 18
x 14
x 13
x 16
x 15
JEOL COMP 15.0kV ×80 100µm WD11mm

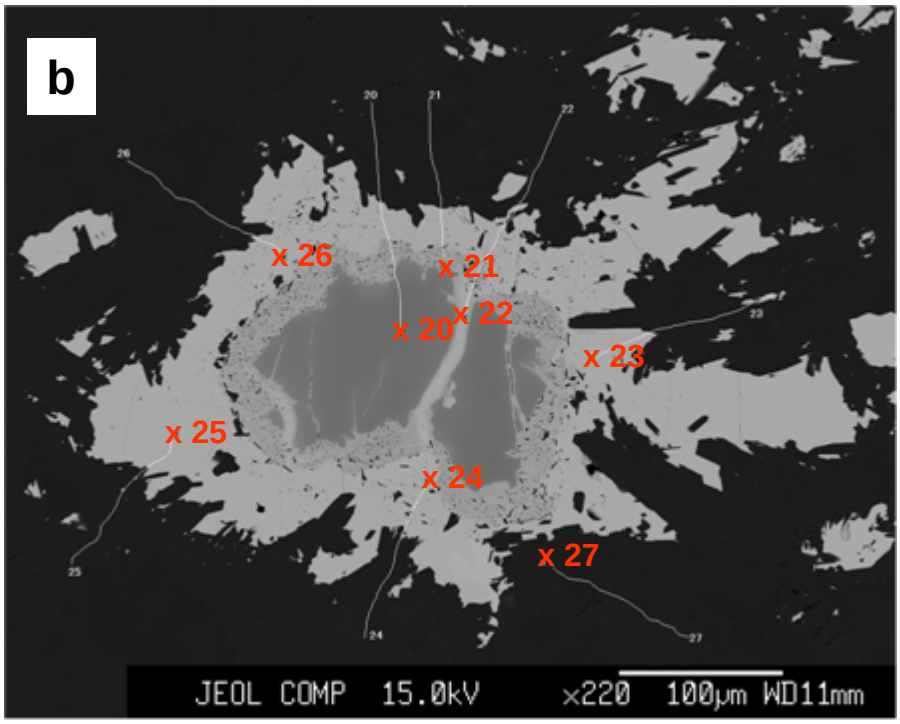
b
x 26
x 21
x 20
x 22
x 23
x 25
x 24
x 27
JEOL COMP 15.0kV ×220 100µm WD11mm

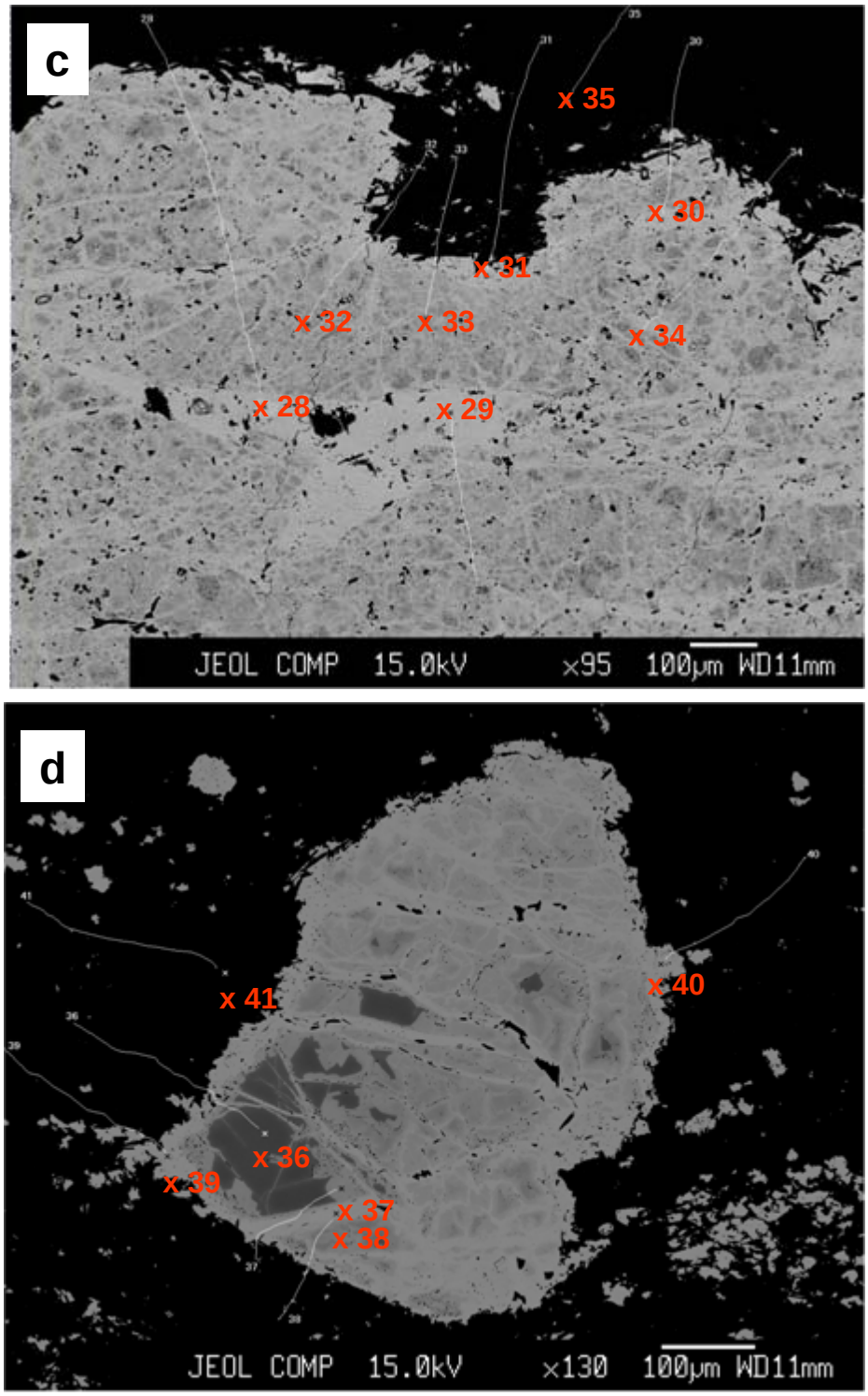

Figure 1.7 Back-scattered electron imagines of thin section of BH-4 and BH-5 using EPMA by Mr. Shibata (Hiroshima University). The numbered "X"'s represent areas where quantitative analyses were done (table 3). The number next to "X" correspond to the number of the scanned spots. **a)** Image on BH-4 circle B shown in Fig. 5 e). The phases of the darkest areas are serpentine (e.g. X19), then chromite (e.g. X13), and bright area are magnetite (e.g. X15);.**b)** Imagine on BH-4 circle F in Fig. 5 k). The major mineral phase of the darkest areas is serpentine (e.g. X27), then chromite (e.g. X20), and brightest areas is magnetite (e.g. X23); **c)** Image of BH-5 circle A in Fig. 5 n, o, p). The mineral phase of the darkest area is serpentine (e.g. X35), and brightest area is magnetite (e.g. X29); **d)** Imagine on BH-5 circle E. The major mineral phase of the darkest areas is serpentine (e.g. X41), then chromite (e.g. X36), and brightest areas is magnetite (e.g. X38).

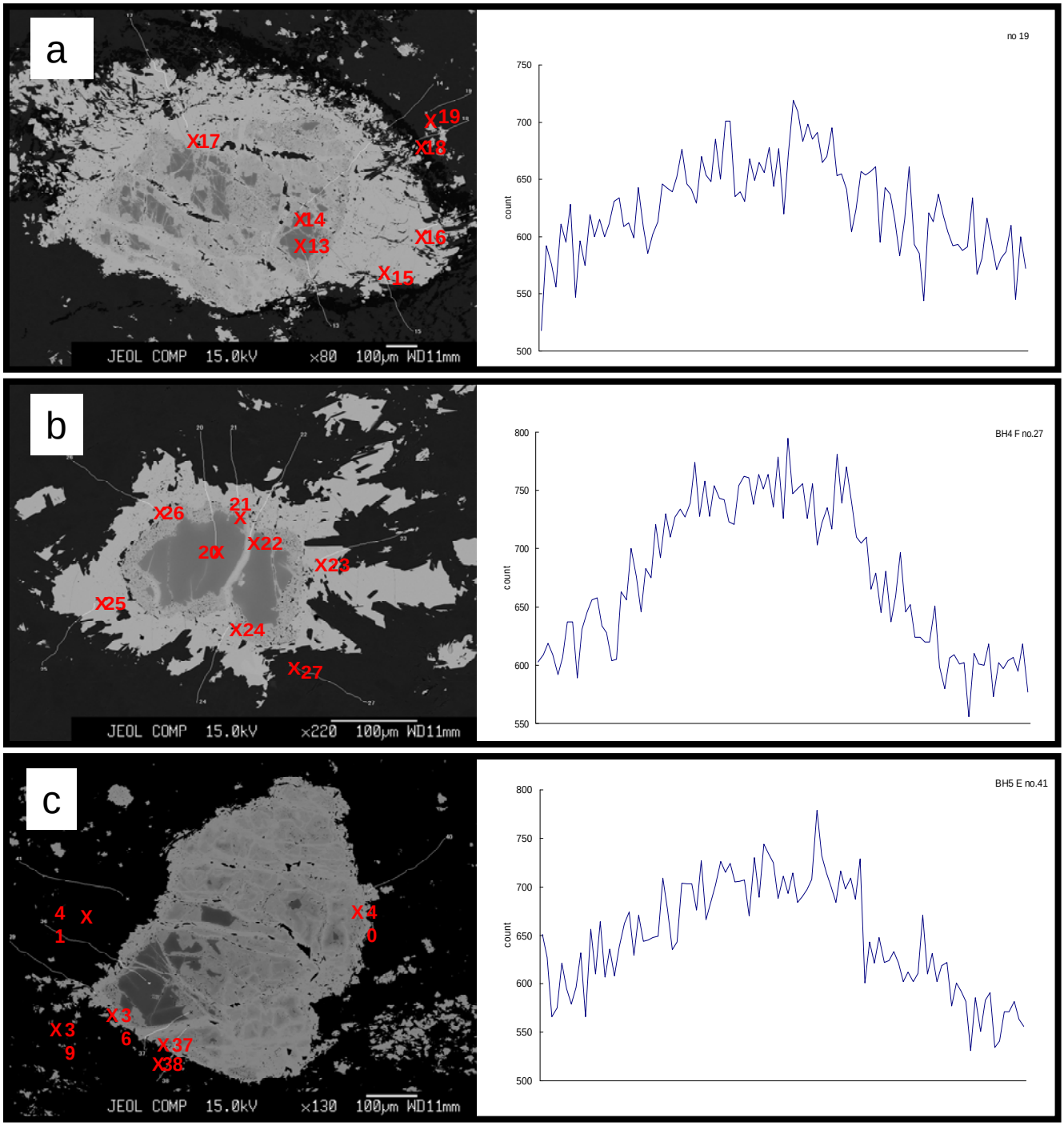

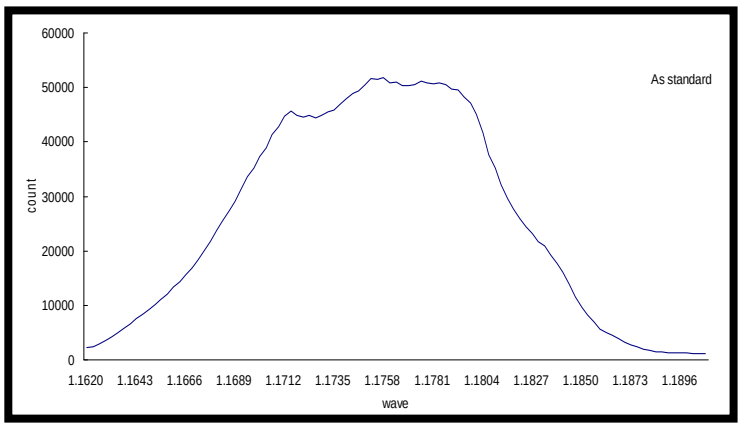

Figure 1.8 EPMA back scattering electron imagine (BSE) of BH-4 and BH-5, and the numbered "X"'s marked the spots for As quantitative analysis on sample thin sections. The plots next to the BSE indicate the presence of As in the samples which is confirmed by the results of As standard (the bottom plot). The X-axis is the wave length of the light intensity and the Y-axis is the count per seconds.

a) BSE imagine of BH-4 circle B in Fig 5 e). Analysis X19 shows X19 contains As since there is increase on counts on the according wave length. **b)** BSE imagine of BH-4 circle F in Fig 5 k). Analysis on circle F, X2 shows that X27 does contain As since there is a clear increase on counts on the according wave length. **c)** BSE imagine of BH-5 circle E. Analysis on X41 shows that X41 does contain As since there is an increase on counts on the according wave length.

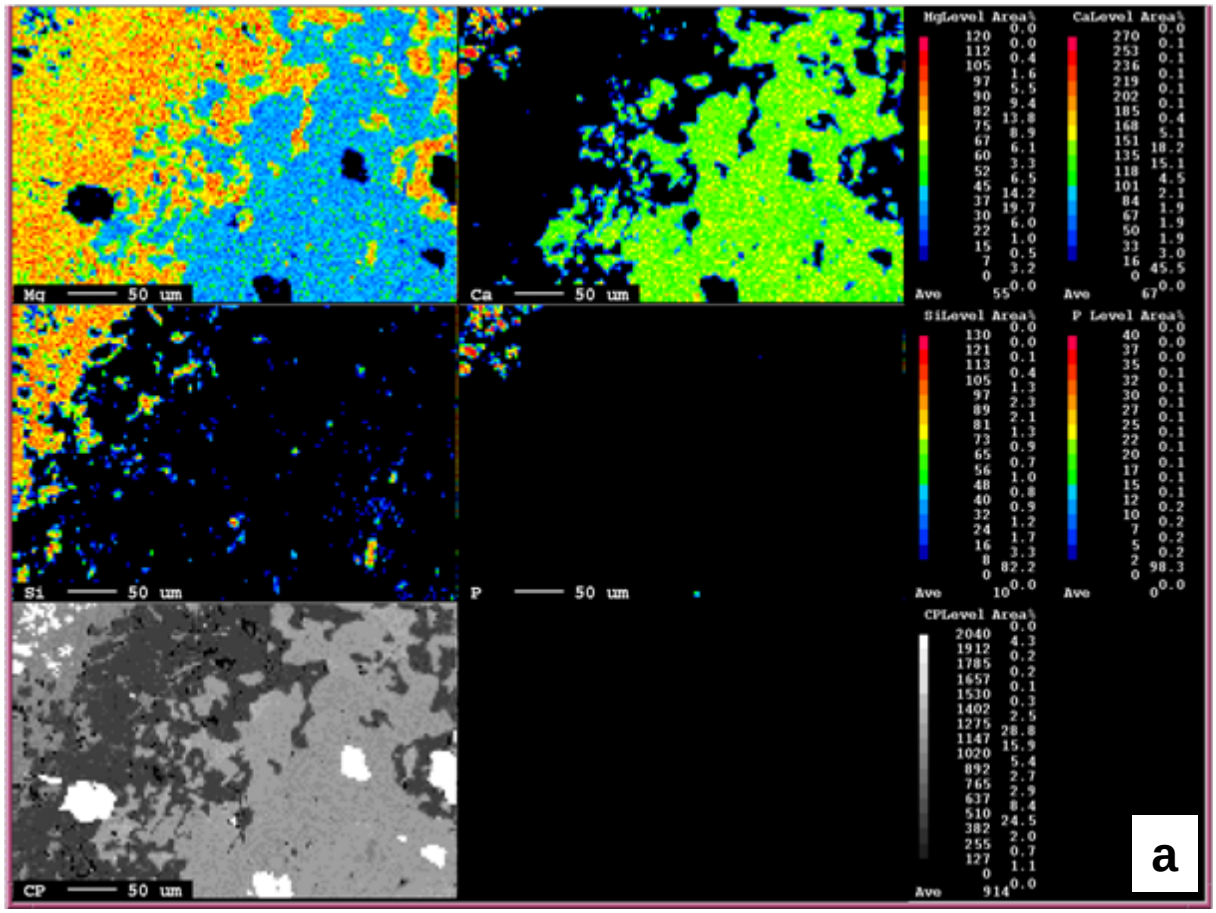
Mg 50 um
Ca 50 um
Si 50 um
P 50 um
CP 50 um
MgLevel Area%
CaLevel Area%
SiLevel Area%
P Level Area%
CPLevel Area%
a

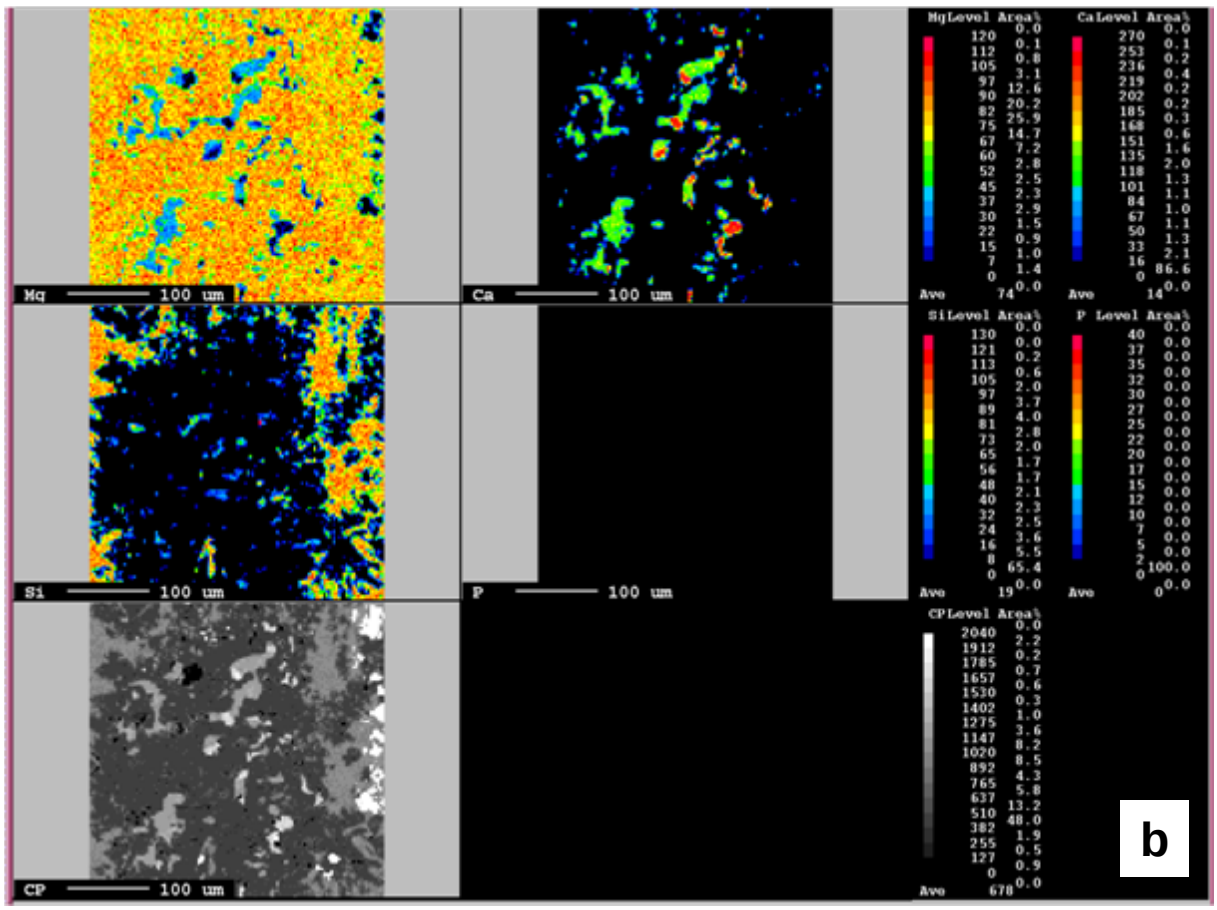
Mg 100 um
Ca 100 um
Si 100 um
P 100 um
CP 100 um
MgLevel Area%
CaLevel Area%
SiLevel Area%
P Level Area%
CPLevel Area%
b

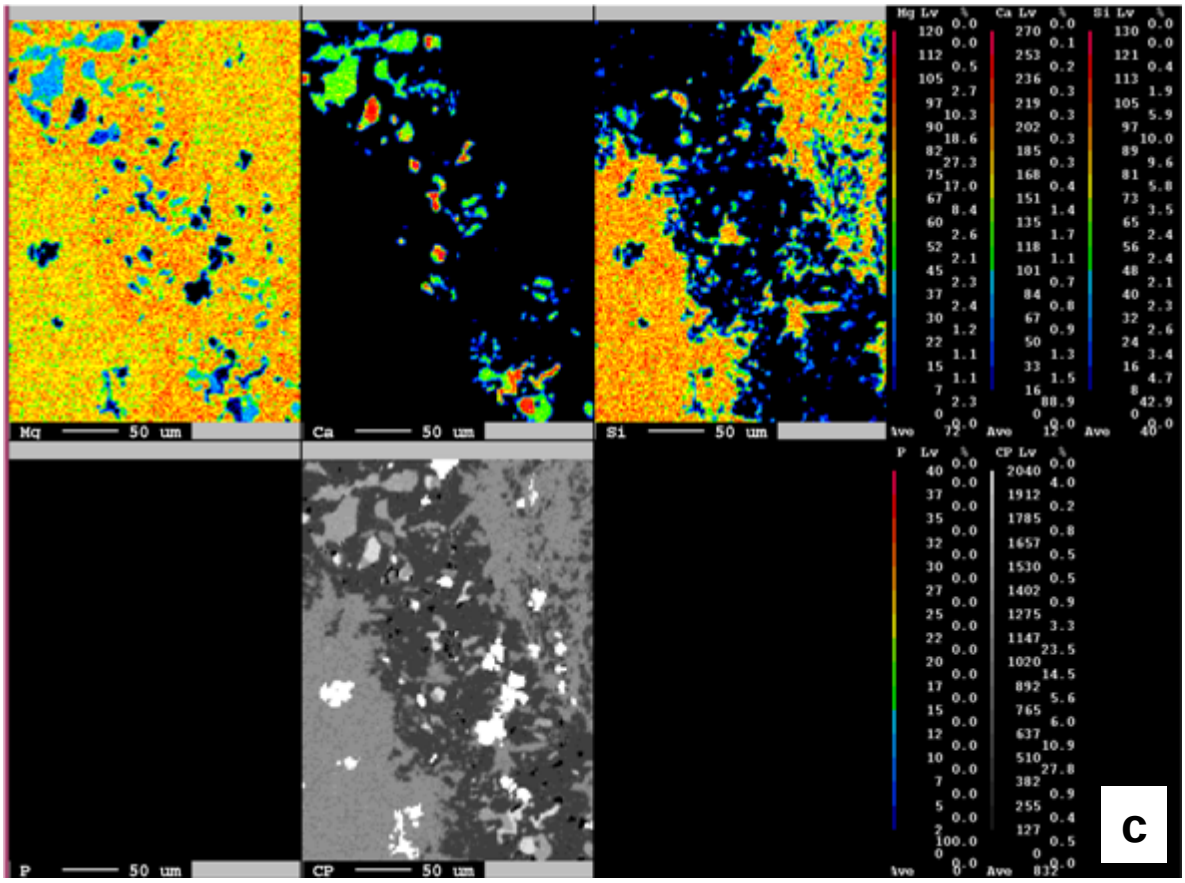
Mg
50 um
Ca
50 um
Si
50 um
P
50 um
CP
50 um
c

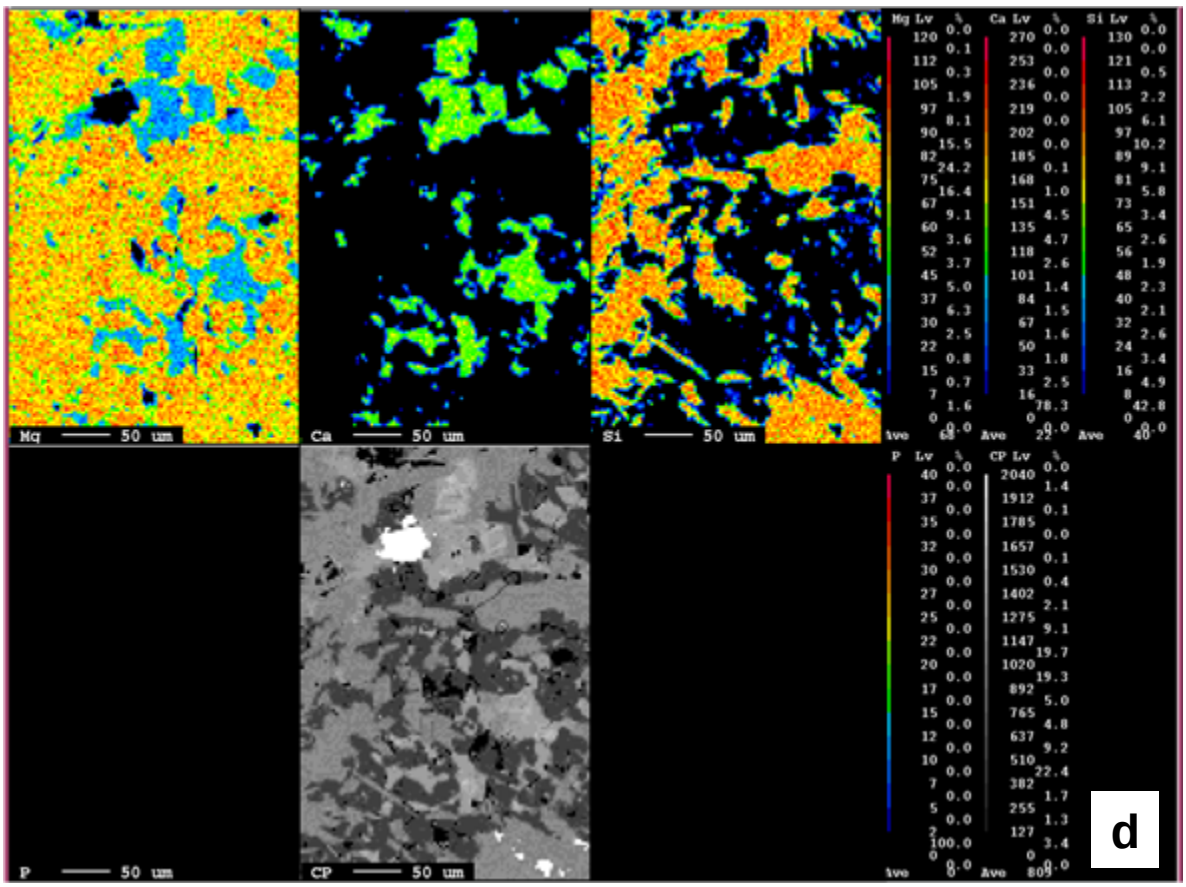
Mg
50 um
Ca
50 um
Si
50 um
P
50 um
CP
50 um
d

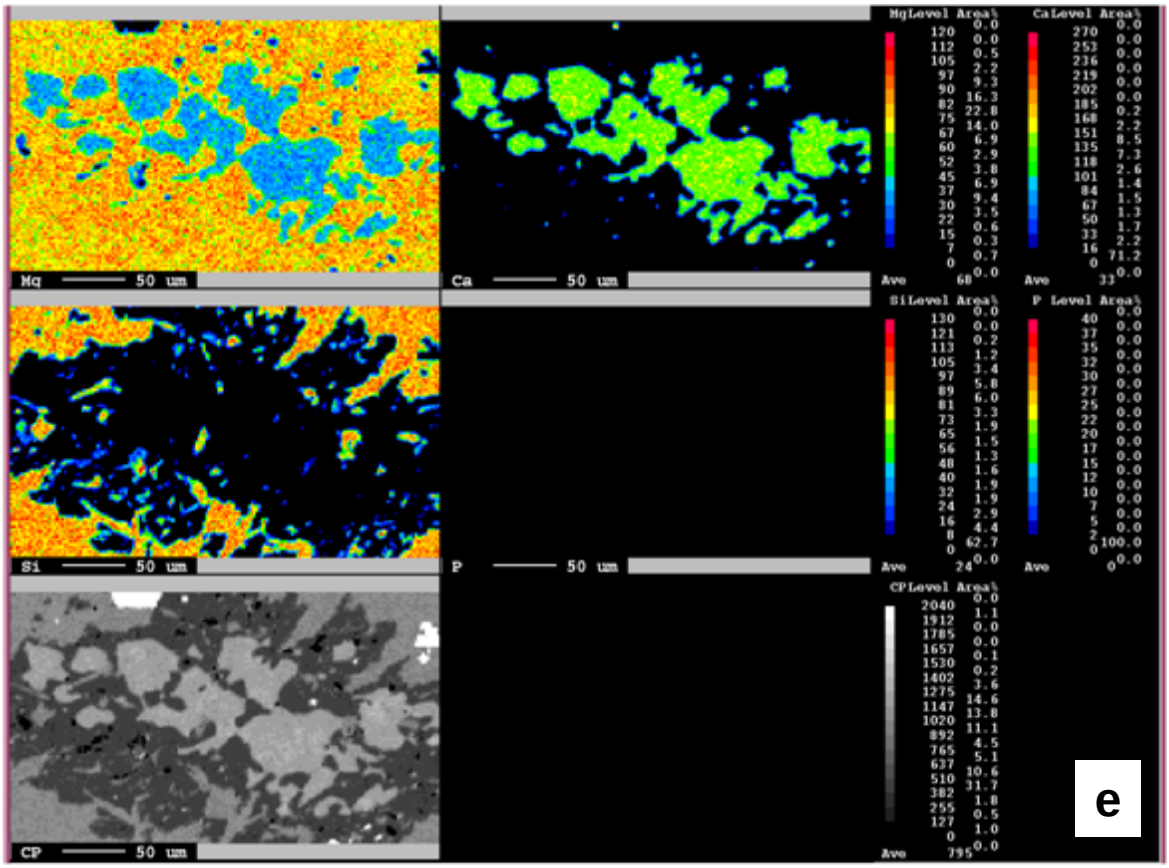

Figure 1.9 EPMA maps of distribution of Mg, Ca, Si, P and a back scattering electron imagine (BSE) on BH-4 and BH-5 on areas that are mainly serpentine (e.g. dark areas on c), d), e) of fig. 5) (conducted by Mr. Chibata, Hiroshima University) . Distribution of Mg is high in all the mapping; level of Ca is high in **a)** and **e)**, low in **b)** and **c)**; **c)** and **d)** are high in Si; all the mappings show very low to undetected P. The distribution of Mg is opposite to Ca, where as Si is distributed in the area ranges of Mg.

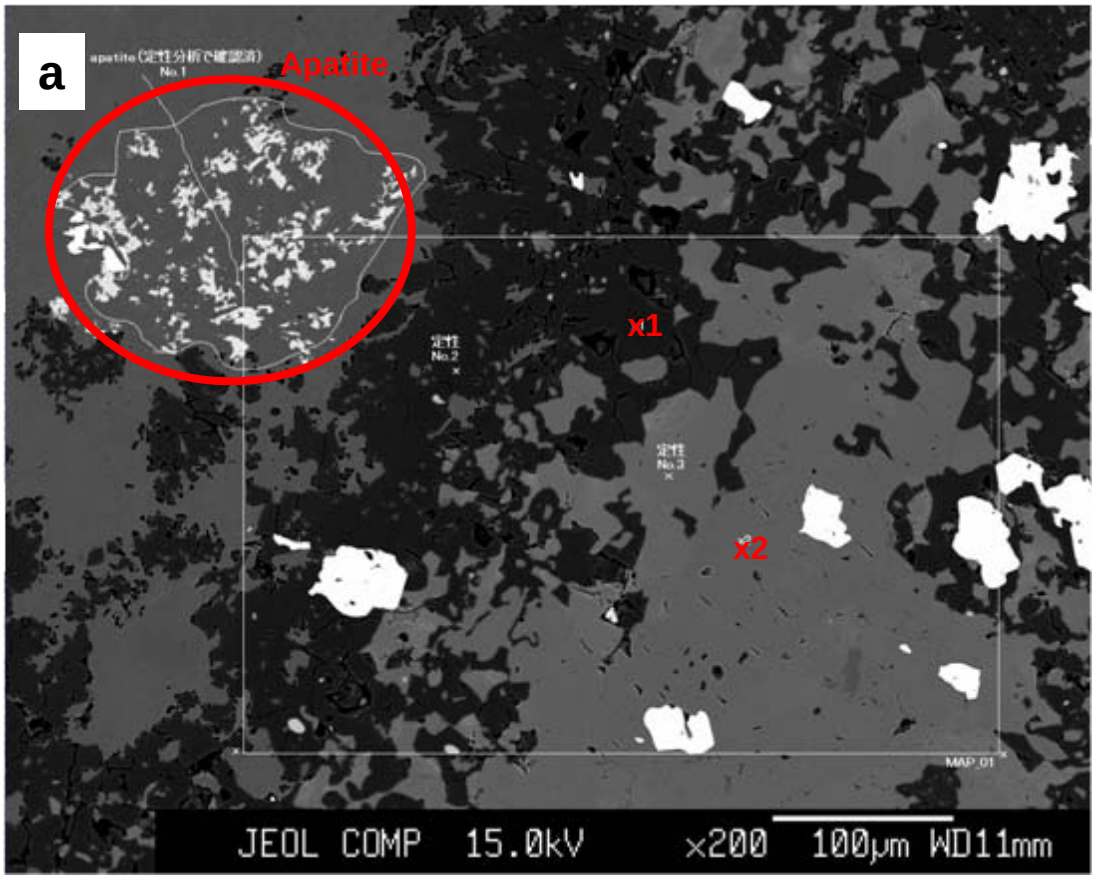
a
Apatite
x1
x2
JEOL COMP 15.0kV ×200 100μm WD11mm

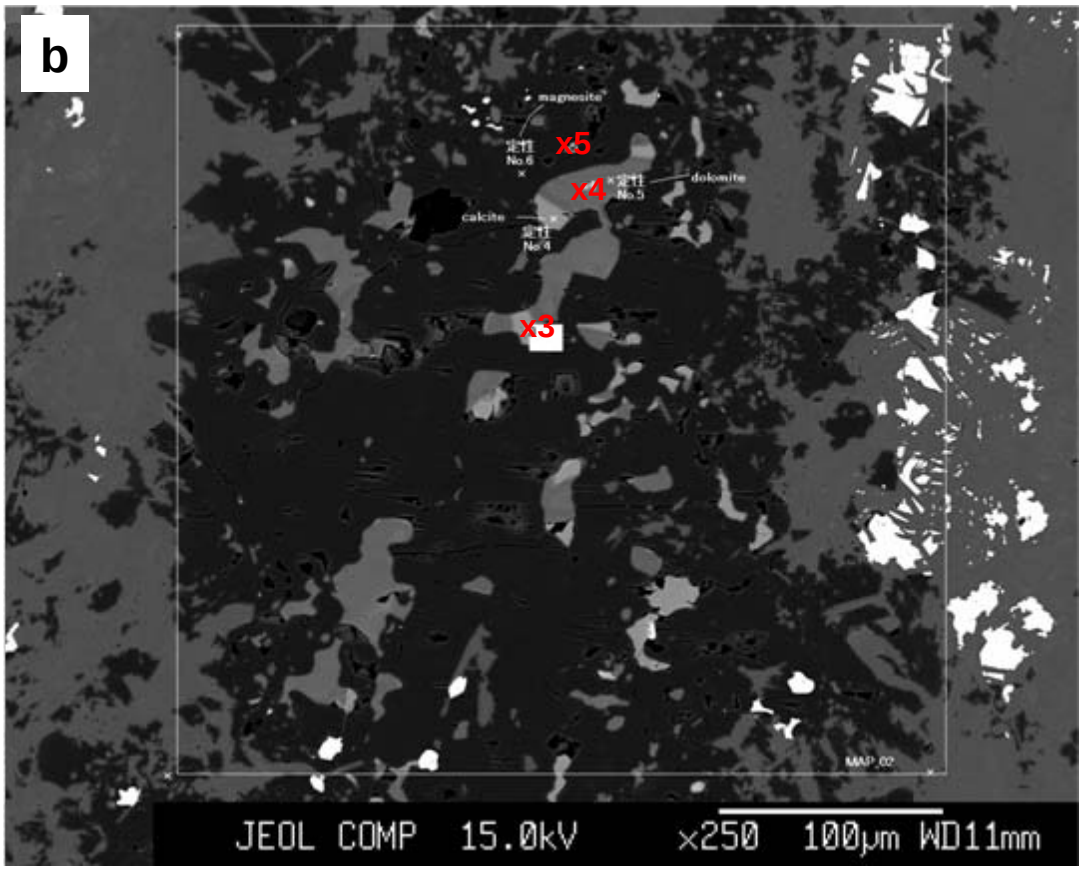
b
magnesite
x5
x4
dolomite
calcite
x3
JEOL COMP 15.0kV ×250 100μm WD11mm

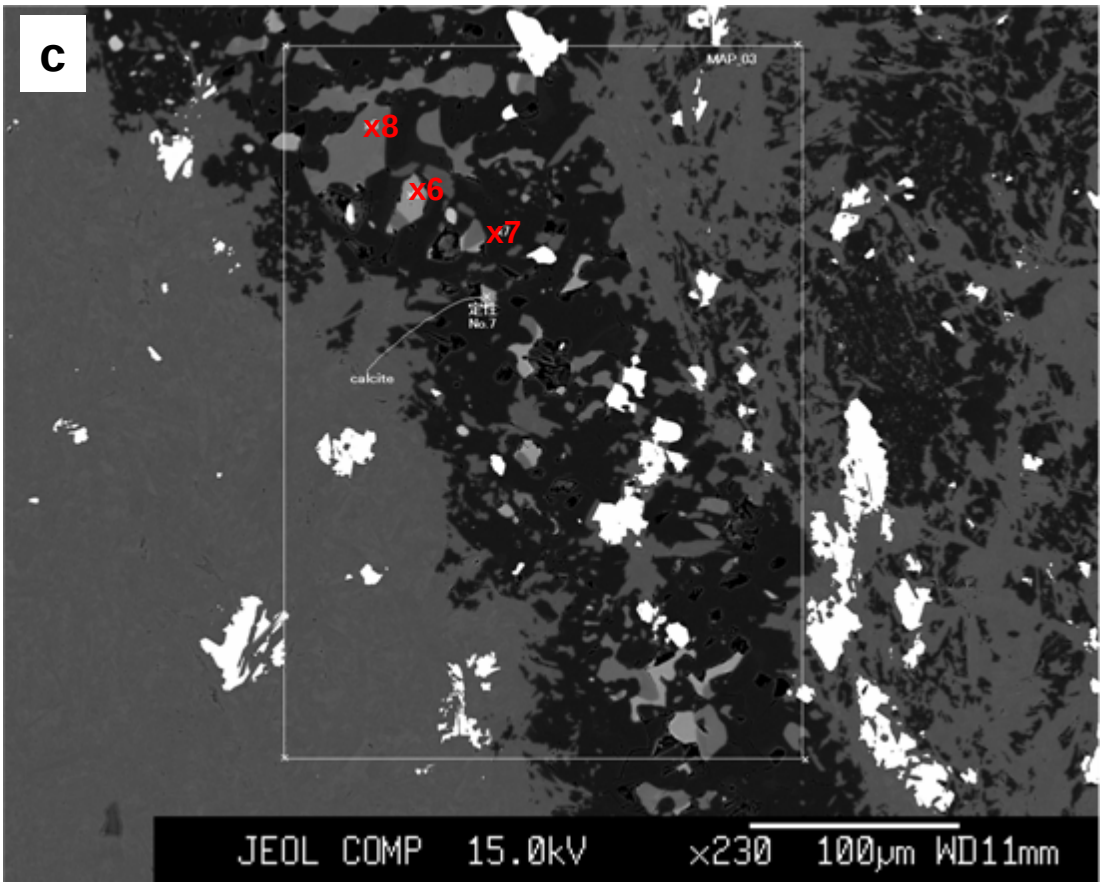
c
MAP 03
x8
x6
x7
No.7
calcite
JEOL COMP 15.0kV ×230 100μm WD11mm

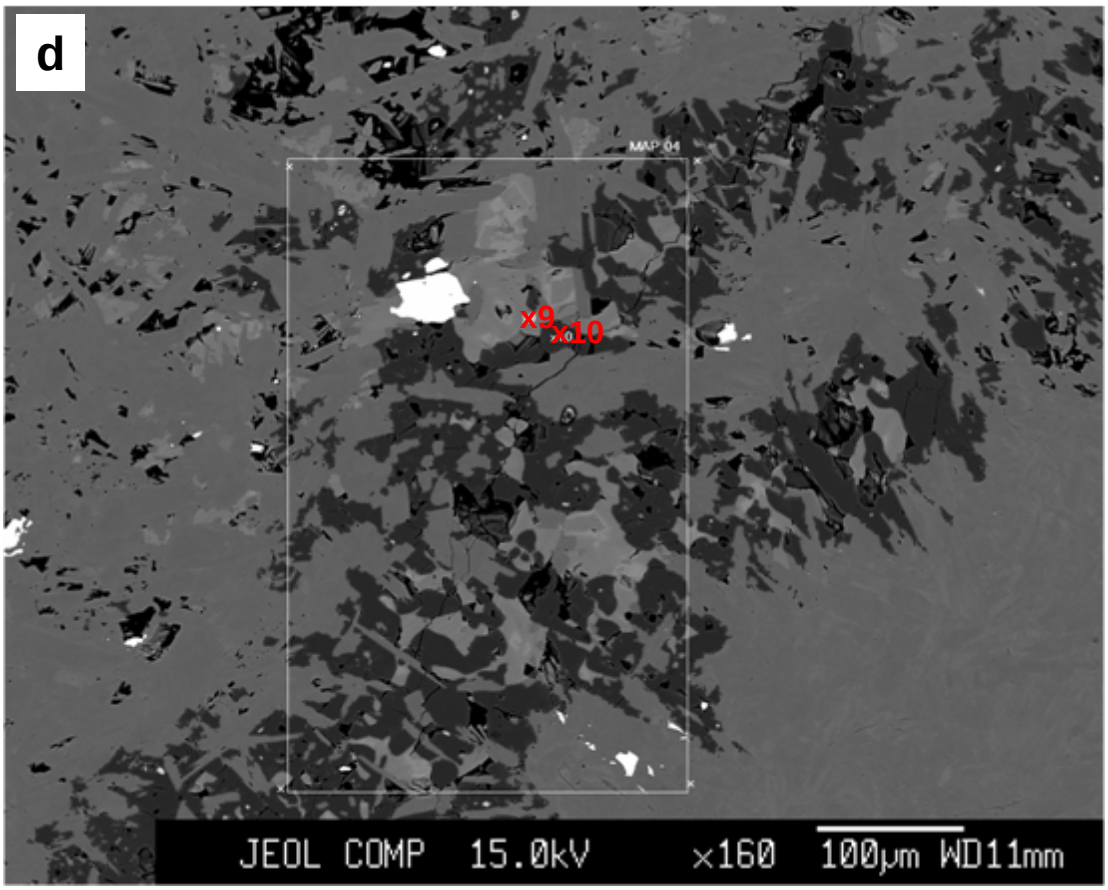
d
MAP 04
x9
x10
JEOL COMP 15.0kV ×160 100μm WD11mm

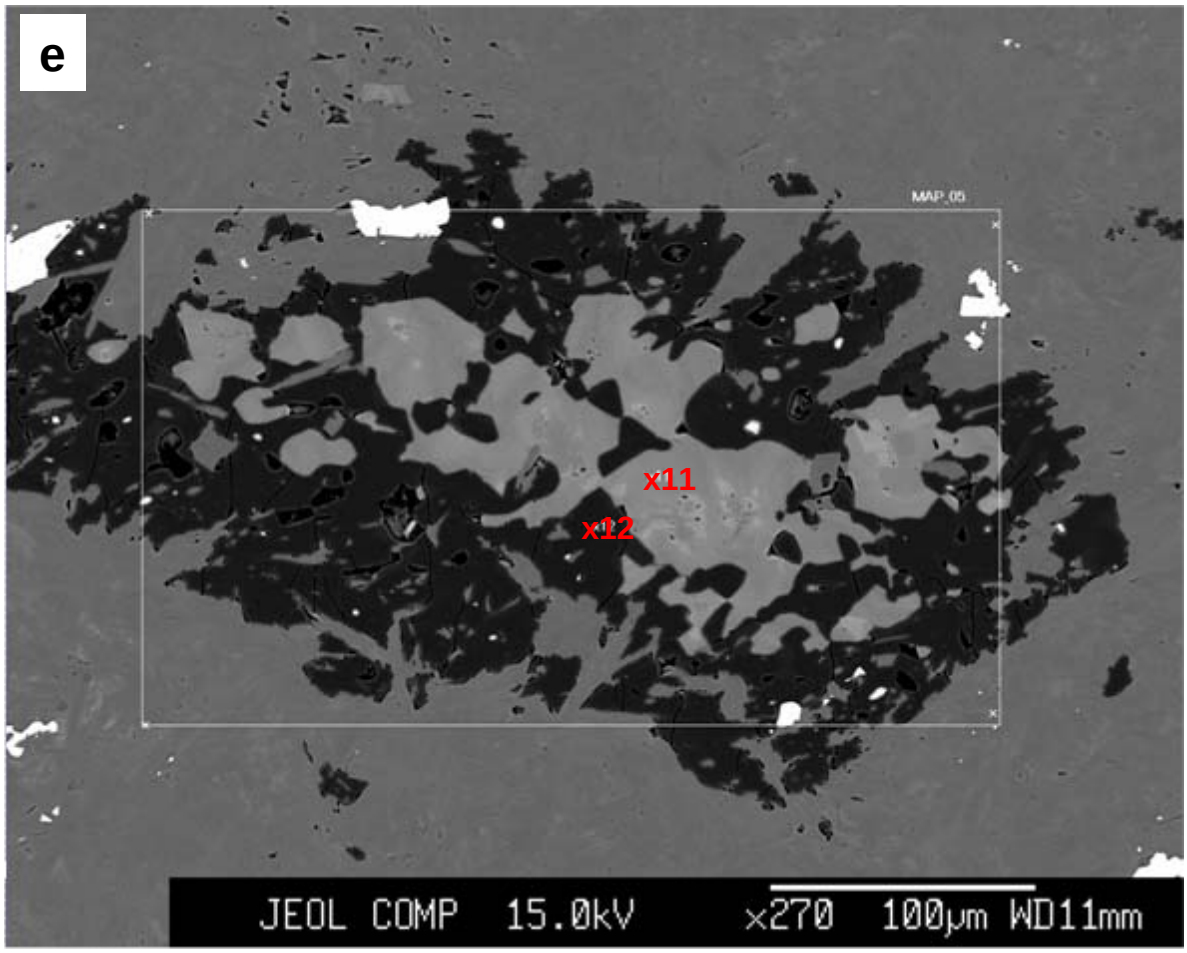

Figure 1.10 BSE images of BH-4 and BH-5 (the squared areas on the images are identical to fig. 9 BSE images). Qualitative and quantitative analysis on carbonate minerals were carried out on numbered “X”’s marked spots (table 4). Apatite was only found in **a)** (on left top bright circled area). Dolomite, magnesit, and calcite all identified

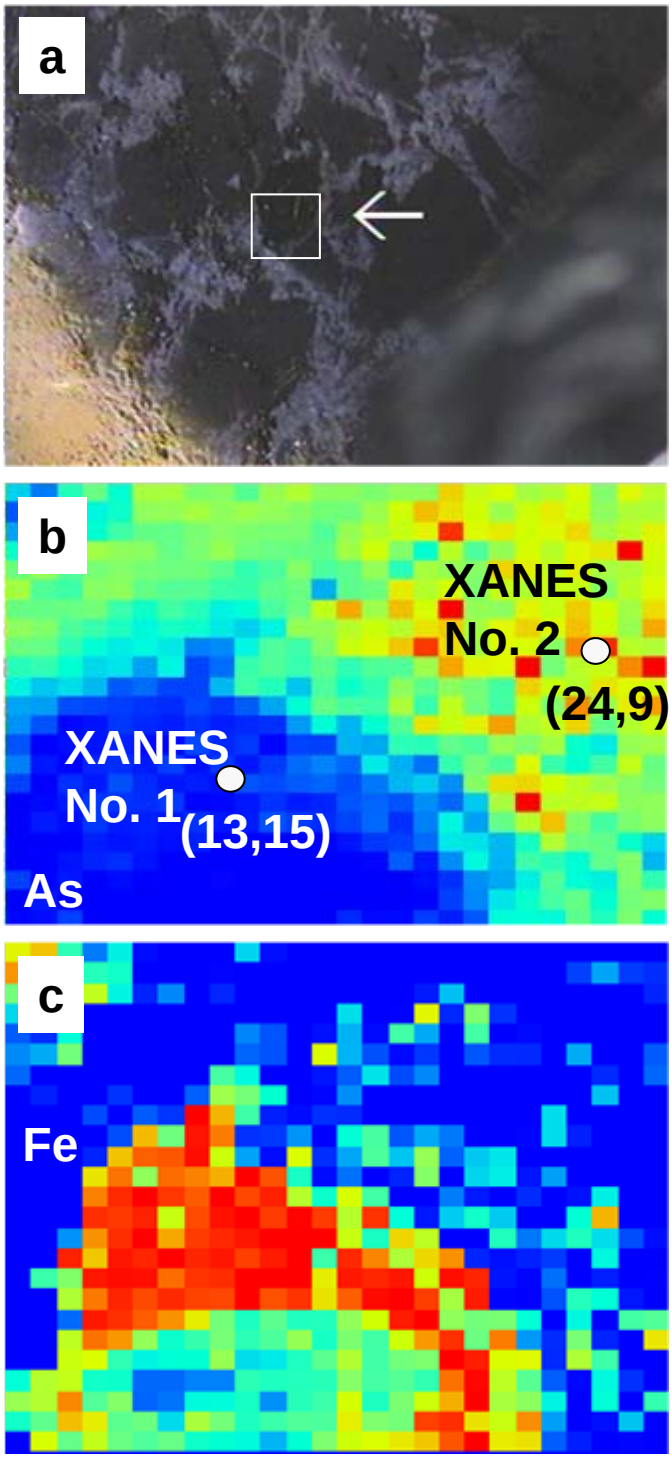
a
b
XANES
No. 2
(24,9)
XANES
No. 1
(13,15)
As
c
Fe

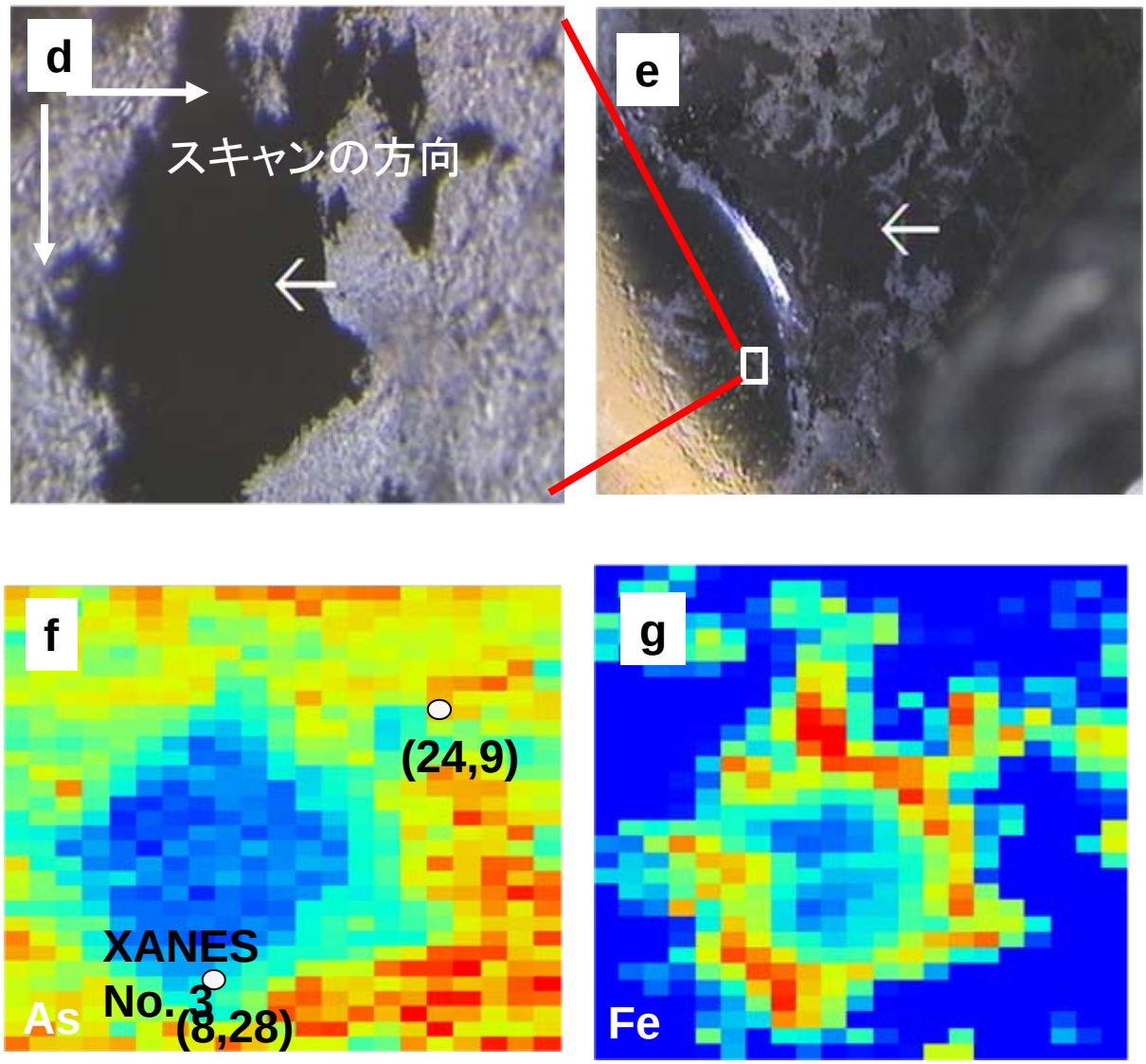

Figure 1.11 Photomicrograph (image **a, d, e**) and X-ray fluorescence (XRF) (image **b, c, e, f**) near the boundary between antigorite and magnetite of sample BH-4 circle B and F in the section shown in Fig. 5 e, k), obtained by Dr. Takahashi (Hiroshima University). **a)** shows the scanned area and the scanning direction（the directions of the arrows. Relative concentrations of As shown on **b), d)** and Fe on **c), e)**. Distributions were presented by the change of color. Red suggests higher concentration where as blue shows the opposites.

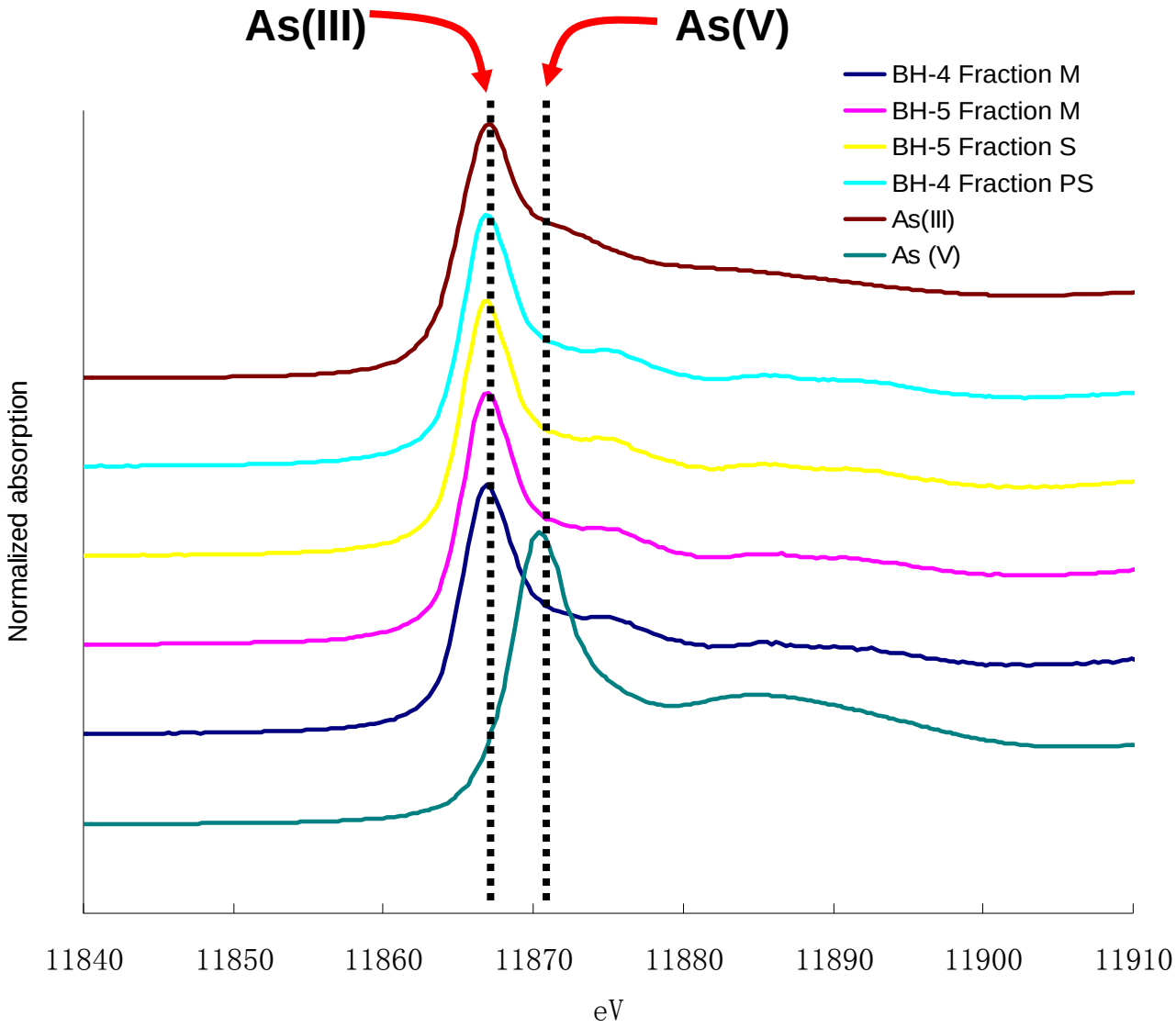

Figure 1.12 XAFS analysis of S fraction of sample BH-4 and BH-5. The valence states of different samples were compared to As(III) ($As^{III}_2O_3$) and As(V) ($As^{V}_2O_5$) solid standards. The vertical line indicated the absorption peak in XANES of As(III). The major As specie presented in the samples is As (III).

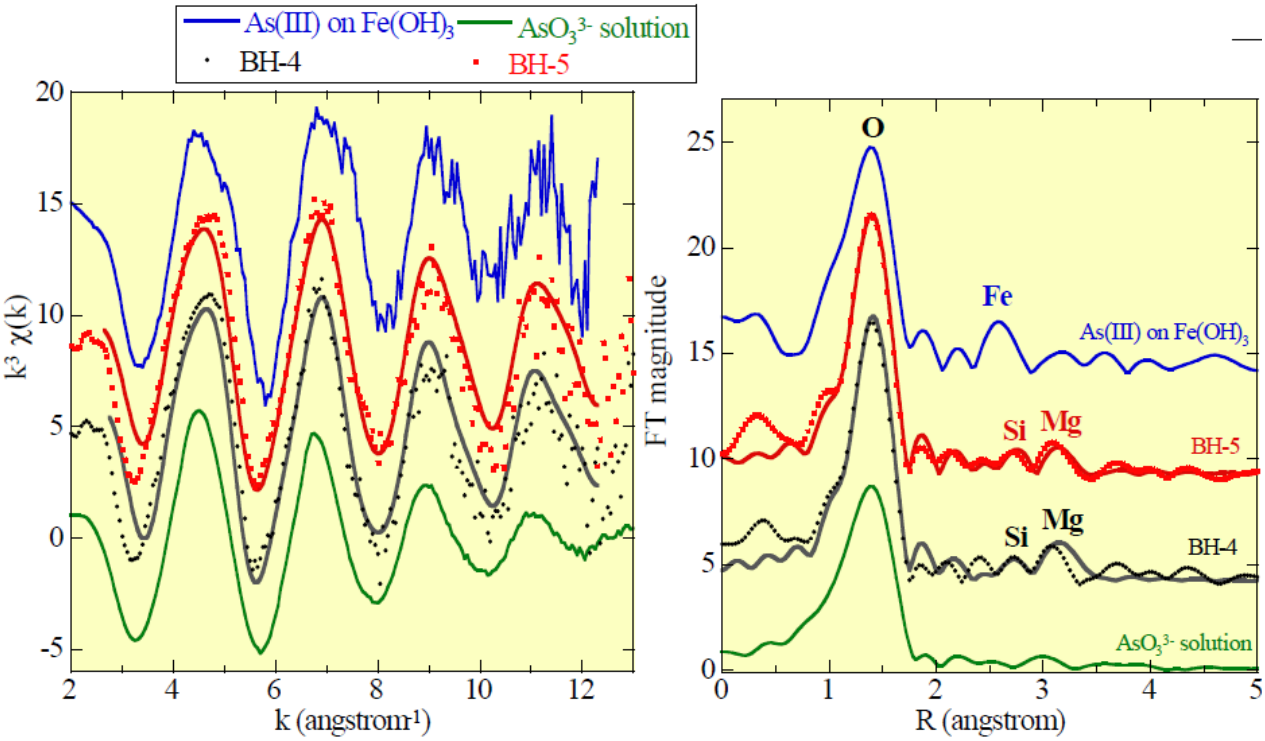

Figure 1.13 EXAFS spectra in k and R spaces for As in S fraction of sample BH-4 and BH-5, As(III) ($NaAs^{III}O_2$) solution, and As(III) adsorbed on $Fe(OH)_3$. Simulation results using FEFF parameters were also shown for BH-4 and BH-5.

Table 1.1 Intensity ratio of peaks of powder X-ray diffraction (XRD) that are above 10 % of the highest peak produced in fraction S and PS of BH4 and BH5 samples. The peak ratios are in parentheses.

	Fraction S		Fraction SP	
	S-BH4	S-BH5	SP-BH4	SP-BH5
d value * (I/Io)	7.22 (1.00) 3.68 (0.71) 2.64(0.62), 2.30(0.13), 1.79(0.12)	7.18(1.00), 2.51(0.97), 3.61(0.76), 3.60(0.75), 2.16(0.24), 1.48(0.23), 1.55(0.18), 4.58(0.16), 2.95(0.15)	7.20(1.00), 3.61(0.74), 2.51(0.19), 2.73(0.16)	7.19(1.00), 3.60(0.67), 2.51(0.32)

Table 1.2 Comparison of powder X-ray Diffraction (XRD) relative intensities (I/Io) of referenced database of possible minerals and relative intensities (I/Io) of Fraction S and SP of BH4 and BH5.

			Sample			
			Fraction S		Fraction PS	
	mineral	* I/Io	BH4	BH5	BH4	H5
Serpentine	antigorite	2.53(1)	P	P	P	P
$Mg_3Si_2O_5(OH)_4$		7.29(1)	P	P	P	P
		3.61(0.8)	P	P	P	P
	Lizardite	7.12(1)	N	N	N	N
		2.379(0.9)				
		3.56(0.8)				
	Chrysotile	7.32(1)	N	N	N	N
		3.65(0.7)				
		4.57(0.5)				
Tale		9.35(1)	N	N	N	N
$Mg_3Si_4O_{10}(OH)_2$		1.53(0.55)				
		4.59(0.45)				
Chromite		2.52(1)	N	N	N	N
$Fe^{2+}Cr_2O_4$		1.46(0.9)				
		1.6(0.9)				
Magnetite		2.53(1)	N	P	N	N
$Fe^{3+}{}_2Fe^{2+}O_4$		1.483(0.85)		P		
		1.614(0.85)		N		
Carbonate	Magnesite*	2.742(1)	<0.1	<0.1	N	N
	$Mg(CO_3)$	2.102(0.45)	N	<0.1	<0.1	<0.1
		1.7(0.35)	N	N	N	N
	Dolomite	2.883(1)	N	N	N	N
	$CaMg(CO_3)_2$	1.785(0.6)				
		2.191(0.5)				
	Calcite	3.035(1)	N	N	N	N
	$CaCO_3$	2.095(0.18)				
		2.285(0.18)				

*I/Io represents an intensity ratio of the according peak to the highest peak.
(http://webmineral.com).
P = the presence of according mineral;
N= the according mineral is not detected;
<0.1 = the according mineral's peak is detected however its ration is lower than 10 % of the highest peak of intensity racial,

Table 1.3.1 representative Cr-spinel and magnetite composition from EPMA quantitative analysis results on BH-4 and BH-5 thin sections.

	Sample	BH-4					BH-4							BH-5				BH-5				
	Circle	B					F							A				E				
	No.*	13	14	15	16	17	20	21	22	23	24	25	26	28	29	30	31	36	37	38	39	40
SiO2		b.d.	b.d.	b.d.	0.01	0.04	0.01	0.06	0.16	0.04	0.10	b.d.	0.10	b.d.	b.d.	b.d.	0.04	b.d.	b.d.	b.d.	0.06	0.14
FeO		17.85	48.70	90.31	90.38	90.32	17.84	46.26	81.47	90.24	88.93	90.31	89.41	90.16	89.74	89.55	90.72	17.76	48.70	90.44	88.90	87.02
MgO		13.55	2.23	0.31	0.26	0.34	12.82	1.54	0.47	0.23	0.41	0.23	0.33	b.d.	0.42	0.32	0.19	13.29	1.68	0.20	0.21	0.27
NiO		0.08	0.71	2.00	2.07	1.78	0.08	0.69	2.07	1.83	1.85	1.79	1.89	1.31	1.21	1.70	1.40	0.06	0.71	1.62	1.74	1.92
Al2O3		25.81	3.19	0.01	0.00	0.01	22.93	1.03	0.20	b.d.	0.09	0.02	0.01	b.d.	b.d.	0.01	b.d.	23.08	1.64	0.04	b.d.	0.02
Cr2O3		41.25	36.33	0.01	0.00	0.24	43.64	38.35	10.10	1.39	1.97	0.21	1.16	1.94	1.57	2.25	0.49	44.14	37.52	1.99	2.31	2.66
TiO2		0.12	b.d.	0.01	0.01	b.d.	0.12	0.14	0.04	0.07	b.d.	0.05	b.d.	b.d.	b.d.	0.02	b.d.	0.01	0.07	0.04	0.01	0.03
MnO		0.71	5.05	0.10	0.09	0.08	1.62	6.72	0.71	0.16	0.16	0.07	0.13	b.d.	b.d.	0.08	0.05	0.96	5.63	0.13	0.18	0.16
	SUM	99.36	96.21	92.75	92.82	92.81	99.07	94.79	95.22	93.97	93.51	92.68	93.03	93.40	92.94	93.92	92.89	99.30	95.95	94.46	93.40	92.22
O = 32																						
Si		0.010	0.012	b.d.	0.003	0.013	0.003	0.017	0.047	0.013	0.030	0.000	0.032	0.000	b.d.	b.d.	0.012	b.d.	b.d.	b.d.	0.017	0.042
Ti		0.022	0.017	0.002	0.002	b.d.	0.023	0.032	0.008	0.015	0.000	0.011	0.000	0.011	0.000	0.003	b.d.	0.002	0.015	0.010	0.002	0.007
Al		7.376	1.106	0.004	0.001	0.002	6.679	0.371	0.073	0.001	0.032	0.007	0.003	0.005	b.d.	0.002	b.d.	6.685	0.578	0.016	b.d.	0.008
Cr		7.909	8.461	0.003	b.d.	0.060	8.527	9.221	2.410	0.336	0.478	0.052	0.281	0.467	0.383	0.543	0.121	8.579	8.876	0.478	0.562	0.654
Fe(iii)		0.651	6.375	15.990	15.988	15.913	0.743	6.310	13.407	15.606	15.430	15.920	15.652	15.505	15.616	15.449	15.856	0.732	6.516	15.487	15.400	15.239
Fe(ii)		2.968	5.619	7.338	7.348	7.394	2.944	5.453	7.159	7.432	7.345	7.437	7.378	7.521	7.496	7.419	7.564	2.918	5.668	7.491	7.447	7.402
Mn		0.146	1.261	0.026	0.023	0.020	0.340	1.730	0.182	0.042	0.042	0.019	0.035	0.009	0.013	0.021	0.013	0.200	1.425	0.033	0.046	0.043
Mg		4.900	0.981	0.140	0.121	0.157	4.725	0.697	0.211	0.106	0.187	0.108	0.152	0.161	0.192	0.146	0.086	4.871	0.750	0.091	0.096	0.123
Ni		0.016	0.168	0.497	0.514	0.442	0.017	0.169	0.504	0.449	0.456	0.445	0.468	0.321	0.299	0.418	0.348	0.012	0.171	0.395	0.431	0.481
Cr#		0.517	0.884			0.970	0.561	0.961	0.971	0.998	0.938	0.888	0.991	0.990	1.000	0.997	1.000	0.562	0.939	0.968	1.000	0.987
Y (Fe3+)		0.041	0.400	1.000	1.000	0.996	0.047	0.397	0.844	0.979	0.968	0.996	0.982	0.970	0.976	0.966	0.992	0.046	0.408	0.969	0.965	0.958
XMg		0.623	0.149	0.019	0.016	0.021	0.616	0.113	0.029	0.014	0.025	0.014	0.020	0.021	0.025	0.019	0.011	0.625	0.117	0.012	0.013	0.016

Cr# : Cr/(Cr+Al);

XMg: Mg/(Mg+Fe2+);

YFe3+: Fe3+/(Cl+Al+Fe3+);

b.d. : under detection limit

CaO and K2O were determined but concentrations were at or below the detection limits.

* The No. of the analyzed spots are shown in figer 7;

No. 13-17 of analysis points correspond to Fig. 7a.;No. 20-26 of analysis points correspond to Fig. 7b.;No. 28-31 of analysis points correspond to Fig. 7c.;No. 36-40 of analysis points correspond to Fig.7 d.

Table 1.3.2 Representative perpentine composition from EPMA quantitative analysis results on BH-4 and BH-5 thin sections.

		BH-4	BH-4	BH-5	BH-5	BH-4				BH4			BH-5							BH5	
	circle	B	F	A	E	F							E								
	No.	19	27	35	41	42	43	44	47	48	49	50	51	52	53	54	55	56	57	58	59
SiO2		42.69	42.54	42.26	42.27	42.63	42.49	42.17	43.06	42.58	42.24	42.37	43.17	42.47	42.62	42.54	42.34	42.09	42.03	42.88	42.76
TiO2		0.03	0.01	0.02	b.d.	0.01	0.03	0.03	0.02	0.02	0.06	0.03	b.d.	0.03	0.02	b.d.	0.02	b.d.	b.d.	0.02	b.d.
Al2O3		0.55	0.64	0.84	0.63	0.63	0.57	0.71	0.76	0.77	0.64	0.58	0.49	0.59	0.64	0.89	0.61	0.84	0.95	0.72	0.76
Cr2O3		0.01	0.12	0.17	0.20	0.06	0.07	0.07	0.07	b.d.	b.d.	0.01	0.02	0.12	0.16	0.30	0.14	0.28	0.39	0.12	0.08
FeO		1.95	1.84	1.65	2.07	2.05	1.74	1.55	1.79	1.86	1.85	1.83	1.41	2.03	2.01	1.60	1.68	1.76	2.02	1.66	1.75
MnO		0.04	0.08	0.06	0.04	0.06	0.06	0.06	0.05	0.06	0.04	0.04	0.06	0.06	0.05	0.05	0.05	0.06	0.06	0.05	0.02
MgO		40.99	40.61	41.02	40.98	41.29	41.22	41.22	41.40	41.16	40.83	41.27	41.70	40.91	41.33	41.05	41.33	40.74	40.89	41.42	41.26
NiO		0.21	0.20	0.14	0.18	0.23	0.22	0.17	0.21	0.17	0.15	0.16	0.14	0.21	0.20	0.11	0.20	0.19	0.19	0.15	0.14
	sum=	86.49	86.07	86.16	86.37	86.97	86.40	85.99	87.36	86.62	85.82	86.28	87.00	86.43	87.04	86.55	86.38	85.95	86.54	87.03	86.78
	O = 7																				
Si		2.001	2.002	1.986	1.987	1.990	1.993	1.986	1.996	1.992	1.994	1.990	2.005	1.994	1.988	1.989	1.987	1.986	1.974	1.994	1.995
Ti		0.001	0.000	0.001	b.d.	0.000	0.001	0.001	0.001	0.001	0.002	0.001	b.d.	0.001	0.001	b.d.	0.001	b.d.	b.d.	0.001	b.d.
Al		0.030	0.036	0.047	0.035	0.035	0.031	0.039	0.042	0.042	0.036	0.032	0.027	0.033	0.035	0.049	0.034	0.047	0.053	0.040	0.042
Cr3+		0.000	0.004	0.006	0.007	0.002	0.002	0.003	0.003	b.d.	b.d.	0.000	0.001	0.005	0.006	0.011	0.005	0.010	0.014	0.004	0.003
Fe+2		0.077	0.072	0.065	0.081	0.080	0.068	0.061	0.070	0.073	0.073	0.072	0.055	0.080	0.078	0.062	0.066	0.069	0.079	0.065	0.068
Mn		0.002	0.003	0.002	0.002	0.002	0.002	0.003	0.002	0.002	0.001	0.001	0.002	0.002	0.002	0.002	0.002	0.002	0.002	0.002	0.001
Mg		2.864	2.850	2.874	2.872	2.873	2.882	2.893	2.861	2.870	2.874	2.890	2.887	2.863	2.873	2.862	2.891	2.865	2.863	2.872	2.869
Ni2+		0.008	0.007	0.005	0.007	0.009	0.008	0.006	0.008	0.006	0.006	0.006	0.005	0.008	0.007	0.004	0.008	0.007	0.007	0.005	0.005
	sum=	4.983	4.978	4.986	4.992	4.991	4.989	4.992	4.981	4.987	4.986	4.993	4.982	4.986	4.991	4.981	4.993	4.986	4.993	4.983	4.983

b.d. : under detection limit

K2O CaO and N2O were determined but concentrations were at or below the detection limits.

* some of the No. of the analyzed spots are shown in figer 7

No.19 of analysis points correspond to Fig. 7a.;No.27 of analysis points correspond to Fig. 7b.;No. 35 of analysis points correspond to Fig. 7c.;No. 41 of analysis points correspond to Fig.7 d.

Table 1.4 EPMA quantitative analysis results on BH-4 and BH-5 thin sections of carbonate minerals.

No. of scan point*	MgO	CaO	FeO	MnO	Total	Comment*
1	46.18	0.22	0.33	0.39	47.12	Magnetite
2	20.96	29.60	0.06	0.11	50.73	Dolomite
3	3.85	51.56	0.11	0.06	55.58	Calcite
4	21.82	28.95	0.08	0.87	51.72	Dolomite
5	46.33	0.15	0.36	0.39	47.23	Magnesite
6	3.79	51.72	0.11	0.06	55.68	Calcite
7	46.97	0.06	0.44	0.36	47.83	Magnesite
8	21.26	29.05	0.28	0.43	51.02	Dolomite
9	21.53	29.88	0.11	0.27	51.79	Dolomite
10	46.17	0.18	0.37	0.61	47.33	Magnesite
11	21.05	29.45	0.02	0.50	51.02	Dolomite
12	45.93	0.25	0.35	0.45	46.98	Magnesite

* The numbers of the scanned points marked as “x” are coordinating with Fig 10; No.1, 2 of analysis points correspond to Fig. 10 a.; No.3- 5 of analysis points correspond to Fig. 10 b.; No. 6, 7, 8 of analysis points correspond to Fig. 10 c.; No. 9, 10 of analysis points correspond to Fig. 10 d. No.11, 12 of analysis points correspond to Fig10 e.

Table 1.5 ICP-AES and ICP-MS data of SP fraction of sample BH-4 and BH-5. ICP-AES data of Ca, Mg, Al, Ai Mn and in phosphoric acid.

		BH4	BH5	Blank	RF*
ICP-AES	[Ca] (ppm)	1490	0	0	
NaH2PO4.H2O (1M)	[Mg] (ppm)	4.58wt%	4.70wt%	0	
	[Al] (ppm)	133	469	0	
	[Si] (ppm)	1.34wt %	2.27wt%	0	
	[Mn] (ppm)	574	441	0	
	[Fe] (ppm)	368	1400	0	
ICP-MS	[As] (ppm)	77.7	123	0	18
NaH2PO4.H2O (1M)		108	135	0	
HF/HNO3 concentrated (1:3)	[As] (ppm)	357	756	0	33

*RF= reference material (Jsd-2，Geological survey of Japan)

Table 1.6 EXAFS parameters for BH-4 and BH-5 shows the coordination number (CN), distances of As-O shells, with peaks well fitted by assuming Si and Mg using FEFF parameters, and As-Si, and As-Mg distances.

	Shell	R (Å)[1]	CN[2]	DW (Å)[3]	Δ E(eV)[4]
	As-O	1.78 +/- 0.009*	4.0 +/- 0.5	0.070 +/- 0.016	
BH-4	As-Si	3.204 +/- 0.070*	0.6 +/- 0.1	0.075	8.9 +/- 2.0
	As-Mg	3.491 +/- 0.31	1.9 +/- 0.9	0.075	
	As-O	1.775 +/- 0.009	3.9 +/- 05	0.069+/- 0.016	
BH-5	As-Si	3.188 +/- 0.062	0.7 +/- 0.6	0.075	8.0 +/- 2.0
	As-Mg	3.484 +/- 0.032	1.8 +/- 0.9	0.075	

[1] R (Å): interatomic distance

[2] CN: Coordination number

[3] DW (Å): Debye-Waller factors

[4] Δ E(eV): adsorption energy

*Error estimates of the fitted parameters in bond distance and coordination number were <0.02 Å and <20%, respectively.

Appendix A

The Effect of pH variation on the diffusion coefficient of inorganic and organic arsenic species in water

Sakamistu, M., Niu, L., Hattori, K., and Takahashi, Y.

a.1 Abstract

Diffusion coefficients of arsenite, arsenate, methylarsonic acid (MMA), and phenylarsonic acid (PAA) at various pH were calculated from acidity constant (pKa) values. The higher the ionic potential, the thicker the hydration layer of the hydrated ion, the smaller the diffusion coefficient. The dependence of hydrated ionic size on the degree of deprotonation decreased from carbonic acid, MMA, PAA, arsenate, arsenite, to phosphoric acid.

a.2 Introduction

In this chapter of the thesis, the major amount of the data, calculations were generated by Mika Sakamitsu, and it is written based on my and her experiements.

In natural systems, migration of metal ions is controlled by mass transfer system, namely advection and diffusion. Advection is caused by water flow, whereas diffusion is driven by concentration gradients. In a system where advection is negligible such as in small porous medium, diffusion is the only transport mechanism for chemicals (Appelo and Postma, 2005). Diffusion also relates to the removal of contaminants and redistribution of materials where water flow is slow, such as in small porous medium, fractured aquifers, and solutes exchange within stagnant water in bulk rocks (Appelo and Postma, 2005). In general, diffusion coefficient (D) under specific condition depends on the ionic potential (Li and Grefory, 1974).

Arsenic is highly toxic yet naturally occurring (Mandal and Suzuki, 2002). Arsenic contaminated groundwater has been found in many areas (Smedley and Kinniburgh, 2002; Polizzotto et al., 2008; Buschmann, et al., 2006); in

consequence, it is important to predict the mobility of arsenic. There are several forms of arsenic, including arsenite, arsenate, monomethylarsonous acid (MMA), and phenylarsonic acid (PAA), and the speciation change depends on the pH and Eh. Diffusion coefficient (D) of arsenic in solution at various pH is not available, although diffusion coefficients of arsenite ($D_{As(III)}$) and arsenate ($D_{As(V)}$) were determined (Li and Grefory, 1974; Leaist, 2007).

a.3 Methods and materials

Experimental design

In this study, $D_{As(III)}$, $D_{As(V)}$, D_{MMA}, and D_{PAA} were measured at several pH ranging from 2 to 12 with diffusion cells method and mass transfer resistance model (Furukawa et al., 2007; Wang et al., 2001). This simple method is able to provide accurate results. This method utilized two solution cells that are separated by a membrane filter. A solution contains the species of interests will be added in only one cell and is allowed to diffuse to the neighboring cell solution, thus the their diffusion speed can be calculated by measuring the concentrations of those species in solution from both cells taken in time intervals.

A set of diffusion cells was composed by a pair of acrylic plastic cells (5.0 cm X5.0 cm), namely source(S) cell and measurement(M) cell, which were separated with a polycarbonate membrane filter (area = 7.07 cm^2, pore diameter =0.80 μm, and thickness =11 μm; ADVANTEC, Japan), with uniform, straight cylindrical pores, as shown in fig. 2.1. Solutions were kept at 25.0 ± 0.2 ˚C in water bath, stirred by magnetic stirrers at a constant speed. Each S cell contain one of 0.10 mg/dm^3 arsenite ($NaAsO_2$; Wako), arsenate

($Na_2HAsO_4 \cdot 7H_2O$; Wako), MMA ($CH_3AsO(OH)_2$; Wako), or PAA ($C_6H_5O(OH)_2$; Wako) with inner standards Sr and Cs dissolved in 0.010 M $NaNO_3$ solutions; M cell was filled with 0.010 M $NaNO_3$ solution. Each paired cell was adjusted to the same pH using HNO_3 and/or NaOH. Solutions were added into the paired cells simultaneously; samples were then taken from both S and M cells every 10 min. for the total length of 90 min. The total loss of solution was less than 0.5 % and was negligible for calculation. Taken samples were diluted with 2% HNO_3 and the concentrations of the taken solutions were measured by ICP-MS (Agilent HP-7500). Arsenic valence states were determined by HPLC-ICP-MS, consisting of a Pu-2089 (JASCO) HPLC pump, Co-2065 Plus (JASCO) column oven, a TSKgel Super IC-AP (Thoso) anion exchange column, and connected to the ICP-MS.

D of arsenic was determined with known D of Sr and Cs, with the model: (1) (Wang et al., 2001)

where C_1 and C_2 are the concentrations for S and M cells respectively, t is the time, A is the membrane area, k is the mass transfer coefficient, V is the volume of the solution in the S and M cells. The slope of

$\ln\{(C_1-C_2)_0/(C_1-C_2)_t\}$ vs t, 2Ak/V,

is determined by linear regression analysis. k is determined by A and V. The total mass transfer resistance R_t is expressed as:

(2),

where R_m is the resistance of the membrane, R_b is the boundary layer resistance, and R_e is the end effect. The employed membrane filter pore radius (0.80 μm) was larger than the radii of the solute molecules, thus the filter did not cause any hinder and the diffusion coefficient in the pores equals

to the diffusion coefficient in the bulk solution（Malone and Anderson, 1977). Deen et al.(1981) suggested that k was related to diffusion coefficient

D: (3),

where the constants k_1, k_2, and k_3, characterized by the membrane properties, cell geometry, and stirring speed, determine the mass transfer through membrane. D can be calculated from Eq. (3) if k_1+k_3 and k_2 are obtained from diffusion experiments, using known D of two or more other species.

The sizes of non-hydrated arsenite, arsenate, MMA, and PAA were estimated by geometric method.

Radii of arsenite and MMA were a (long axis) = (4); (a is R_C in table 2.2), and

b(short axis) = (5),

where m is the long distance of arsenite or MMA and n is the short distance of arsenite or MMA. The m and n of arsenite were calculated from the distances of As(III)-O (181 pm) in water solution, O-O (272 pm) (Ramírez-Solí et al., 2004), ionic sizes of As^{3+} (58 pm) and 4 coordinations of O^{2-} (140 pm, r_O). MMA's m and n were also calculated from the distances of As-C (190 pm) (Jing et al., 2005), r_O, and C^{4+} (15 pm). The radius of arsenate was R_C = $r_{As(V)}$ + r_O (table 2.2). The $r_{As(V)}$ of H_3AsO_4 was the average of 176 pm (As^V-OH) and 160 pm (As^v-O), and $r_{As(V)}$ of $H_2AsO_4^-$ was the average of 181 pm (As^v-OH) and 163 pm (As^v-O). The $r_{As(V)}$ of $HAsO_4^{2-}$ was the average of 187 pm (As^v-OH) and 168 pm (As^v-O) (Myneni, 1998). The R_C of PAA was calculated with equation: long axis = $r_{As=O}$ + r_{As-C} + $r_{benzene\ ring}$ = 166 + 189 + 81 = 325 pm (Lyoyd, 2008).

The effective sizes of the species with hydration layer were calculated from D with Stokes-Einstein equation (Cussler, 1997). Arsenite and MMA have the shapes of prolate ellipsoid, and their hydrated ionic radius of those species and the D is:

(6) (Cussler, 1997), where k_B is the Boltzmann's constant, T is the absolute temperature, and μ is the coefficient of viscosity of solvent. The b/a value 0.552 calculated from a and b were applied to arsenite, where a is regarded as R_H. PAA are oblate ellipsoid, thus the function of the hydrated ionic radius D is: (7) (Cussler, 1997).

Stokes-Einstein equation for spherical Arsenate is:

,

where R_H is the effective radius of diffusion species(Cussler, 1997). Arsenite was detected less than 10% of the total As species during the diffusion experiment, so as arsenate of arsenite. MMA and PAA were not altered during the experiment.

a.4 Results

Fig. 2.2 shows the pH dependence of $D_{As(III)}$, $D_{As(V)}$, D_{MMA}, D_{PAA}. $D_{As(III)}$ was 1.6 times larger than $D_{As(V)}$, illustrating that the effective size of arsenate is larger than arsenite. D_{MMA} is smaller than D_{PAA}. The range of variation of $D_{As(III)}$, $D_{As(V)}$, D_{MMA}, and D_{PAA} when the pH changed from pH 2 to 12 were 18%, 29%, 33%, and 19%, respectively. Thirdly, $D_{As(V)}$ was slightly smaller than D_{MMA} at pH 2. Finally, D_{MMA} and D_{PAA} had similar values at neutral pH. The results show that D decreased with increasing ionic potential z/r (z: charge, r: ionic radius) (Li, 1974). The curve of D on pH dependence was

determined by multiplying D of the charge of each dissolved species by the percentage of dissolved species (Fig. 2.2).The true D of each species at different charges were obtained by fitting the experimental data to the ratios of each species estimated in the speciation calculation. D values at particular pH with the presence of various species were calculated from the speciation of arsenic (table 1.1).

The size of oxyanion for diffusion coefficient calculated from geometric method R_C was almost constant independent of pH. However, R_H calculated from D changed with the variation of pH. In Fig. 2.3, D was plotted against R_C calculated by geometric method (Eq. 4, 5). D values decrease while R_C values increases. It proposed that such features in Fig. 2.2 could be calculated from D of other oxyanions. Fig. 2.3 showed that the D of phosphoric acid, arsenic, and antimonic acid of D were very similar.

R_H of oxyanion, arsenite, arsenate, MMA, and PAA were plotted against the number of charges in Fig. 2.4, and the slopes showed the differences of electrostatic interactions between dissolved species and water molecules with deprotonation. The strength of R_H dependence on the charges is ranked as follow: carbonic acid > MMA > PAA > arsenate > arsenite > phosphoric acid.

Fig. 2.5 was produced by adding Li's (1974) data to this study. The similarity of the slopes in Fig. 2.5 indicates that the trends of ionic potential and D were similar. Though D decreased with increasing ionic potential of cations with same valence, the slopes in Fig. 2.5 were similar among oxyanion. The slopes decrease in the order of carbonic acid, MMA, arsenate, arsenite, phosphoric acid, and PAA.

a.5 Discussion

The pH dependence of $D_{As(III)}$, $D_{As(V)}$, D_{MMA}, D_{PAA}. $D_{As(III)}$ shown in Fig. 2.2 suggesting that the effective size of arsenate is larger than arsenite because of the presence of an extra oxygen in arsenate. D_{MMA} is smaller than D_{PAA} suggests that PAA may have weaker electrostatic interaction between the species and water molecule due to its hydrophobic functional group. In solutions with increasing pH, more anion group can be attached to the specie that has higher ionic charges; therefore the decrease in D with increasing pH reflects the increase of ionic charges.

The hydrated ionic radius of arsenate was larger than MMA, which can cause the size of $D_{As(V)}$ being slightly smaller than D_{MMA} at pH 2, and MMA and PAA had similar hydrated ionic radius can be the reason that D_{MMA} and D_{PAA} had similar values at neutral pH. The deprotonation with increasing pH caused increasing in ionic potential thus the decreased D. The curve of D on pH dependence was determined by multiplying D of the charge of each dissolved species by the percentage of dissolved species (Fig. 2.2).

Variations of D with the increases in the negative charges shown in Fig. 2.3 indicates the larger interaction between water and the diffusive species for more negatively charged ions. Figs. 2.4 and 2.5 show that the carbonic acid has the strongest R_H dependence on the charges, then followed by MMA, PAA, arsenate, arsenite, phosphoric acid. Thus, carbonic acid is the most sensitive to the pH change to variation of charge, and the following species has decreasing in sensitivity.

a.6 Conclusion

D at around pH 2, where there is no significant deprotonation, decreases in the order of arsenite, arsenate, MMA, and PAA. Thus, D depended on the non-hydrated size of species, whereas, D_{MMA} and D_{PAA} had similar values because PAA does not hydrate to a large size than MMA.

a.7 References

Appelo C. A. J. and Postma D. (2005) Geochemistry, Groundwater and pollution, second ed. A.A. Balkema, Rotterdam, pp. 93-96

Buschmann J., Kappeler A., Lindauer U., Kistler D., Berg M. and Sigg L. (2006) Arsenite and arsenate binding to dissolved humic acids: influence of pH, type of humic acid, and aluminum.

Cussler E. L. (1997) Diffusion, Mass Transfer in Fluid System, Second ed. Cambridge Univ. Press, Cambridge, 111-121

Deen W. M., Boher M. P. and Epstein N. B. (1981) Effect of molecular size and configuration on diffusion in microporous membranes. AIChE J., 27, 952-959

Furukawa K., Takahashi Y. and Sato H. (2007) Effect of the formation of EDTA complexes on the diffusion of metal ions in water. Geochim. Cosmochim. Acta, 71, 4416-4424

Jing C., Meng X., Liu S., Baidas S., Patraju R., Christodoulatos C. and Korfiatis G. P. (2005) Surface complexation of organic arsenic on nanocrystalline titanium oxide. J. Colloid Interface Sci., 290, 14-21

Leaist D. (2007) Mutual diffusion coefficients for binary aqueous solutions of arsenous, arsenic, and malonic acids. J. Chem. Eng. Data., 52, 1319-1325

Li Y. H. and Grefory S. (1974) Diffusion of ions in sea water and in deep-sea sediments. Geochim. Cosmochim. Acta, 38, 703-714

Lyoyd N. C., Morgan H. W., Nicholson B. K. and Ronimus R. S. (2008) Substituted phenylarsonic acids; structures and spectroscopy. J. Organometallic Chemistry, 693, 2443-2450

Malone D. M. and Anderson J. L. (1977) Diffusional boundary-layer resistance for membranes with low porosity. AIChE J., 23, 177-184

Mandal B. K. and Suzuki K. T. (2002) Arsenic round the world: a review. Talanta, 58, 201-235

Myneni C. B., Traina S. J., Waychunas G. A. and Logan T. J. (1998) Experimental and theoretical vibrational spectroscopic evaluation of arsenate coordination in aqueous solutions, solids, and at mineral-water interfaces. Geochim. Cosmochim. Acta, 62, 3285-3300

Polizzotto M., Kocar B. D., Benner S. G., Sampson M. and Fendorf S. (2008) Near-surface wetland sediments as a source of arsenic release to ground water in Asia. Nature, 454, 505-508

Ramírez-Solí A., Mukopadhyay R., Rosen B. P. and Stemmler T. L. (2004) Experimental and theoretical characterization of arsenite in water: insights into the coordination environment of As-O. Inorg. Chem., 43, 2954-2959

Shannon R. D. (1976) Revised effective ionic radii and systematic studies of interatomic distances in
halides and chalcogenides. Acta Cryst., A32, 751-767

Smedley P.L. and Kinniburgh D. G. (2002) A review of the source, behaviour and distribution of arsenic in natural waters. Applied Geochemistry, 17, 517-568

Wang Y., Combe C. and Clark M. M. (2001) The effects of pH and calcium on the diffusion coefficient of humic acid. J. Membr. Sci., 183, 49-60

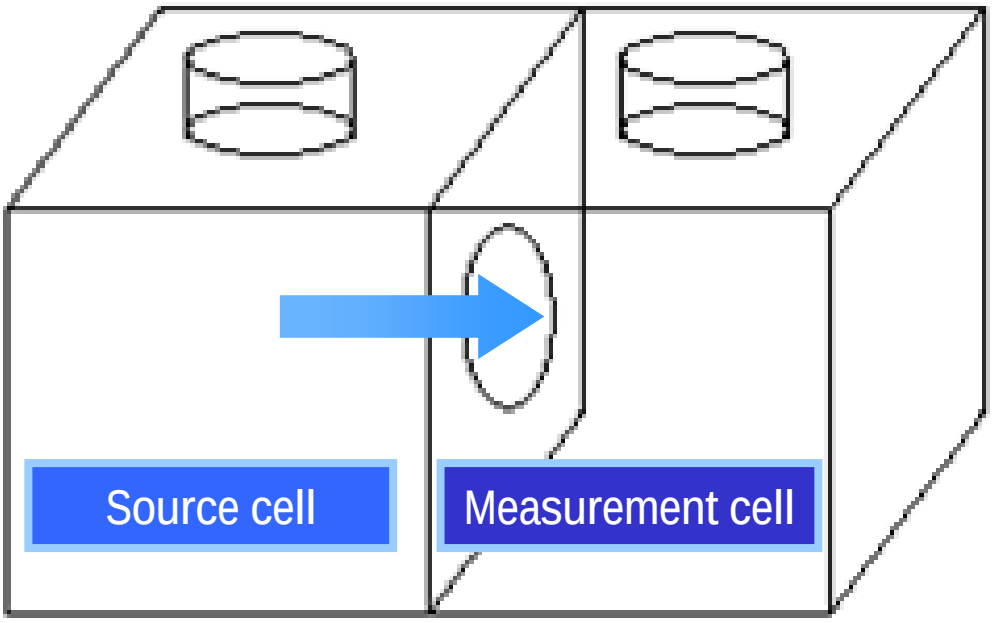

Figure a.1 schematic diagram of experimental setting. The experimental method is based on those by Furukawa et al. (2007) and Wang et al. (2001).

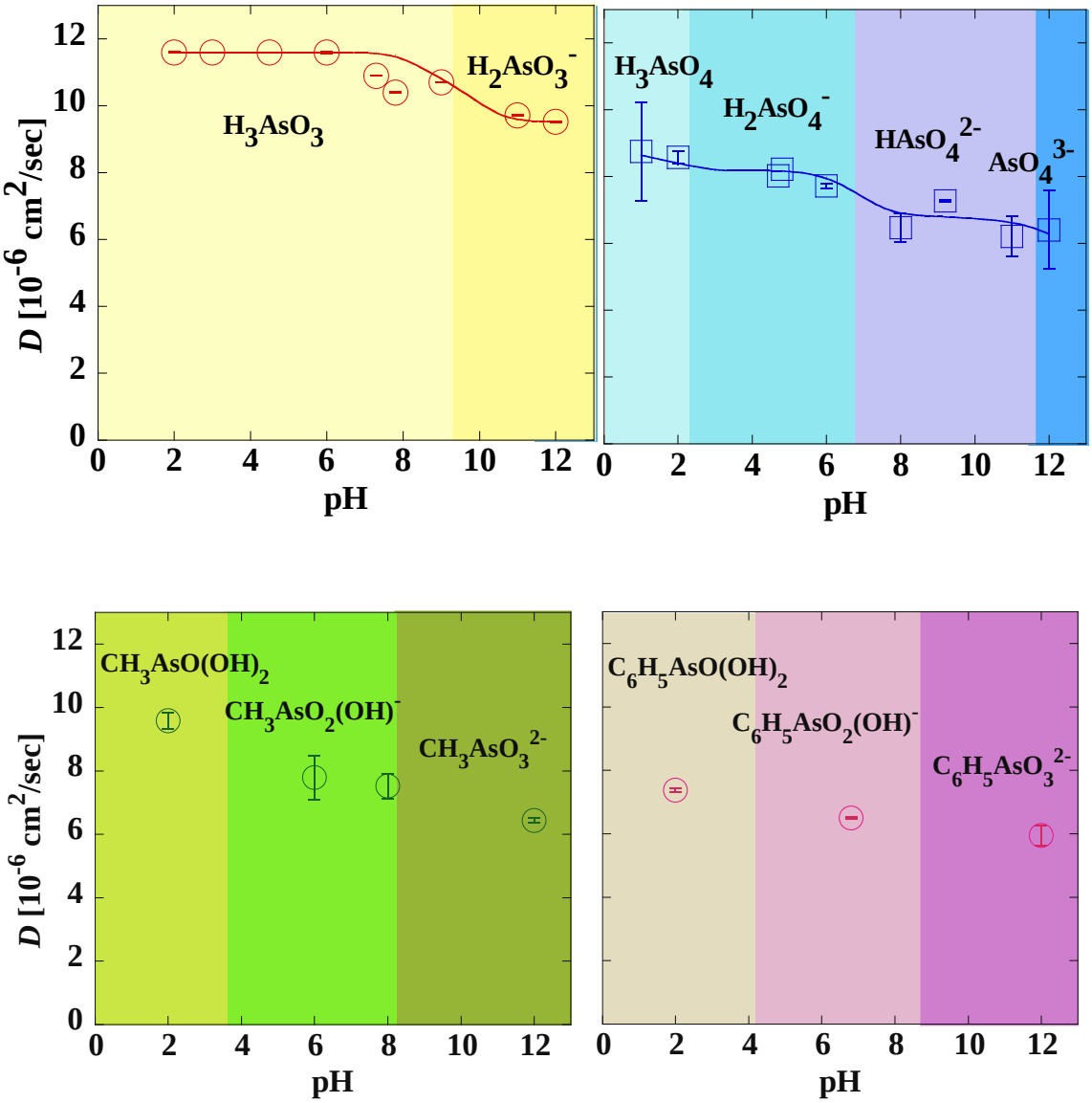

Figure a.2 D of arsenite, arsenate, MMA, and PAA as a function of pH. The positive and negative stander deviations are shown as vertical bars above and blow the average values. The column colors changes representing change of D values with the increase of pH. D values of arsenite at pH 2, 3, 4 and arsenate at pH 2 is measured by myself and added onto Mika Sakamistu's graphs.

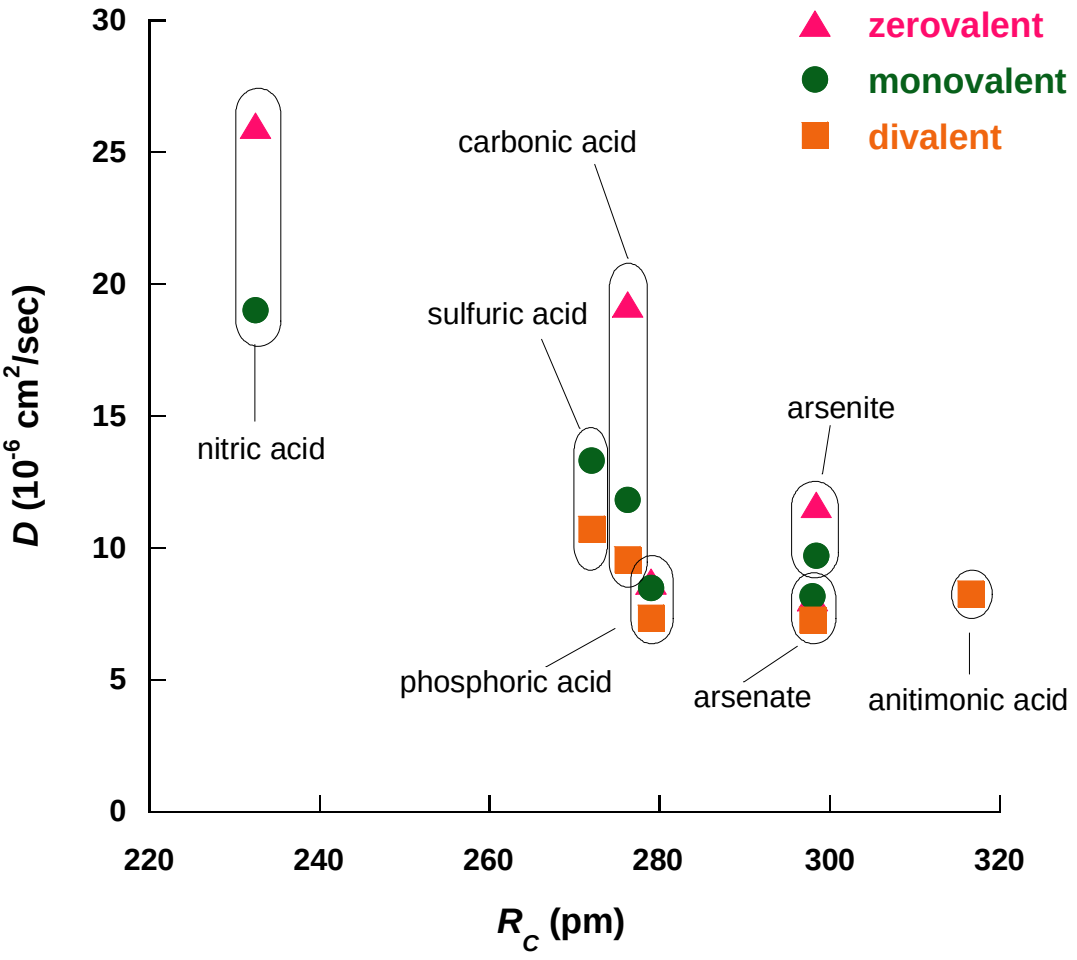

Figure a.3 correlation of *D* value and molecular radius(R_C) of different chemical species, R_C was calculated by geometric method explained in Section 2.2.1. *D* of nitic acid: Cussler, 1997; Li and Gregory, 1974. *D* of carbonic acid: Leaist, 1987; Li and Gregory, 1974. *D* of sodium nitrite acid: Li and Gregory, 1974. *D* of phosphoric acid: Leaist, 1984; Noulty and Leaist, 1987; Li and Gregory, 1974. *D* of arsenious and arsenic acid: this study. *D* of antimonic acid: Li and Gregory, 1974.

.

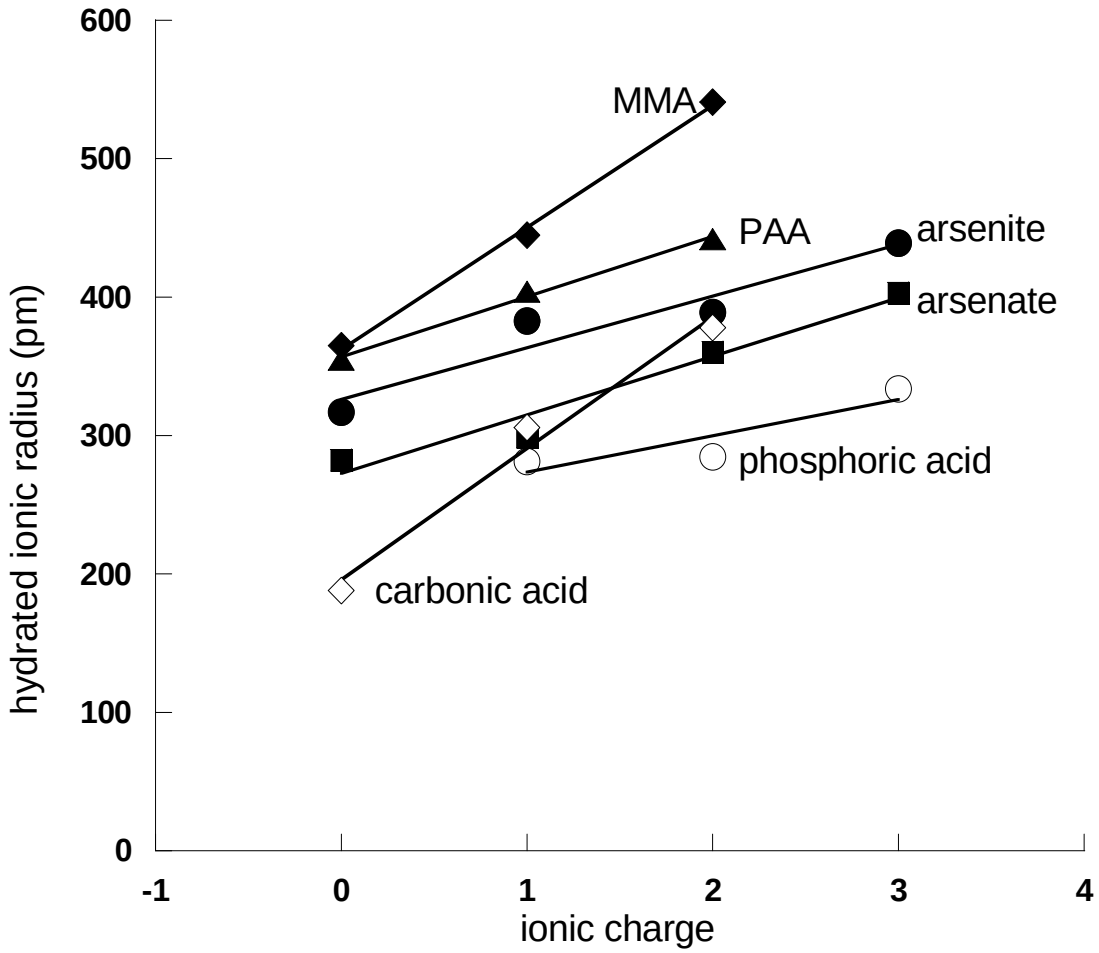

Figure a.4 The charge dependence of hydrated ionic radius (pm) in solution calculated by Stokes-Einstein equation. The graph is prepared by Mika Sakamistu and edited by the added data points from myself.

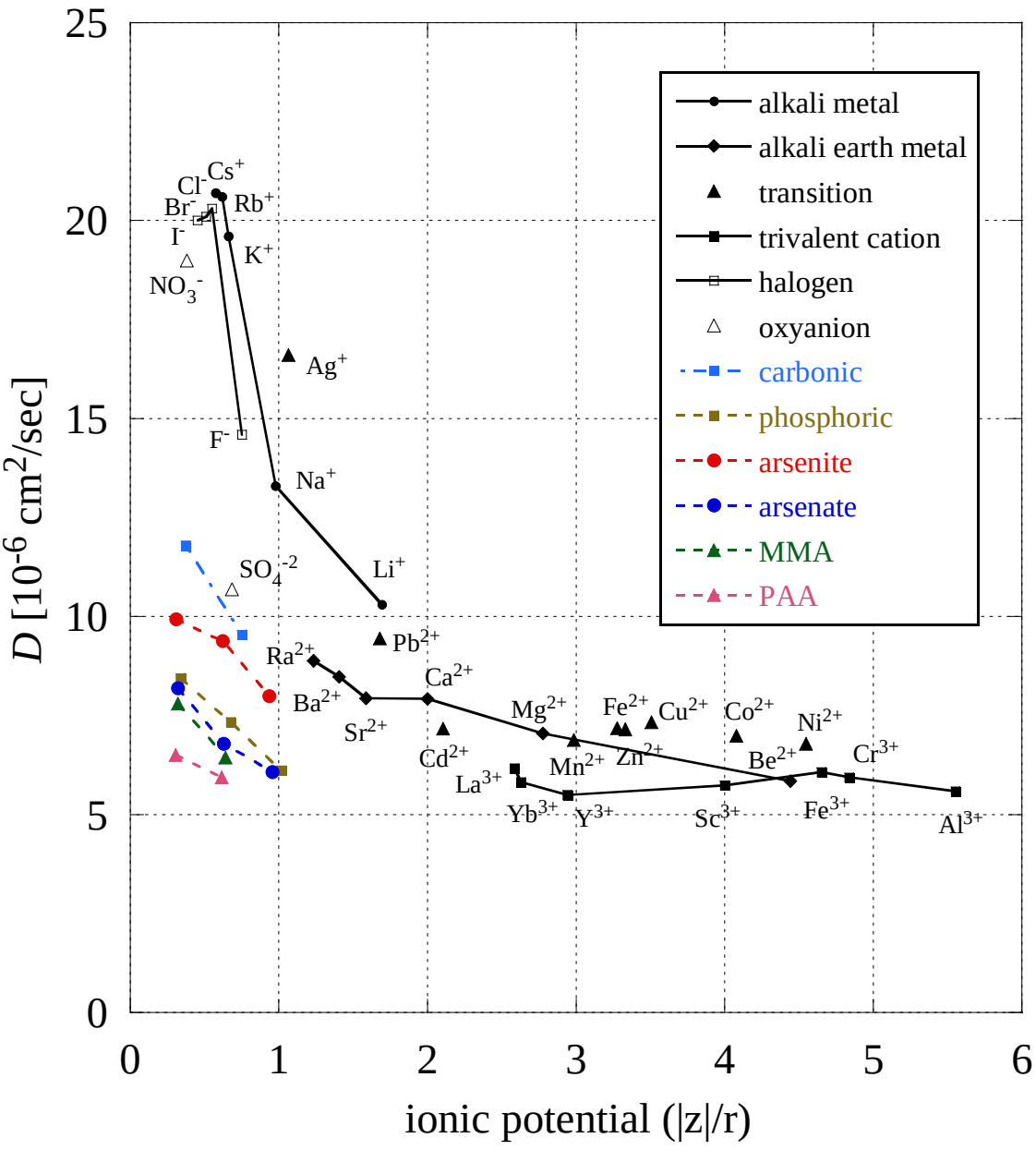
25
20
15
10
5
0
0
1
2
3
4
5
6
D [10-6 cm2/sec]
ionic potential (|z|/r)
alkali metal
alkali earth metal
transition
trivalent cation
halogen
oxyanion
carbonic
phosphoric
arsenite
arsenate
MMA
PAA
Cl-
Br-
I-
NO3-
Cs+
Rb+
K+
Ag+
F-
Na+
Li+
SO4-2
Pb2+
Ra2+
Ba2+
Sr2+
Ca2+
Cd2+
La3+
Yb3+
Mg2+
Mn2+
Y3+
Fe2+
Zn2+
Cu2+
Sc3+
Co2+
Be2+
Ni2+
Fe3+
Cr3+
Al3+

(a)

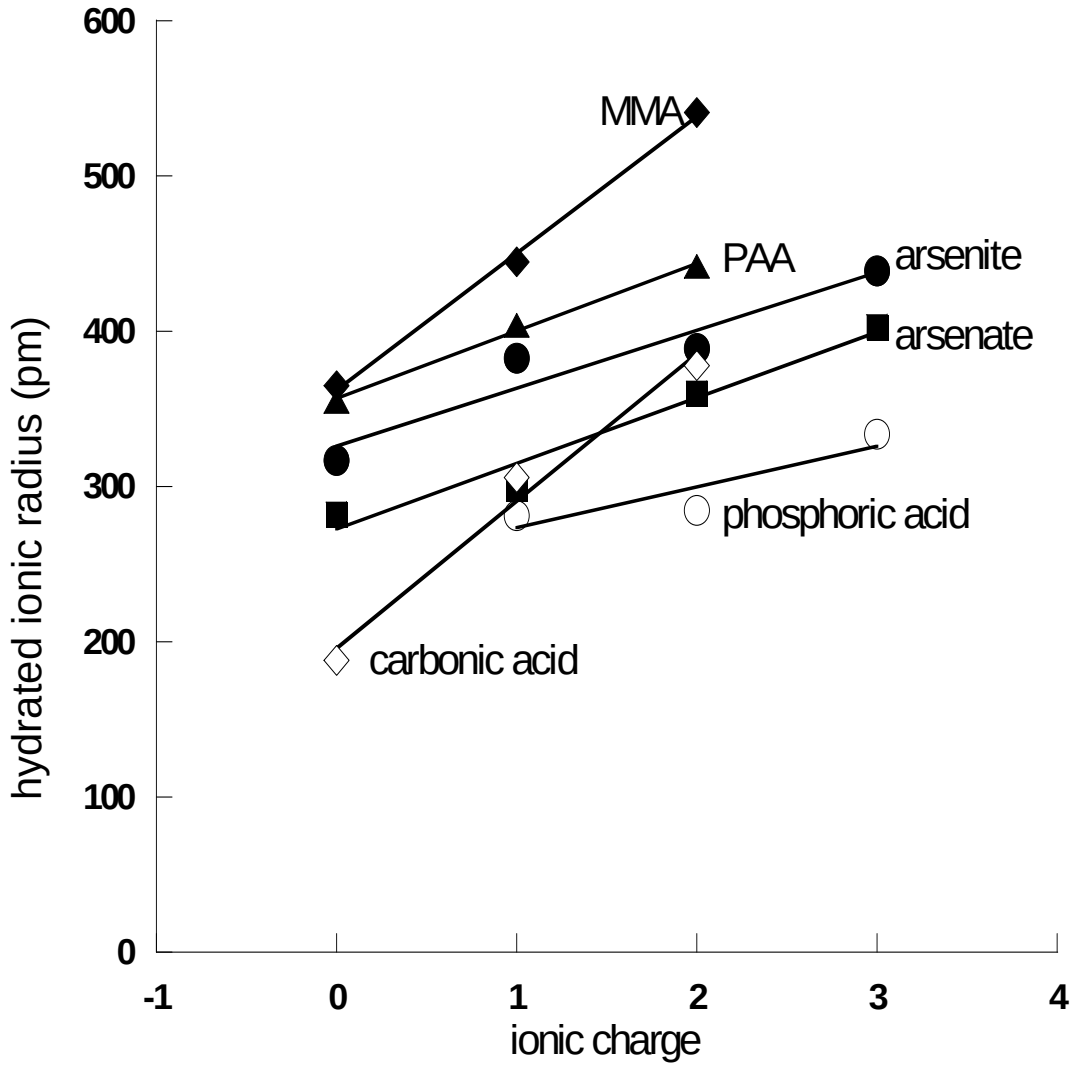

Figure a.5 The charge dependence of hydrated ionic radius (pm) in solution calculated by Stokes-Einstein equation. The graph is prepared by Mika Sakamistu and edited by the added data points from myself.

Table a.1 D of various species of arsenite, arsenate, MMA, and PAA in solutions.

arsenite				
	H_3AsO_3	$H_2AsO_3^-$	$HAsO_3^{2-}$	AsO_3^{3-}
	11.6	9.94	9.38	8
arsenate				
	H_3AsO_4	$H_2AsO_4^-$	$HAsO_4^{2-}$	AsO_4^{3-}
	8.76	8.2	6.79	6.08
MMA[1]				
	$CH_3AsO(OH)_2$	$CHAsO_2(OH)^-$	$CH_3AsO_3^{2-}$	
	9.62	7.88	6.44	
PAA[2]				
	$C_6H_5AsO(OH)_2$	$C_6H_5AsO_2(OH)^-$	$C_6H_5AsO_3^{2-}$	
	7.4	6.51	5.94	

*D (cm^2/sec): diffusion coefficient
[1] MMA = ethylarsonic acid
[2] PPA = phenylarsonic acid

Table a.2 The radius (R_C) of various dissociation species of arsenite, arsenate, MMA, and PAA in solution.

arsenite	H_3AsO_3	$H_2AsO_3^-$	$HAsO_3^{2-}$	AsO_3^{3-}
	314	314	314	314
arsenate	H_3AsO_4	$H_2AsO_4^-$	$HAsO_4^{2-}$	AsO_4^{3-}
	316	312	318	313
MMA	$CH_3AsO(OH)_2$	$CHAsO_2(OH)^-$	$CH_3AsO_3^{2-}$	
	313	313	313	
PAA	$C_6H_5AsO(OH)_2$	$C_6H_5AsO_2(OH)^-$	$C_6H_5AsO_3^{2-}$	
	325	325	325	

*units: pm
(Shannon, 1976).

Appendix B

Photomicrographs and Back Scatter Electron image of 100609 -11 and 121306-5 hand samples and thin sections

1 cm

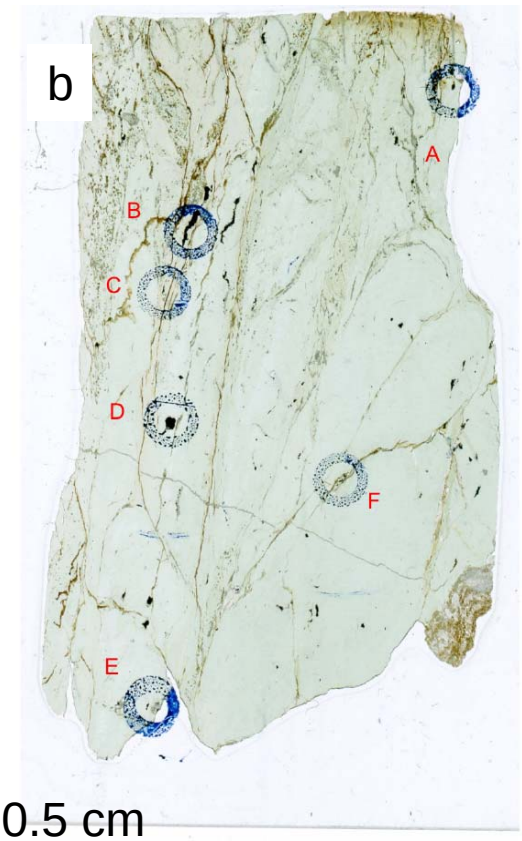

0.5 cm

Circle A

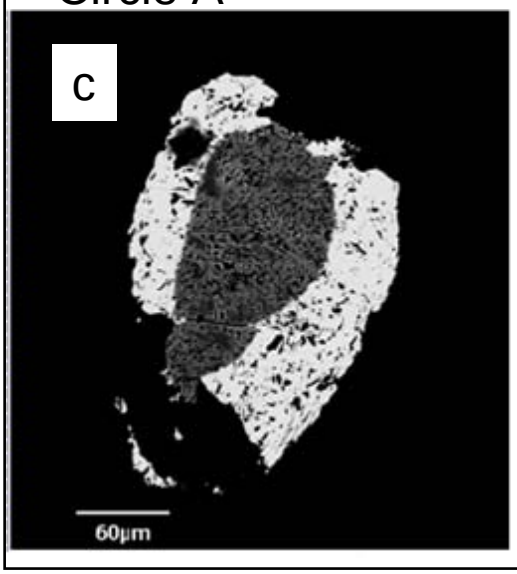

Circle D

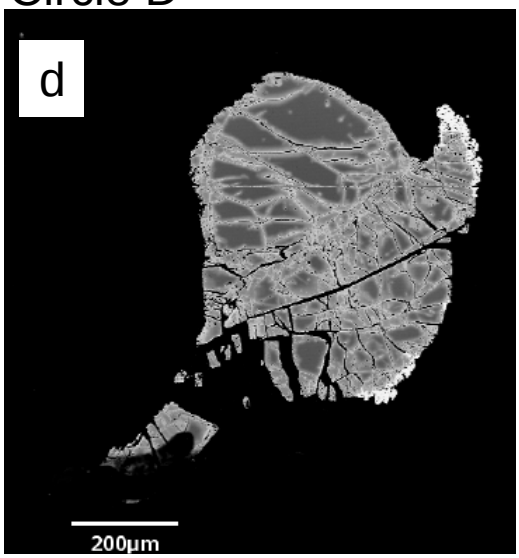

Circle E

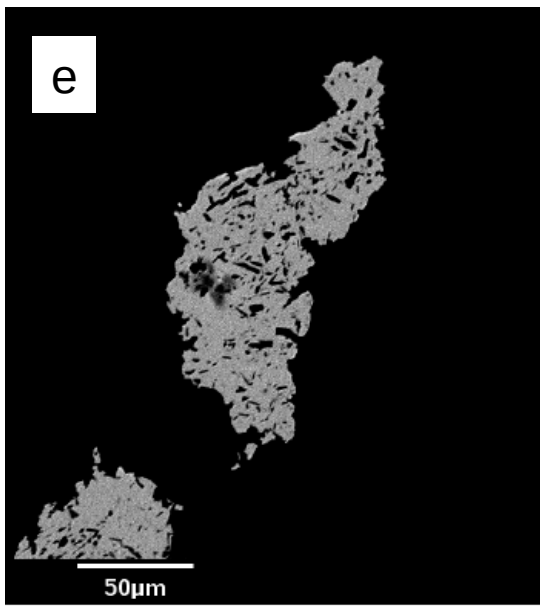

Circle F

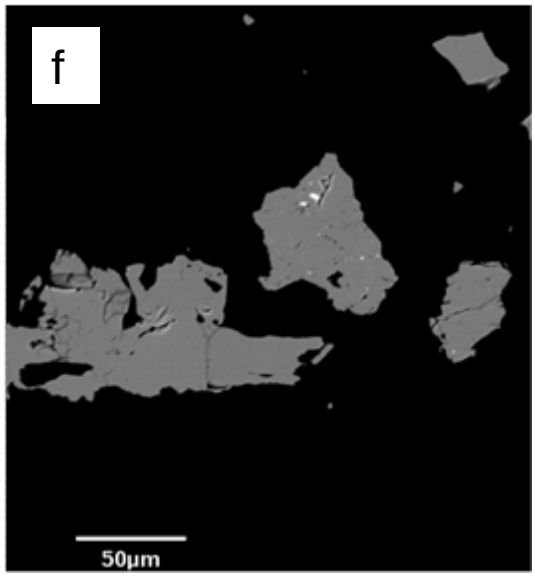

Various photos, photomicrographs and Back Scatter Electron (BSE) imagines of sample100109-11 and 121306-5 hand samples and thin sections. **a)** Photograph of hand specimen 100109-11; **b)** Thin section of 100109-11. **c, d, e, f)** BSE imagine of 100109-11 circle A, D, E, F. **g)** Photo of hand sample 121306-5

Appendix C

Electron Microprobe Data

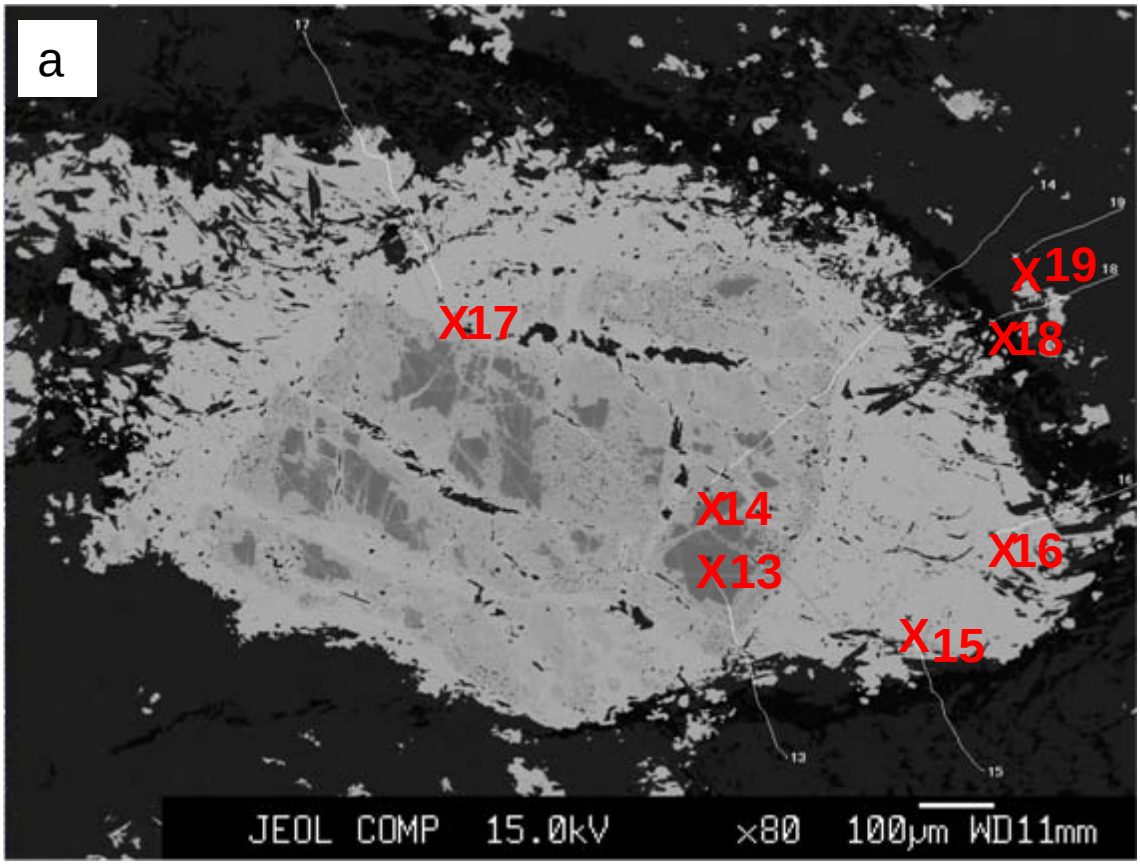
a
X17
X19
X18
X14
X13
X16
X15
JEOL COMP 15.0kV ×80 100µm WD11mm

b

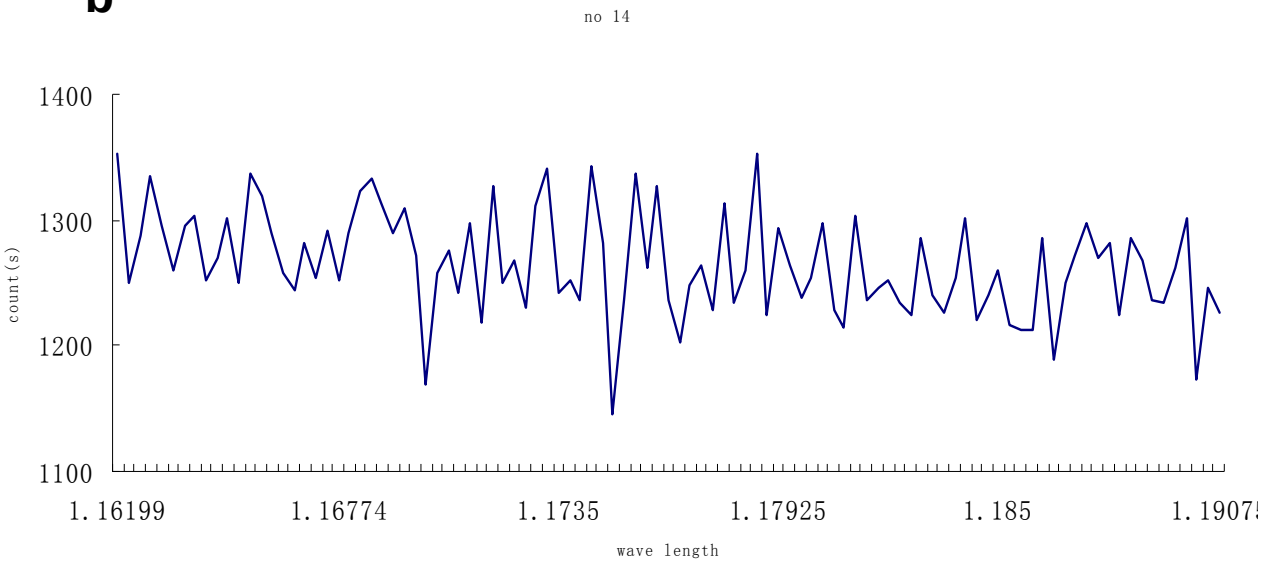
no 14
1400
1300
1200
1100
count(s)
1.16199
1.16774
1.1735
1.17925
1.185
wave length

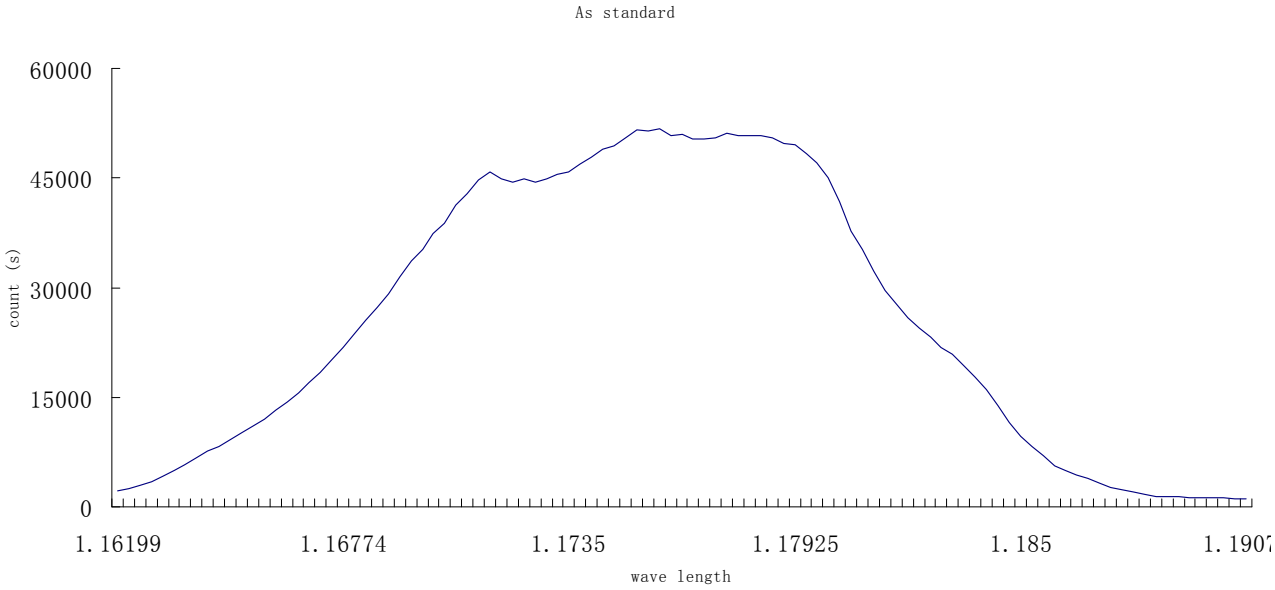
As standard
60000
45000
30000
15000
0
count (s)
1.16199
1.16774
1.1735
1.17925
1.185
wave length

C

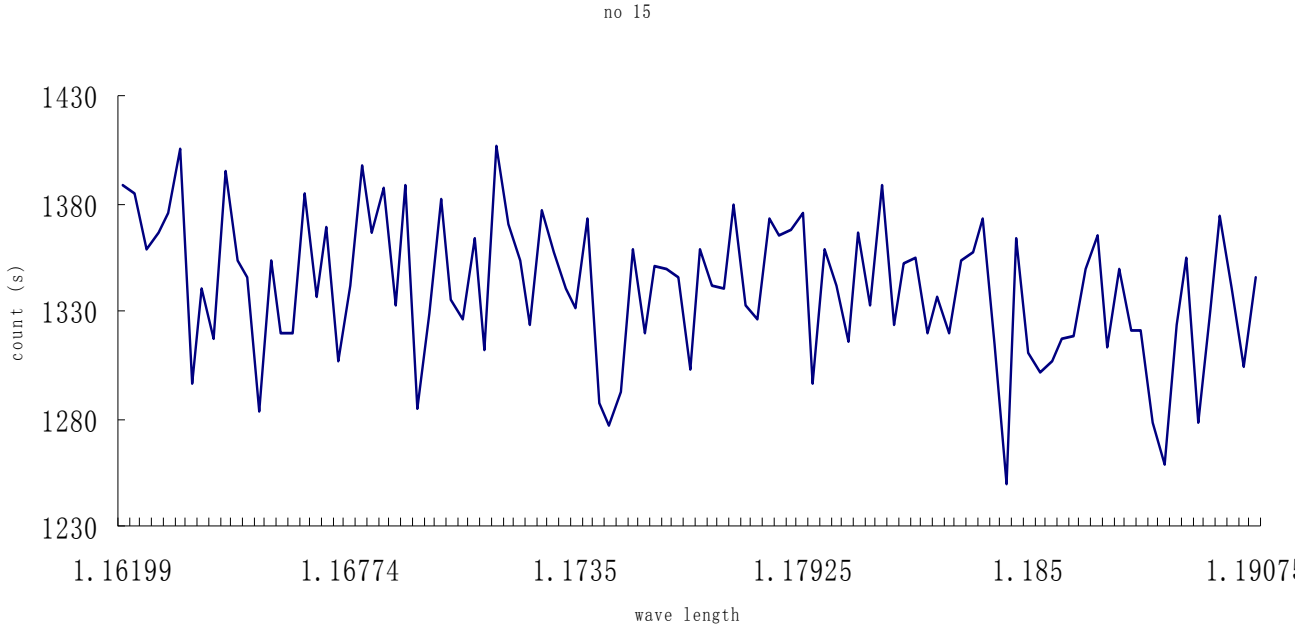
no 15
1430
1380
1330
1280
1230
count (s)
1.16199
1.16774
1.1735
1.17925
1.185
wave length

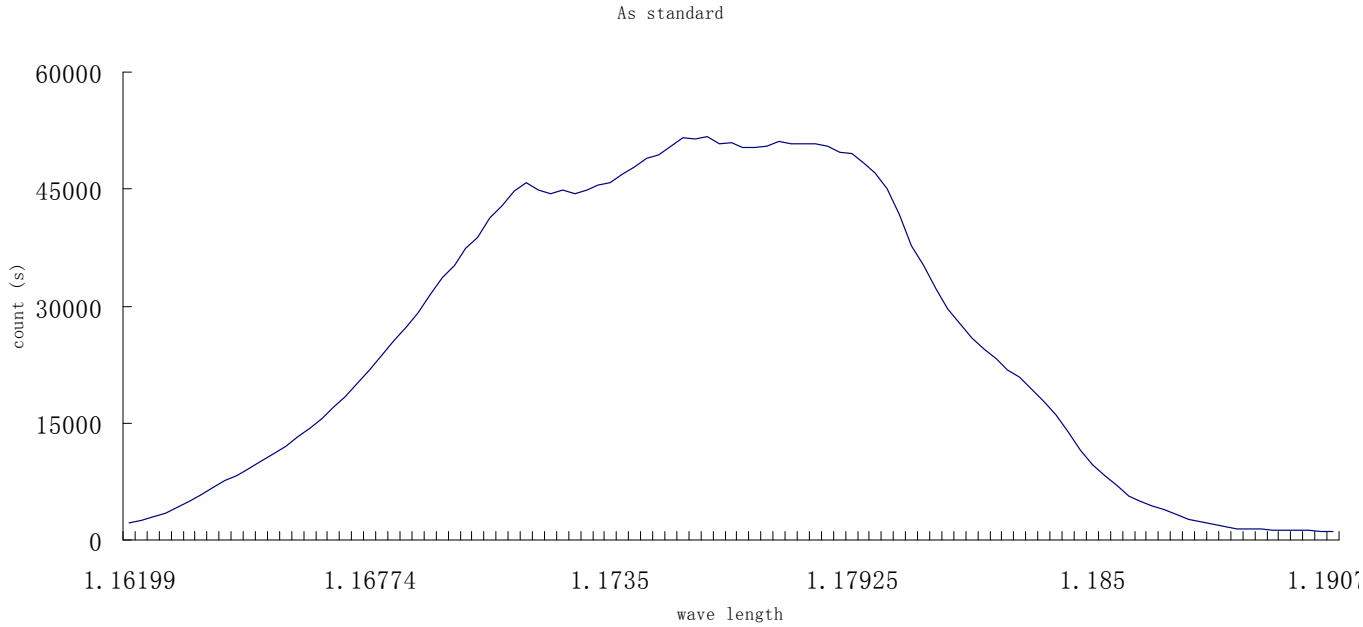
As standard
60000
45000
30000
15000
0
count (s)
1.16199
1.16774
1.1735
1.17925
1.185
wave length

d

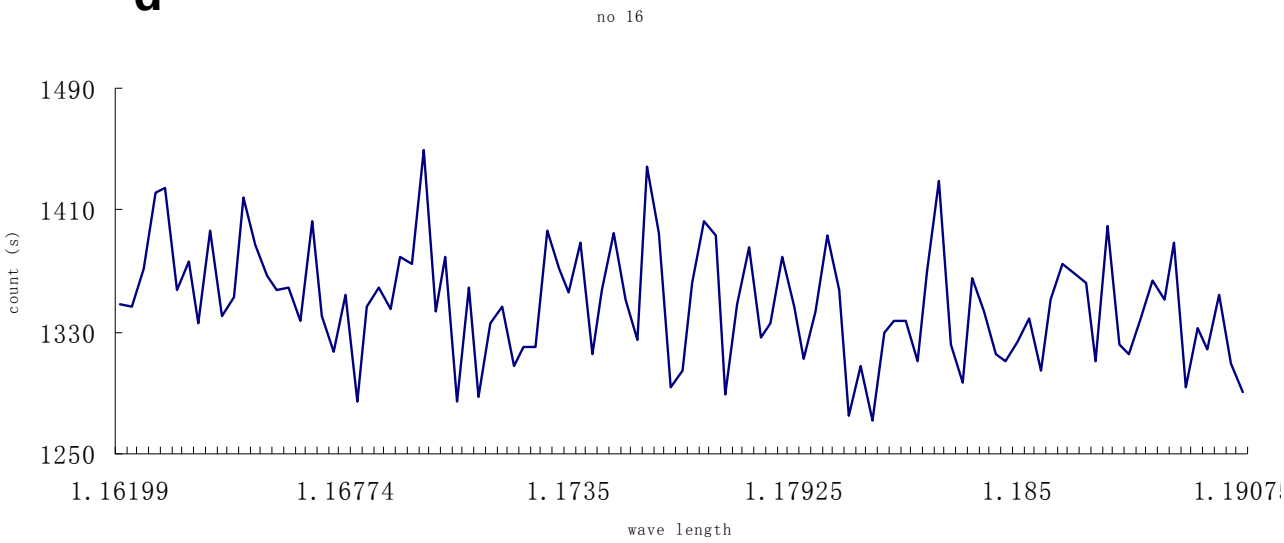
no 16
1490
1410
1330
1250
count (s)
1.16199
1.16774
1.1735
1.17925
1.185
wave length

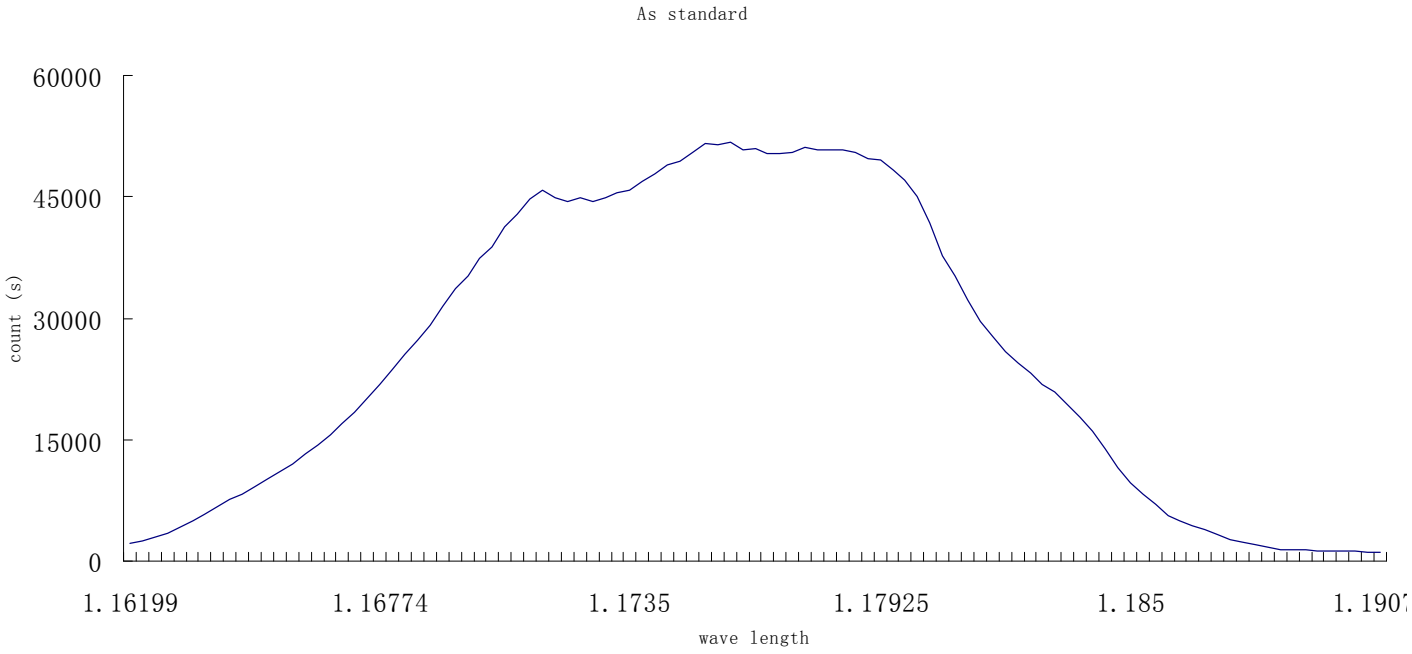
As standard
60000
45000
30000
15000
0
count (s)
1.16199
1.16774
1.1735
1.17925
1.185
wave length

e

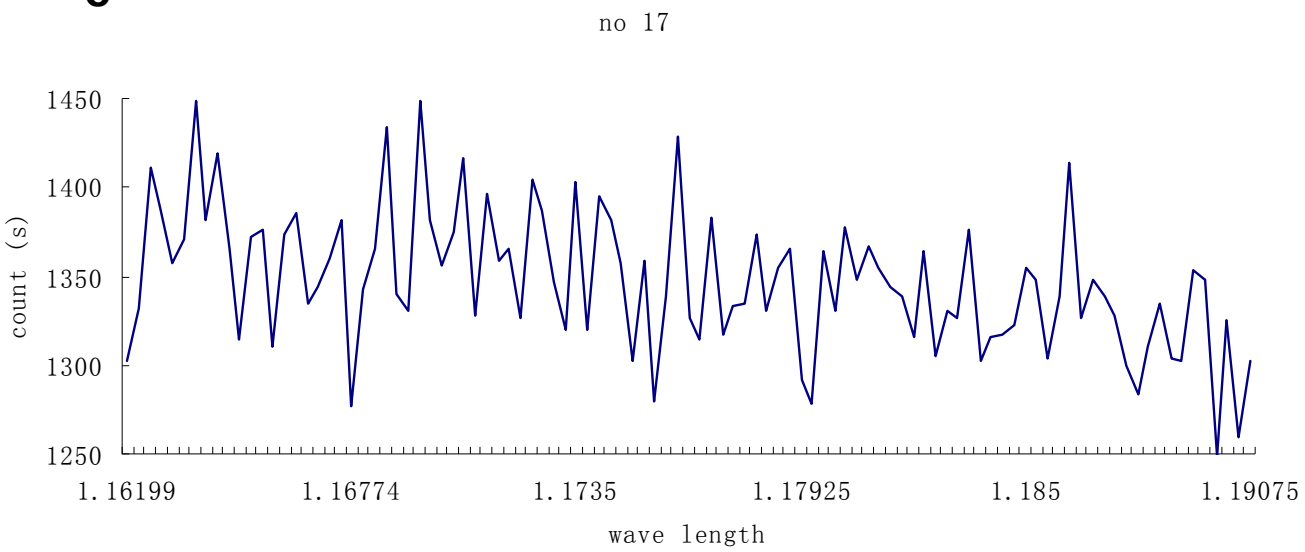
no 17
1450
1400
1350
1300
1250
count (s)
1.16199
1.16774
1.1735
1.17925
1.185
1.19075
wave length

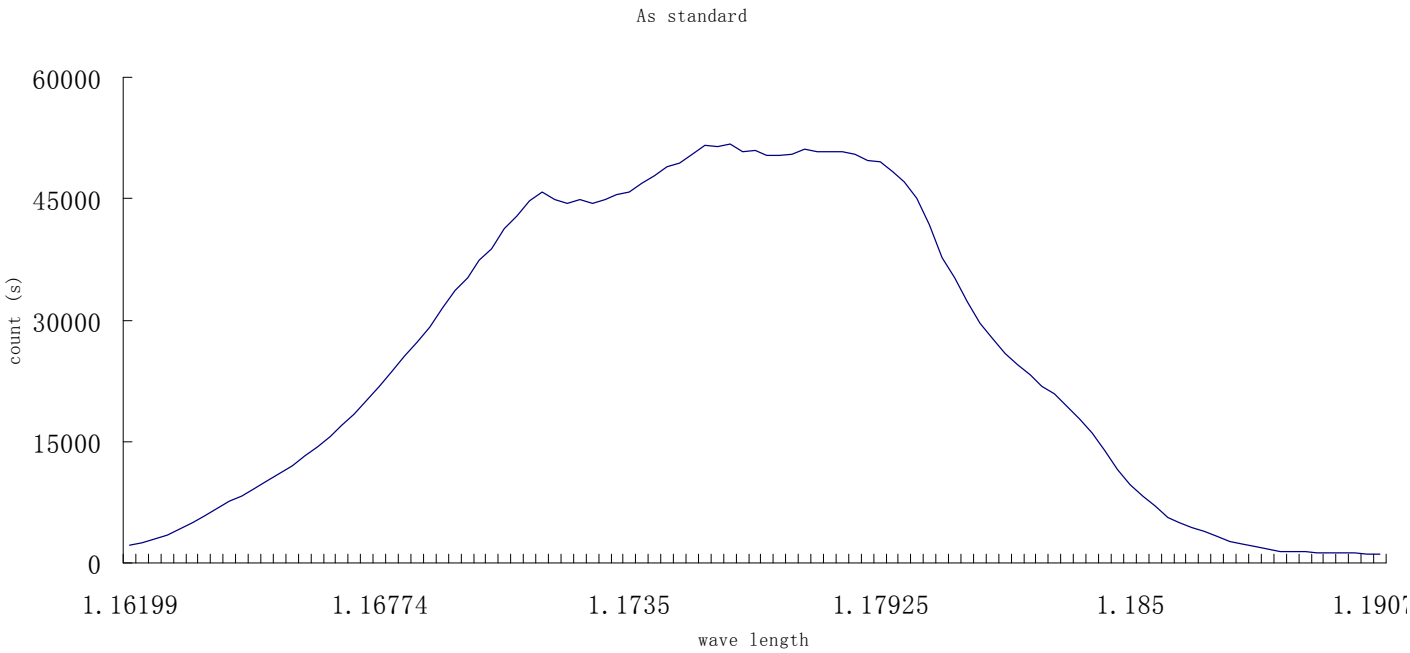
As standard
60000
45000
30000
15000
0
count (s)
1.16199
1.16774
1.1735
1.17925
1.185
wave length

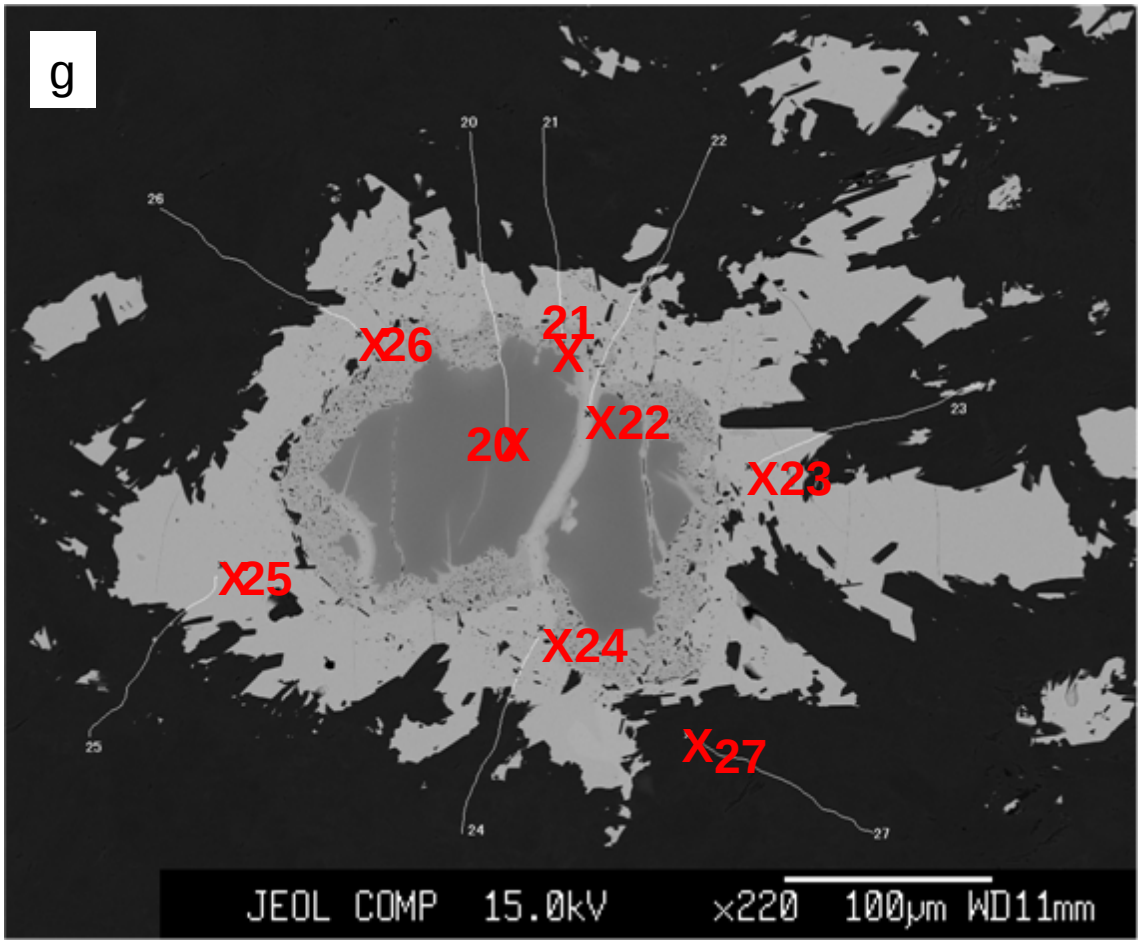
g
20
21
22
26
X26
21
X
X22
20X
23
X23
X25
X24
25
X27
24
27
JEOL COMP 15.0kV ×220 100μm WD11mm

h

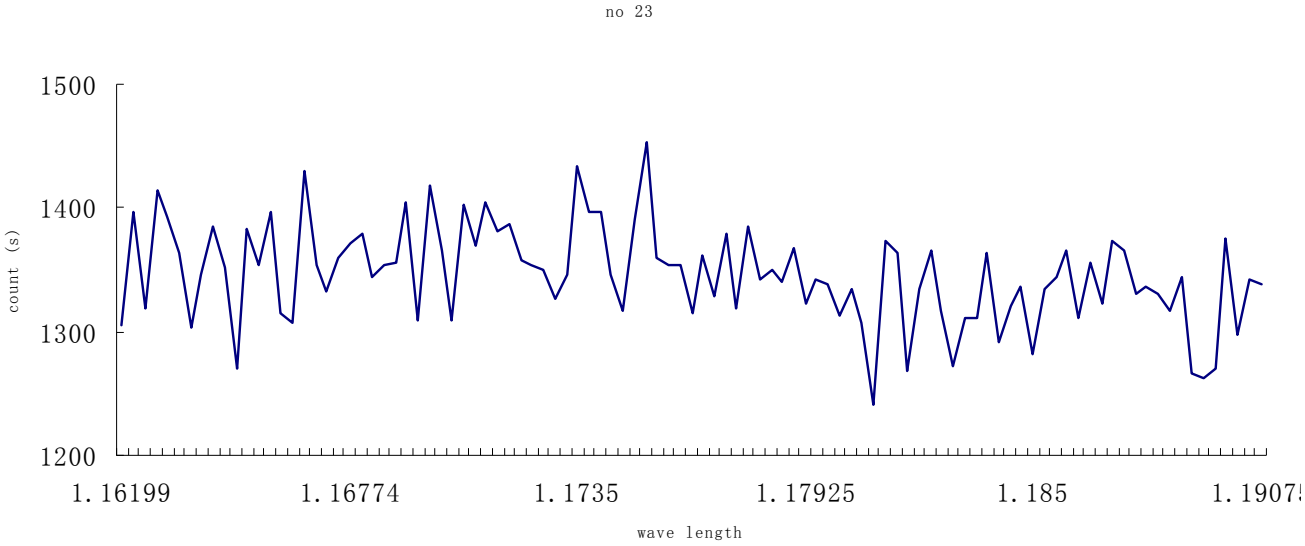
no 23
1500
1400
1300
1200
count (s)
1.16199
1.16774
1.1735
1.17925
1.185
wave length

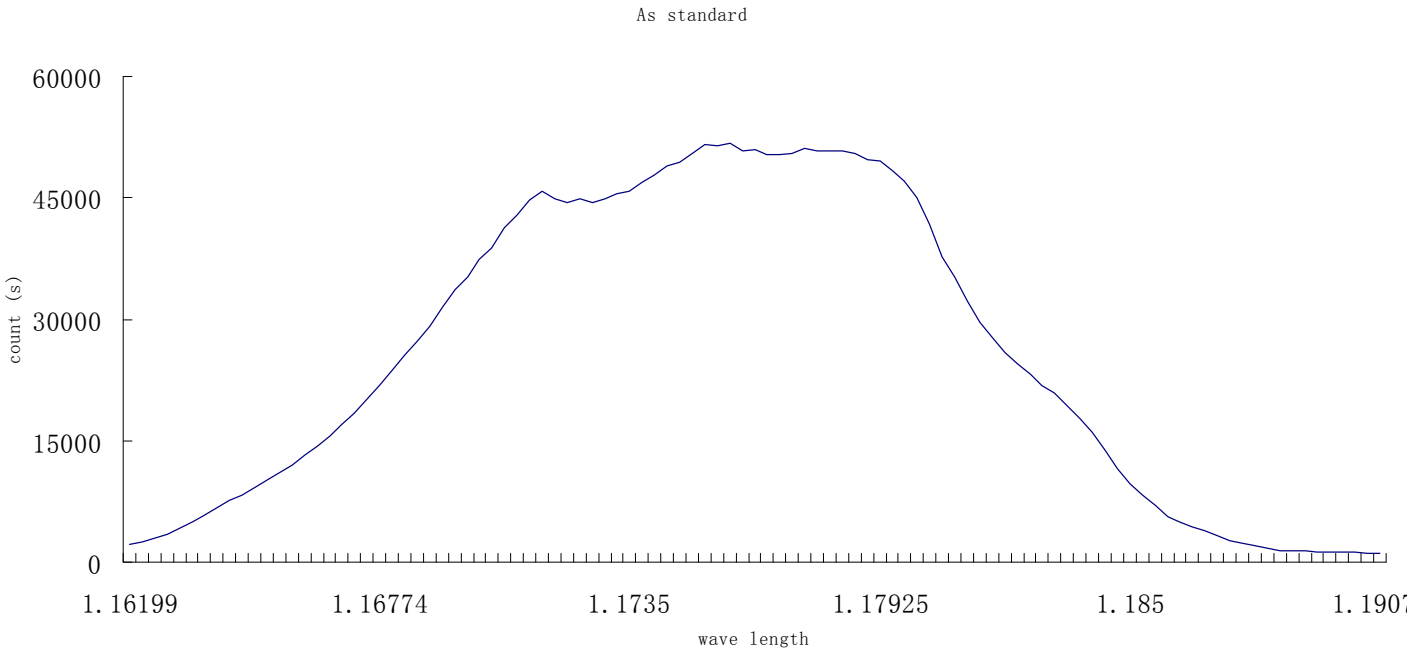
As standard
60000
45000
30000
15000
0
count (s)
1.16199
1.16774
1.1735
1.17925
1.185
wave length

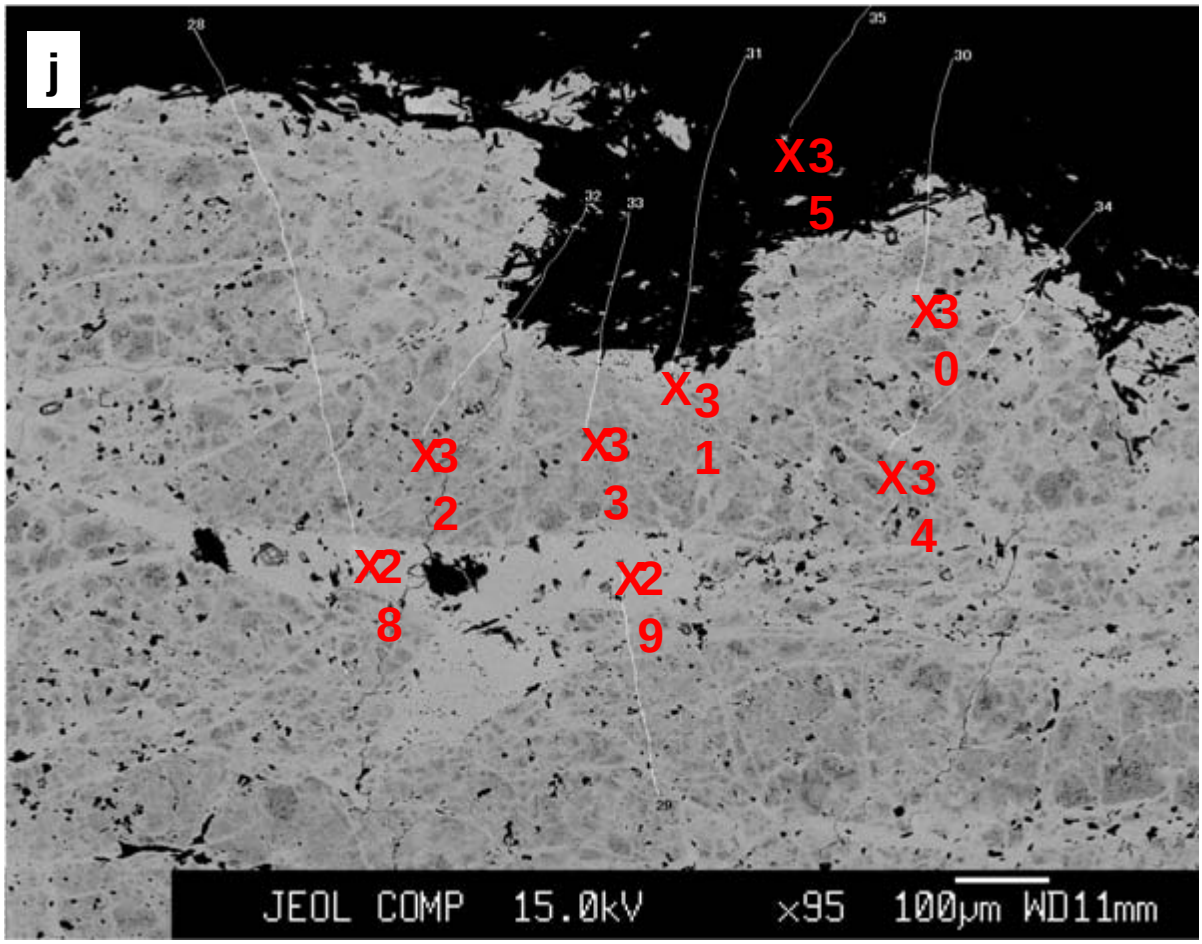
j
28
35
31
30
X35
32
33
34
X30
X31
X33
X32
X34
X28
X29
JEOL COMP 15.0kV ×95 100µm WD11mm

k

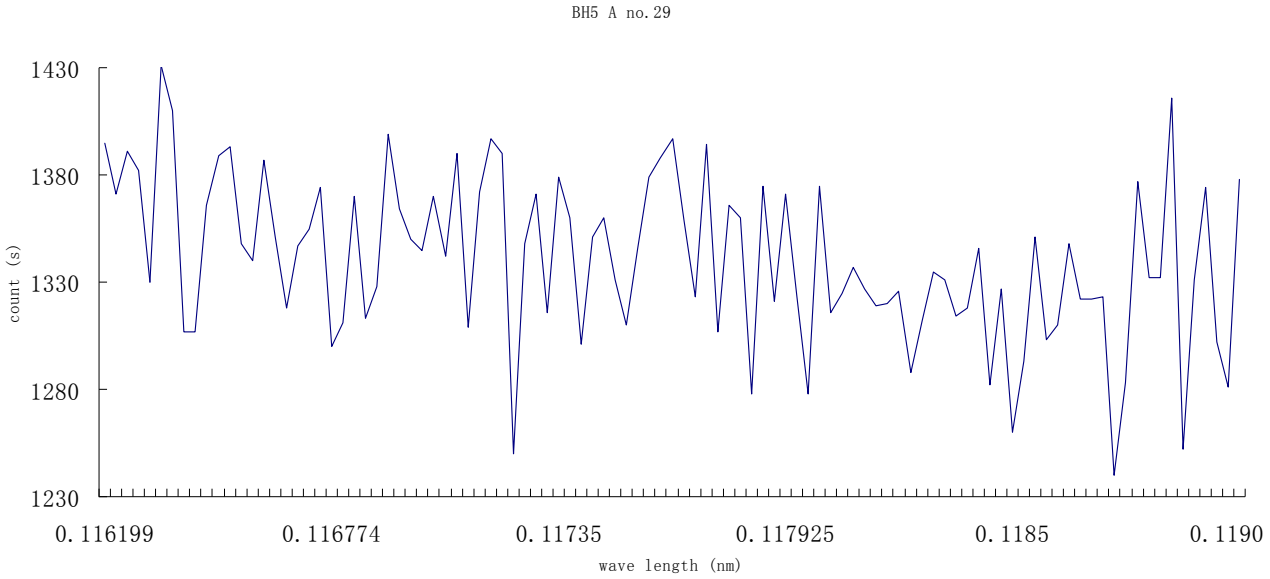
BH5 A no.29
1430
1380
1330
1280
1230
count (s)
0.116199
0.116774
0.11735
0.117925
0.1185
0.1190
wave length (nm)

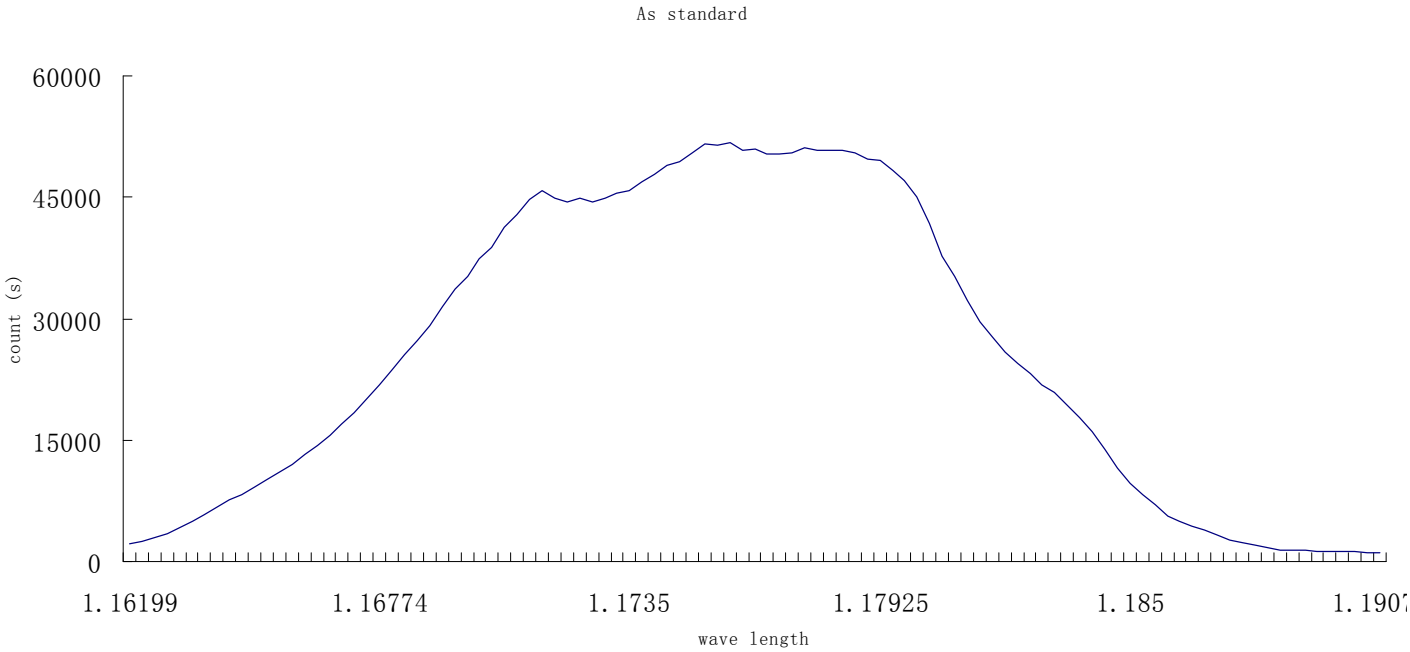
As standard
60000
45000
30000
15000
0
count (s)
1.16199
1.16774
1.1735
1.17925
1.185
wave length

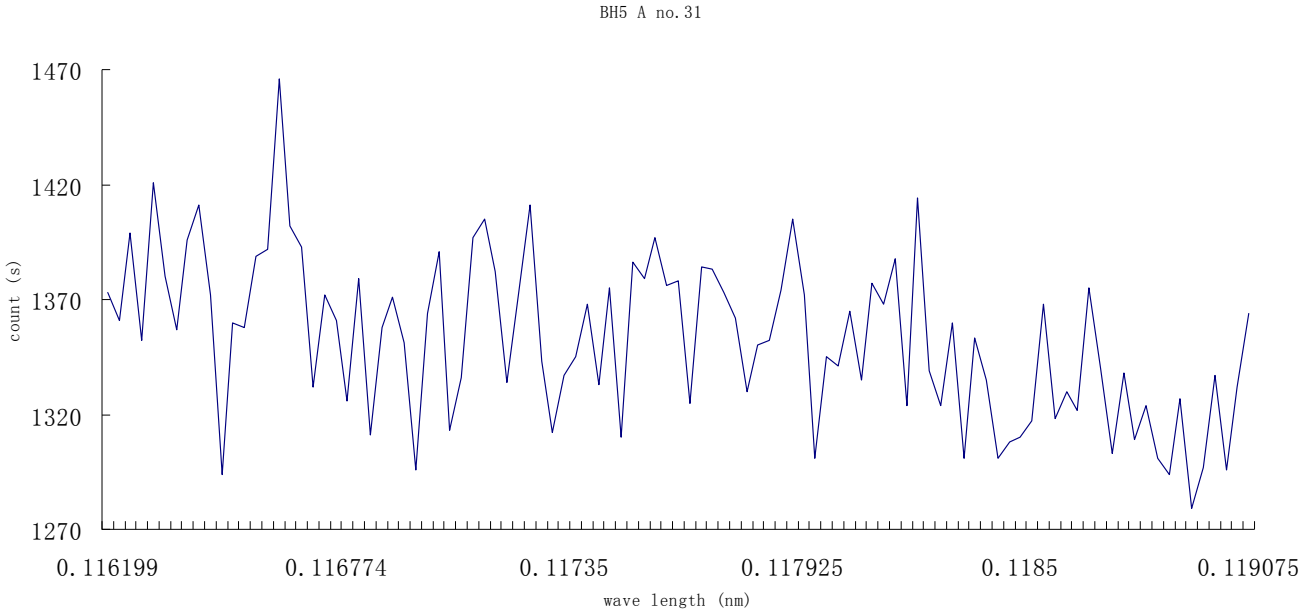
BH5 A no.31
1470
1420
1370
1320
1270
count (s)
0.116199
0.116774
0.11735
0.117925
0.1185
0.119075
wave length (nm)

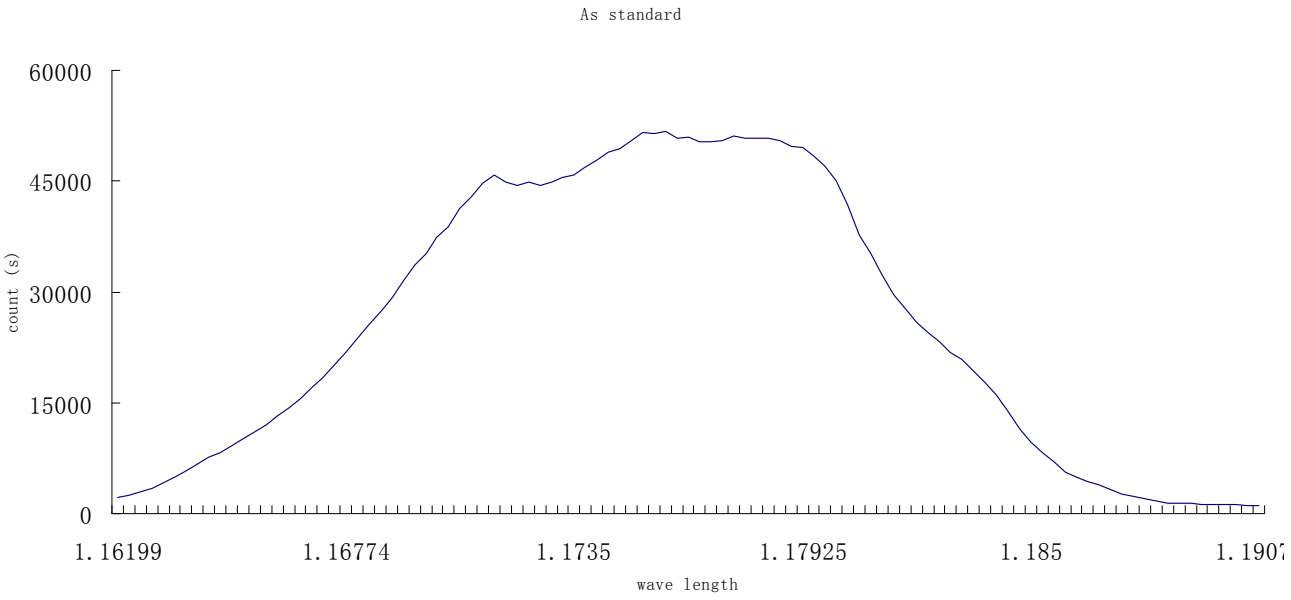
As standard
60000
45000
30000
15000
0
count (s)
1.16199
1.16774
1.1735
1.17925
1.185
wave length

m

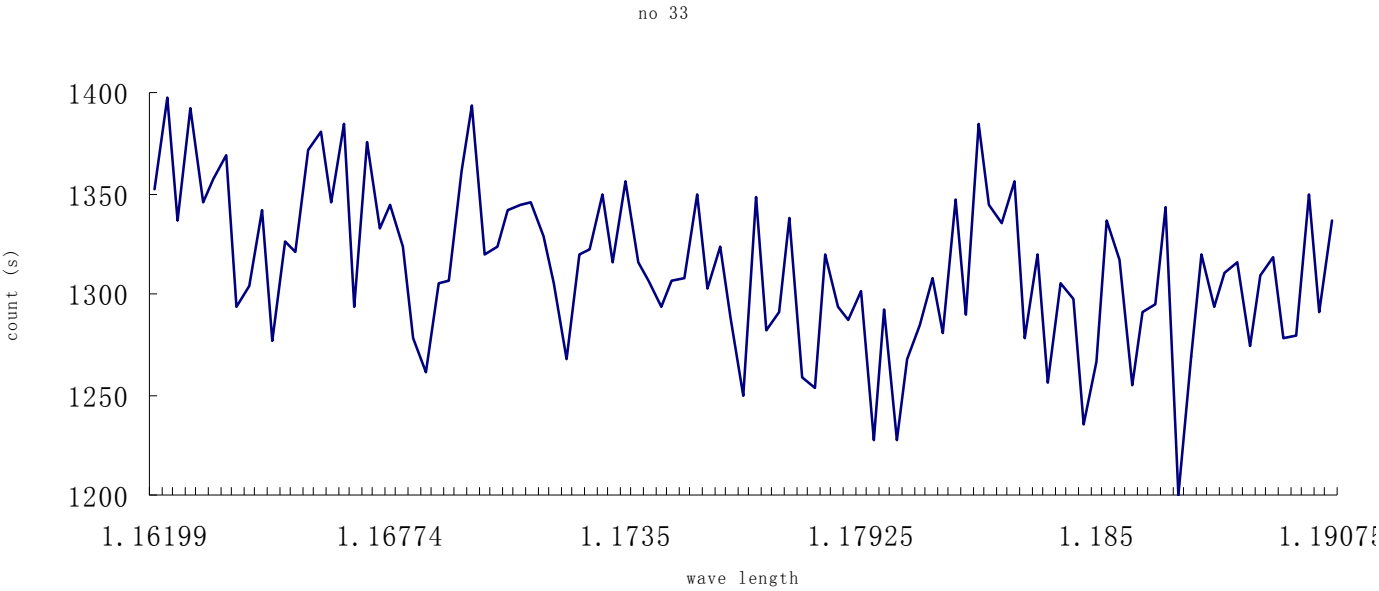
no 33
count (s)
1400
1350
1300
1250
1200
1.16199
1.16774
1.1735
1.17925
1.185
wave length

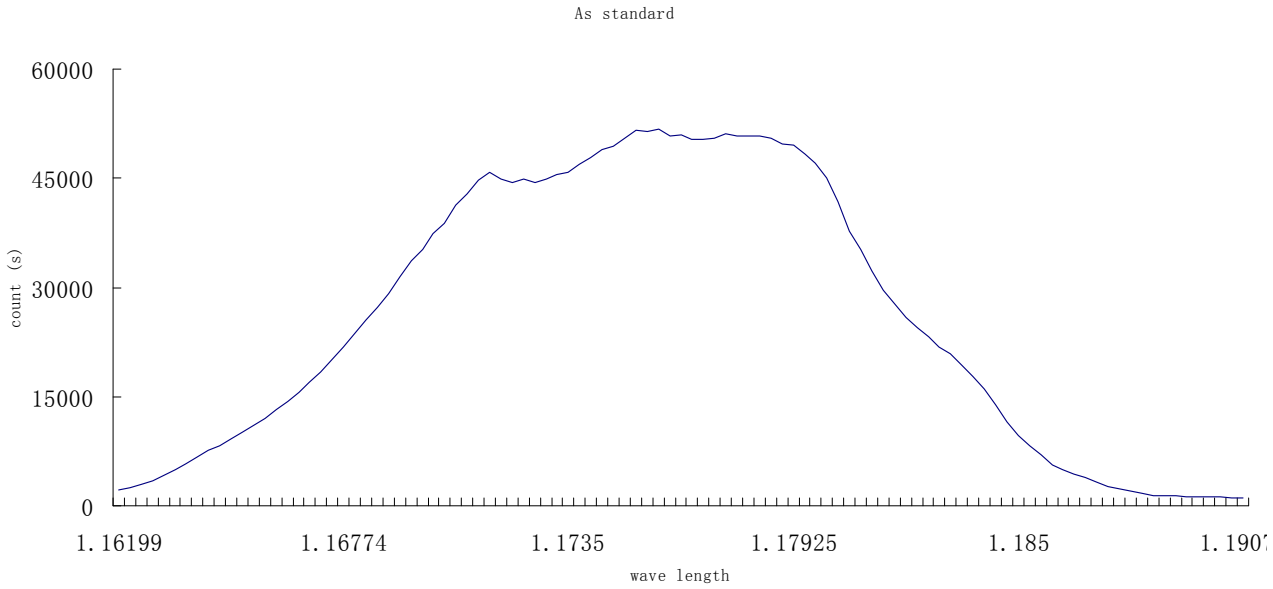
As standard
count (s)
60000
45000
30000
15000
0
1.16199
1.16774
1.1735
1.17925
1.185
wave length

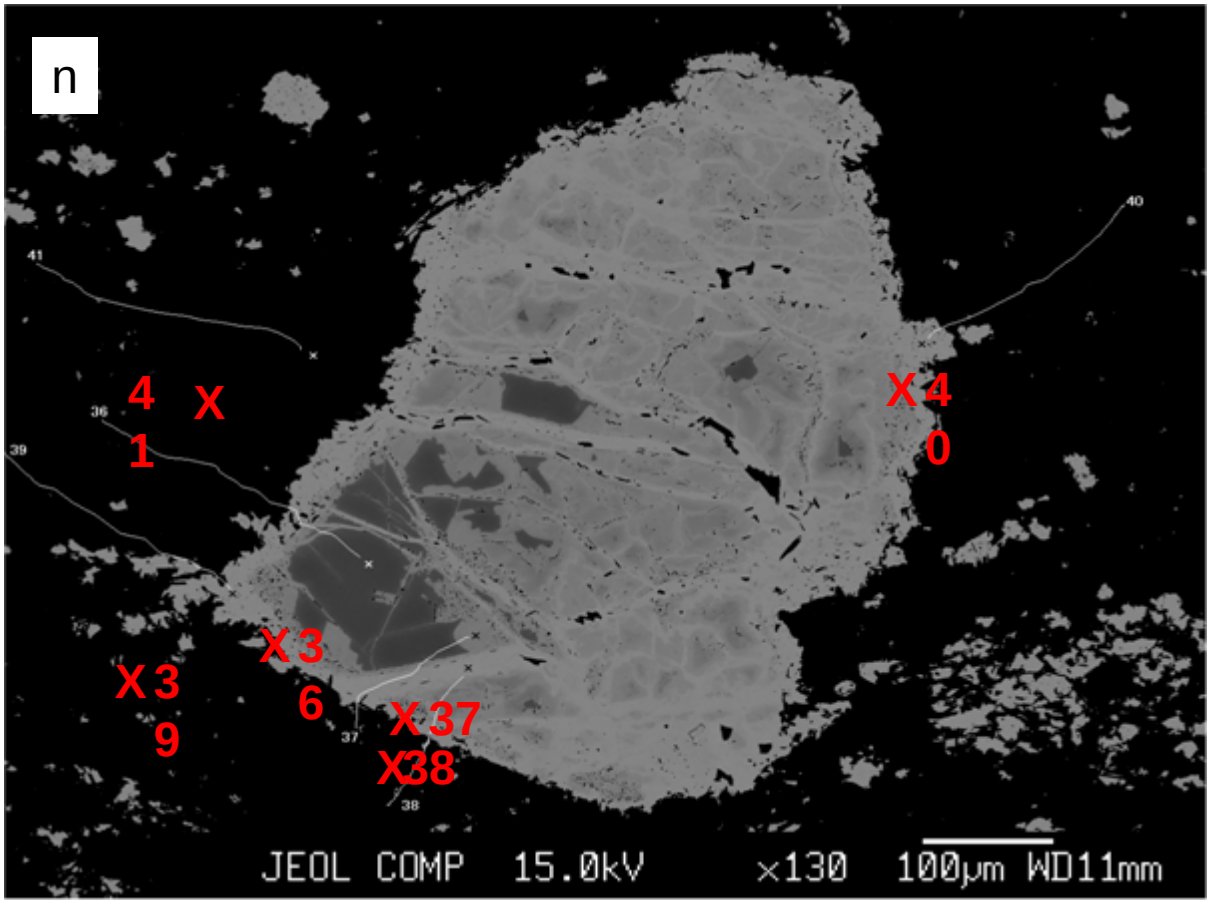
n
41
40
36
39
37
38
X 41
X 40
X 39
X 36
X 37
X 38
JEOL COMP 15.0kV ×130 100µm WD11mm

O

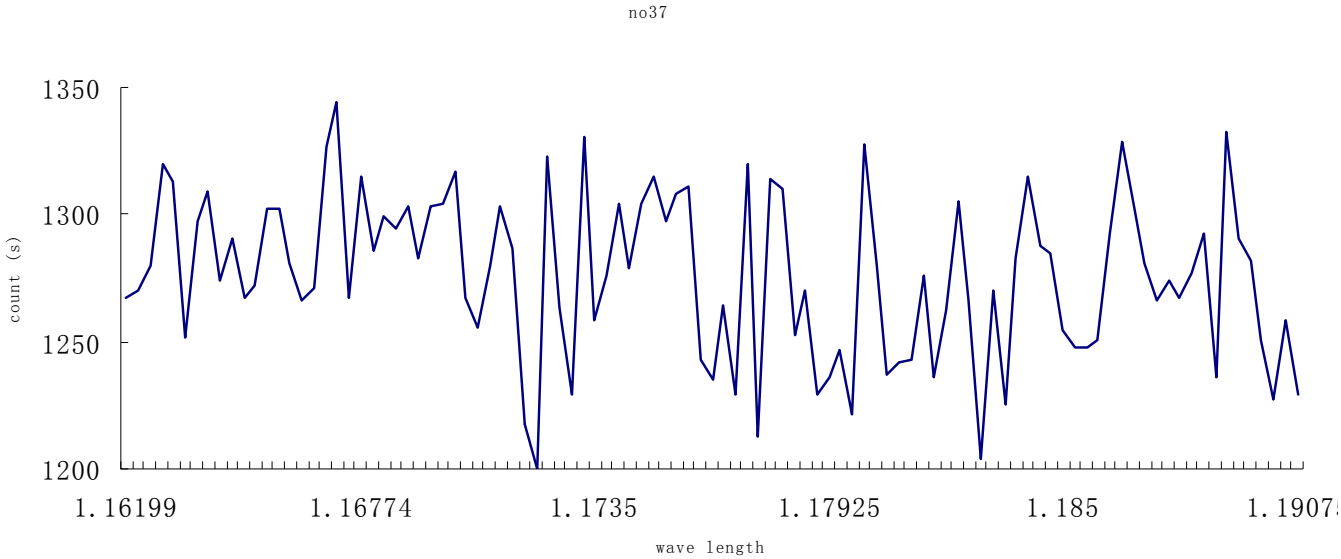
no37
1350
1300
1250
1200
count (s)
1.16199
1.16774
1.1735
1.17925
1.185
wave length

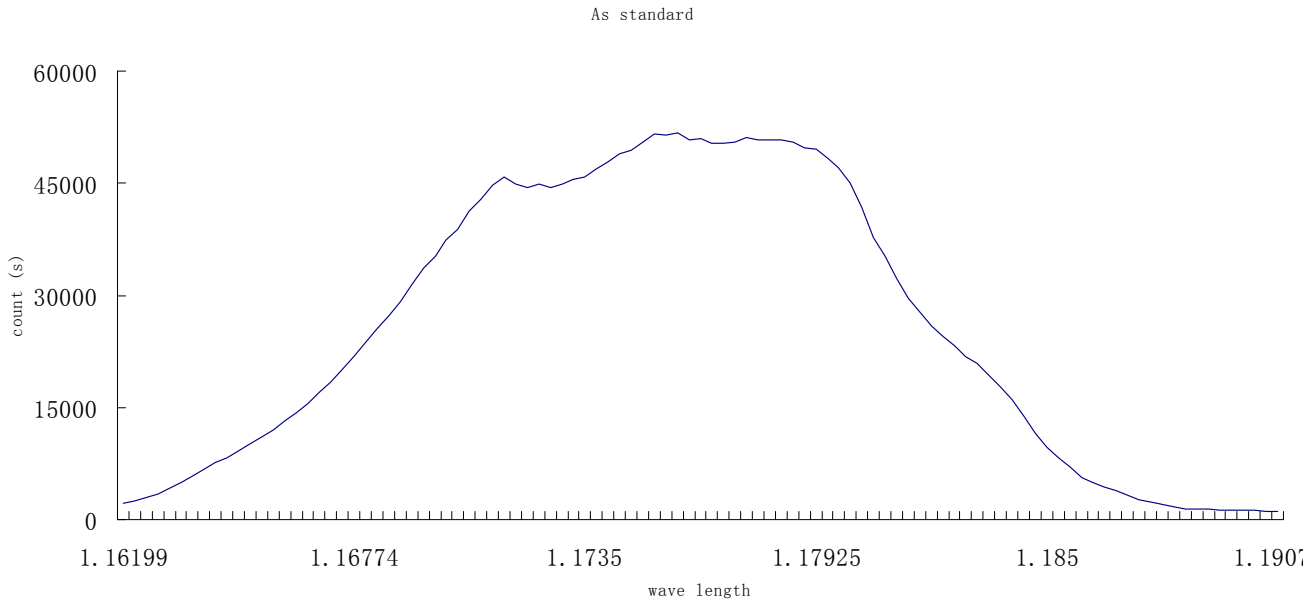
As standard
60000
45000
30000
15000
0
count (s)
1.16199
1.16774
1.1735
1.17925
1.185
wave length

p

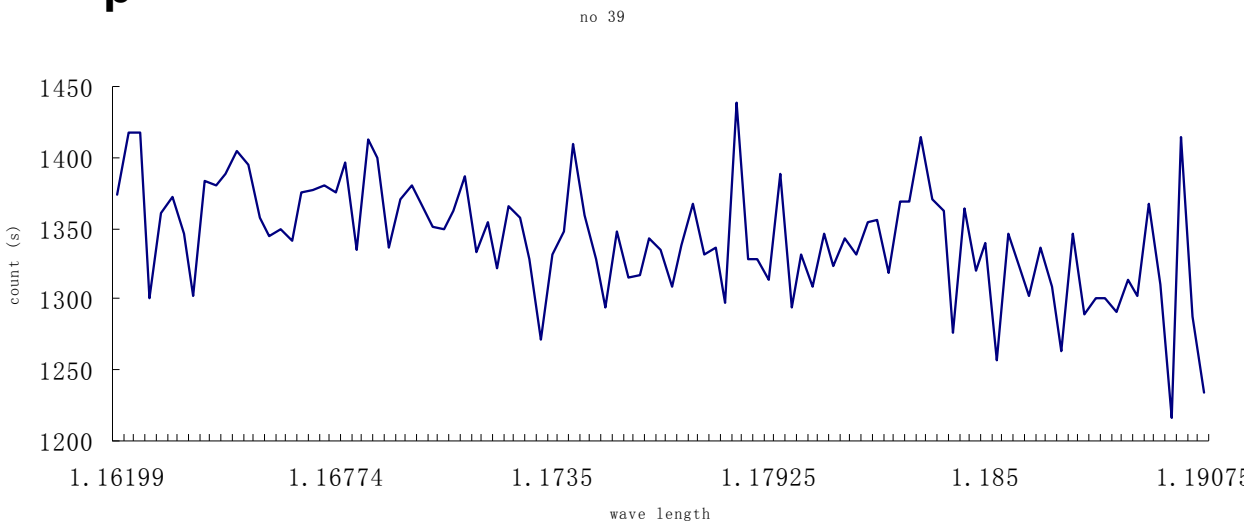
no 39
1450
1400
1350
1300
1250
1200
count (s)
1.16199
1.16774
1.1735
1.17925
1.185
wave length

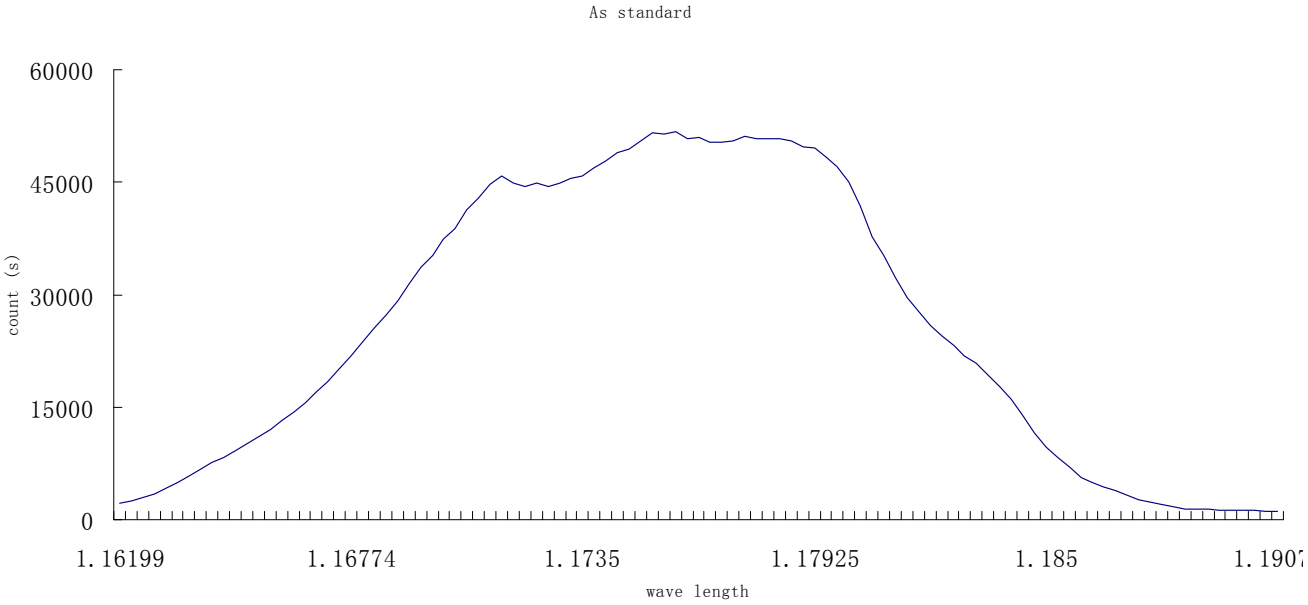
As standard
60000
45000
30000
15000
0
count (s)
1.16199
1.16774
1.1735
1.17925
1.185
wave length

EPMA back scattering electron imagine (BSE) of BH-4 and BH-5, and the numbered "X"'s marked the spots for As quantitative analysis on sample thin sections. The plots after the BSE indicate the presence of As in the samples (the top plot) which is confirmed by the results of As standard (the bottom plot). The X-axis is the wave length of the light intensity and the Y-axis is the count per seconds. **a)** EPMA back scattering imagine of BH-4 circle B in Fig 5 e). **b)** EPMA quantitative analysis of As species on BH-4 circle B, X14, **c)** on X15, **d)** on X16, **e)** on X17. X14 -- X17 do not contain As since there is no increase on counts on the according wave length. **g)** EPMA back scattering imagine of BH-4 circle F in Fig 5 k). **h)** analysis on BH-4 circle F, X23 shows X23 does not contain As since there is no increase on counts on the according wave length, whereas. **j)** EPMA back scattering imagine of BH-5 circle A in Fig 5 n, o, p). **k)** Analysis on BH-5 circle A, X29 , **l)** on X31 and **m)** on X33 shows that X29, X31 and X33 do not contain As since there is no increase on counts on the according wave length. **n)** EPMA back scattering imagine of BH-5 circle E. **o)** EPMA quantitative analysis of As species on BH-5 circle E, X37 and **p)** on X39 shows that. X37 and X39 do not contain As since there is no increase on counts on the according wave length.

Appendix D

Raw ICPMS data of As, Sr, Cs mean concentrations and relative stander deviations

		As concentration		Sr concentration		Cs concentration	
pH	ID	Mean(ppb)	RSD	Mean(ppb)	RSD	Mean(ppb)	RSD
	HCl	b.d.	32.4	b.d.	26.9	0.0	19.7
	BLANK	b.d.	43.4	0.0	63.8	0.0	15.6
	100PPT	0.1	2.0	0.1	1.1	0.1	1.4
	500PPT	0.5	4.5	0.5	0.6	0.5	0.9
	1PPB	1.0	1.8	1.0	0.6	1.0	0.8
	5PPB	5.1	1.3	5.1	0.6	5.1	1.1
	10PPB	9.2	1.3	9.2	0.5	9.2	1.0
2	I-L0	2.6	1.5	2.8	0.5	2.7	0.7
2	I-R0	b.d.	32.4	b.d.	17.3	0.0	9.0
2	I-R1	0.3	4.6	0.3	1.1	0.6	1.0
2	I-R2	0.6	2.9	0.6	1.8	1.2	0.6
2	I-R3	1.0	2.0	1.0	0.3	1.7	0.4
2	I-R4	1.2	2.2	1.2	1.0	2.2	0.8
2	I-R5	1.5	1.4	1.5	0.6	2.6	0.9
2	I-R6	1.7	1.4	1.7	0.1	3.0	1.0
2	I-R7	1.8	1.9	2.0	1.0	3.4	1.0
2	I-R8	2.2	1.7	2.3	0.4	3.8	1.1
2	I-R9	2.4	1.0	2.5	0.8	4.1	1.2
3	II-R1	0.4	3.0	0.4	0.8	0.7	0.8
3	II-R2	0.7	2.4	0.7	1.2	1.2	0.3
3	II-R3	1.0	3.4	1.1	0.7	1.9	0.7
3	II-R4	1.2	2.0	1.3	0.6	2.3	1.1
3	II-R5	1.5	1.2	1.6	0.9	2.7	0.4
3	II-R6	1.8	2.5	1.9	0.6	3.1	0.5
3	II-R7	2.0	1.2	2.1	0.7	3.6	0.6

3	II-R8	2.3	2.2	2.4	0.7	3.9	0.4
3	II-R9	2.5	2.3	2.7	0.5	4.3	0.8
3	II-L1	18.3	0.6	6.4	0.8	5.3	1.1
3	II-L2	18.4	1.1	6.4	0.6	5.2	0.6
3	II-L3	15.1	1.4	5.3	0.4	4.3	0.4
3	II-L4	16.6	1.1	5.8	0.6	4.6	0.7
3	II-L5	16.1	1.7	5.6	1.1	4.4	0.8
3	II-L6	15.9	0.8	5.5	0.5	4.2	0.5
3	II-L7	16.7	0.7	5.9	0.6	4.5	0.8
3	II-L8	13.8	1.4	4.9	0.4	3.7	0.8
3	II-L9	15.1	1.4	5.3	1.1	3.9	1.2
	HCl wash	b.d.	16.2	b.d.	26.9	0.0	19.7
	BLANK	b.d.	44.5	0.0	63.8	0.0	15.6
	100PPT	0.1	2.0	0.1	1.1	0.1	1.4
	500PPT	0.5	4.5	0.5	0.6	0.5	0.9
	1PPB	1.0	1.9	1.0	0.6	1.0	0.8
	5PPB	5.1	1.3	5.1	0.6	5.1	1.1
	10PPB	9.2	1.3	9.2	0.5	9.2	1.0
2	I-R0	b.d.	31.7	b.d.	17.3	0.0	9.0
2	I-R1	0.3	4.6	0.3	1.1	0.6	1.0
2	I-R2	0.6	2.9	0.6	1.8	1.2	0.6
2	I-R3	1.0	2.0	1.0	0.3	1.7	0.4
2	I-R4	1.2	2.2	1.2	1.0	2.2	0.8
2	I-R5	1.5	1.4	1.5	0.6	2.6	0.9
2	I-R6	1.7	1.4	1.7	0.1	3.0	1.0
2	I-R7	1.8	1.9	2.0	1.0	3.4	1.0
2	I-R8	2.2	1.7	2.3	0.4	3.8	1.1
3	II-R1	0.4	3.0	0.4	0.8	0.7	0.8
3	II-R2	0.7	2.4	0.7	1.2	1.2	0.3

3	II-R3	1.0	3.4	1.1	0.7	1.9	0.7
3	II-R4	1.2	2.0	1.3	0.6	2.3	1.1
3	II-R5	1.5	1.2	1.6	0.9	2.7	0.4
3	II-R6	1.8	2.5	1.9	0.6	3.1	0.5
3	II-R7	2.0	1.2	2.1	0.7	3.6	0.6
3	II-R8	2.3	2.2	2.4	0.7	3.9	0.4
3	II-R9	2.5	2.3	2.7	0.5	4.3	0.8
2	I-L0	2.6	1.5	2.8	0.5	2.7	0.7
2	I-R9	2.4	1.0	2.5	0.8	4.1	1.2
2	II-L1	18.3	0.6	6.4	0.8	5.3	1.1
2	II-L2	18.4	1.1	6.4	0.6	5.2	0.6
2	II-L3	15.1	1.4	5.3	0.4	4.3	0.4
2	II-L4	16.6	1.1	5.8	0.6	4.6	0.7
2	II-L5	16.1	1.7	5.6	1.1	4.4	0.8
2	II-L6	15.9	0.8	5.5	0.5	4.2	0.5
2	II-L7	16.7	0.7	5.9	0.6	4.5	0.8
2	II-L8	13.8	1.4	4.9	0.4	3.7	0.8
2	II-L9	15.1	1.4	5.3	1.1	3.9	1.2
	HCl wash	b.d.	32.5	b.d.	26.9	0.0	19.7
	blank	b.d.	29.9	0.0	24.6	0.0	22.0
	100ppt	0.1	7.0	0.1	1.9	0.1	2.5
	500ppt	0.5	3.5	0.5	1.2	0.5	0.9
	1ppb	1.0	1.8	1.0	0.8	1.0	0.6
	5ppb	5.0	2.1	5.2	0.6	5.1	1.0
	10ppb	9.0	1.4	9.4	0.8	6.5	53.1
8	iL0	26.3	14.8	29.5	6.2	38.6	3.1
8	iR0	1.2	21.5	1.0	7.3	2.8	2.7
8	iR1	3.3	16.1	3.9	6.5	8.5	6.8
8	iR2	5.4	11.1	7.4	4.1	16.7	5.9

8	iR3	9.0	11.7	10.8	3.0	24.8	3.2
8	iR4	5.8	10.1	7.1	4.3	15.2	3.7
8	iR5	15.1	8.7	16.3	2.6	34.7	0.9
8	iR6	15.7	17.5	18.3	5.9	42.3	4.4
8	iR7	19.8	9.2	21.9	3.7	49.2	3.9
8	iR8	20.1	6.2	23.7	2.9	53.9	4.1
8	iR9	24.3	9.3	26.5	7.1	58.0	6.6
10	iiR1	2.8	16.2	3.2	5.4	6.8	6.0
10	iiR2	5.5	16.7	7.1	6.0	14.2	4.2
10	iiR3	7.8	8.3	9.0	5.8	21.2	4.9
10	iiR4	10.0	9.8	12.9	6.4	27.7	4.3
10	iiR5	14.2	8.2	15.4	3.3	34.2	2.5
10	iiR6	19.4	14.3	16.8	3.6	37.8	2.1
10	iiR7	15.2	8.6	18.4	7.6	42.8	9.3
10	iiR8	19.2	15.9	21.4	8.0	47.2	2.9
10	iiR9	20.3	11.3	23.9	4.2	51.9	5.1
	HCl wash	b.d.	90.6	b.d.	8.7	b.d.	0.1

ID: each of the “I”, “II”, “I”, ii” stands for 1 complete set of experiments of a given pH value shown in the first column;

RSD: relative standard deviation expressed in percent

b.d.= below detection limit

The concentrations of As, Sr, and Cs were measured using the mass peaks of 75, 88 andn 133, respectively.

“L” stands for the source cells; “R” stands for the measurement cell; 0 to 9 in the final digit in the sample identification number (ID) is the number of the sequence of the solution taken from the cells every 10 minutes

Appendix E

Abstract submitted to International Mineralogical Association (IMA) 2010 congress;

The occurrence and speciation of arsenic in serpentinites in northern Vermont, USA

Niu, L.[1], Hattori, K.[1*], Takahashi, Y.[2] & Ryan, P.C.[3]

1- Dept. of Earth Sciences, University of Ottawa, Ottawa, Ontario, Canada (*khattori@uottawa.ca)
2- Dept. of Earth and Planetary Systems Science, Hiroshima University, Higashi-Hiroshima, Japan
3- Geology Dept., Middlebury College, Middlebury, Vermont, U.S.A.

High concentrations of As are reported in ground waters and bedrocks in many parts of New England [1]. Ryan et al. [2] reported that hyss contain high concentrations of As (up to 449 ppm in serpentinites and 1,100 ppm in talc-magnesite rocks) in northern Vermont. Altered ultramafic rocks are common in the Appalachians in New England. We investigated the occurrence of As in representative serpentinites from northern Vermont (103-450 ppm As in bulk rocks). The study includes the examination of polished-thin sections, electron microprobe analysis of minerals, mechanical separation of mineral fractions (ferrihydrite films, antigorite-rich fraction, magnetite-rich fraction), acid leaching and digestion of these fractions, and X-ray absorption spectroscopic study of As. Magnetite-rich fractions yielded high concentrations of As in hot HNO_3 digestion at 90 ºC. Brown films of ferrihydrite along cracks and on surfaces contain very low concentrations of As. Antigorite-rich fractions contain minor As (<50 ppm). X-ray absorption spectra of these fractions show that the As is predominantly +3 in magnetite- and antigorite- fractions.

Magnetite commonly forms a fine dusting in serpentine since the hydration of olivine releases Fe(II). Magnetite also forms rims of chromite grains during serpentinization. Our data suggest that As(III) in water was fixed in magnetite and minor amounts in serpentine during the hydration of ultramafic rocks. Our earlier study of serpentinites in northwestern Himalayas show that As (V) is fixed in serpentinites by replacing Si(IV) in antigorite [3]. The results of these studies suggest that hydrating ultramafic rocks are capable of fixing both As (III) and As(V) and that the speciation of As in serpentinites is controlled by the oxidation state of As in the hydrating fluids.

[1] Ayotte, J.D. et al. (2003) *Environ. Sci. Technol.*, **37,** 2075-2083. [2] Ryan, P.C. et al. (2009) *Abst. GSA Mtg*., **77**-**3**. [3] Hattori, K. et al. (2005) *Geochim. Cosmochim. Acta*, **69**, 5585-5596.

Appendix F

Abstract submitted to annual meeting of the Geological Association of Canada (GAC) and Mineralogical Association of Canada 2011

Arsenic Distribution and Speciation in Appalachian Serpentinites in Northern Vermont, USA

Niu, Lijie[1], Hattori, Keiko[1]*, Takahashi, Yoshio[2] & Ryan, Peter C.[3]
1- Dept. of Earth Sciences, University of Ottawa, Ottawa, Ontario, Canada (*khattori@uottawa.ca)
2- Dept. of Earth and Planetary Systems Science, Hiroshima University, Higashi-Hiroshima, Japan
3- Geology Dept., Middlebury College, Middlebury, Vermont, U.S.A.

High concentrations of As in ground waters are noted in many parts of New England (Ayotte et al., 2003). Previous work by Ryan et al. (2009) documented that serpentinites in northern Vermont contain high As, up to 449 ppm. We selected representative samples of serpentinite and examined the distribution and speciation of As in the samples. The serpentinites are composed of serpentine with minor Cr-spinal, magnetite, and carbonates. The XRD spectra of the samples show that antigorite is the serpentine phase. Carbonate minerals are magnesite and dolomite with very minor calcite. Cr-spinel grains are variably altered to ferritchromite and magnetite in their rims. Samples are separated into a magnetic fraction and a non-magnetic, serpentine-rich fraction. Leaching of a serpentine-rich fraction with NaH_2PO_4 (0.1M) yielded As, which is less than 10 % of the total As recovered by hot HF/HNO_3. The data suggest that As is mostly incorporated in the crystal structure of antigorite. This is further confirmed by the quantitative analysis of

minerals using an electron microprobe. Antigorite contains variable, but high concentrations of As, up to 1300 ppm. X-ray absorption spectra at As K-edge show that As is +3. Local atomic structures around As are calculated based on the EXAFS spectra. The results show that the coordination number of As is 4.0 and that the atomic distances are 1.778±0.009 Å between As and O, 3.196±0.070 Å between As and Si, and 3.4875±0.032 Å between As and Mg. The data suggest that As replaces Si in the tetrahedral site of antigorite.

Earlier study of serpentinites in north western Himalayas suggested that As is +5 replacing Si in antigorite (Hattori et al., 2005). The data from the two locations suggest that antigorite is capable to incorporate As (+3) and As (+5) into its tetrahedral site.